



UNIVERSIDADE FEDERAL DO CEARÁ
CENTRO DE CIÊNCIAS
PROGRAMA DE PÓS-GRADUAÇÃO EM QUÍMICA

SAMUEL VELOSO CARNEIRO

**CHEMICAL SENSING BASED ON CARBON QUANTUM DOTS FOR FOOD
ADDITIVES ANALYSIS**

FORTALEZA

2022

SAMUEL VELOSO CARNEIRO

CHEMICAL SENSING BASED ON CARBON QUANTUM DOTS FOR FOOD
ADDITIVES ANALYSIS

Doctoral thesis submitted to the Programa de Pós-graduação em Química of the Universidade Federal do Ceará as a requirement for the degree of doctor of chemistry.
Concentration area: Physical Chemistry.

Supervisor: Pierre Basílio Almeida Fachine.

Co-supervisor: Rafael Melo Freire.

FORTALEZA

2022

Dados Internacionais de Catalogação na Publicação
Universidade Federal do Ceará
Biblioteca Universitária

Gerada automaticamente pelo módulo Catalog, mediante os dados fornecidos pelo(a) autor(a)

- C29c Carneiro, Sammel Veloso.
Chemical sensing based on Carbon Quantum Dots for food additives analysis / Samuel Veloso
Carneiro. – 2022.
153 f. : il. color.
- Tese (doutorado) – Universidade Federal do Ceará, Centro de Ciências, Programa de Pós-Graduação em Química, Fortaleza, 2022.
Orientação: Prof. Dr. Pierre Basílio Almeida Fechine.
Coorientação: Prof. Dr. Rafael Melo Freire.
1. Carbon Quantum Dots. 2. Chemical sensing. 3. Fluorescence. 4. Nanocomposite. 5. Food additives.
- I. Título.

CDD 540

SAMUEL VELOSO CARNEIRO

CHEMICAL SENSING BASED ON CARBON QUANTUM DOTS FOR FOOD
ADDITIVES ANALYSIS

Tese de doutorado apresentada ao Programa de Pós-Graduação em Química da Universidade Federal do Ceará, como requisito parcial à obtenção do título de doutor em Química.
Área de concentração: Físico-Química.

Aprovada em: ___/___/_____.

BANCA EXAMINADORA

Prof. Dr. Pierre Basílio Almeida Fechine (Orientador)
Universidade Federal do Ceará (UFC)

Prof^a. Dr^a. Gisele Simone Lopes
Universidade Federal do Ceará (UFC)

Prof. Dr. Claudenilson da Silva Clemente
Universidade Federal do Ceará (UFC)

Prof. Dr. Renato Altobelli Antunes
Universidade Federal do ABC (UFABC)

Prof. Dr. José Heriberto Oliveira do Nascimento
Universidade Federal do Rio Grande do Norte (UFRN)

I dedicate this work to my mother, Idalina de Andrade Veloso, and to all my teachers and friends, who throughout my life have contributed to the professional I have become today.

ACKNOWLEDGMENTS

To God, for all the blessings he has bestowed on me throughout my life;

To my parents, Idalina de Andrade Veloso and Francisco Zaneval Rodrigues Carneiro. I especially thank my mother, for accompanying, encouraging and supporting me throughout my school and academic journey;

To Professor Pierre Basílio Almeida Fachine, for his patience, guidance and advice throughout the doctor's degree. Since when I took the Fundamentals of Physical Chemistry course, I always had him as a reference, because I was sure of his greatness as a professional and as a human being; I thank God for the opportunity to have him as my doctoral supervisor;

To my friend and co-supervisor Rafael Melo Freire, for all the hours of conversations and support in order to show me the best ways to conduct my work;

To the scientific initiation students who helped me throughout my doctor's degree. I would like to especially thank Vivian, Harisson and Marcos, for having accompanied me at all times, especially the most rushed. Without you I would not have achieved all the results I have and in such a short time;

To my friend Joelson Oliveira, for accompanying me at all times, from the easiest to the most complicated in my personal and professional life. Thank you for having him as a friend for all hours;

To my friend Sheyliane Pontes, for having accompanied me in my doctoral experiments and for sharing her laboratory experience, which contributed to the achievement of the objectives of this work;

To the Advanced Materials Chemistry Group (GQMat), which made it possible to develop and carry out the experiments. I thank all the members of the group, my friends who helped me at all times, and especially Lillian Fachine, for all the monitoring of my project, for all the conversations and tips, which strongly contributed to the improvement of this work. Nor could I fail to mention the friends who shared their experiences and contributed to my formation: Alvernes, Anderson, Roberta, Tiago, Fernando, Elayne and Eduardo;

To my friends from other laboratories, who accompanied me throughout my master's and doctoral time: David, Ribamar, Bruno, Alexandre, Ana Aline, Malena and Luan;

To my friends from the Chemistry (bachelor's) and (licenciatura) courses, who contributed to my professional training;

To professor and friend Rafael Audino Zambelli, for all the partnerships and for always keeping the food engineering laboratory open;

To Prof. Renato Antunes, from Universidade Federal do ABC, for making the XPS measurements available, essential for the development of the works presented in this thesis;

To Professors Adonay Rodrigues Loiola, Gisele Simone Lopes and Odair Pastor Ferreira, who were part of my Qualification Exam, for all the suggestions that made this work even better;

To Professor Francisco Belmino Romero, for accompanying me since graduation, for his advice and the great learning both in Physical Chemistry as well as in academic life;

To the Department of Analytical Chemistry and Physical Chemistry for having been my second home since graduation;

To the Federal University of Ceará and the State University of Ceará, where I acquired all my academic experience and made possible the realization of my dream of being a doctor and graduated in Chemistry.

To the Graduate Program in Chemistry for all the infrastructure made available for the development of the work;

To everyone who contributed directly and indirectly to the realization of my experiments;

This study was financed in part by the Coordenação de Aperfeiçoamento de Pessoal de Nível Superior – Brasil (CAPES) – Finance Code 001.

RESUMO

Plataformas de sensoriamento químico fluorescente têm sido aplicadas na detecção de diferentes tipos de analitos, incluindo aditivos alimentares. Dentre as suas vantagens, destaca-se a produção com baixo custo e alta sensibilidade no controle de qualidade, seguindo os limites máximos recomendados pelos órgãos competentes. Esses sensores podem se tornar mais versáteis quando são baseados em materiais nanoestruturados, tais como os da classe OD, conhecidos como Pontos Quânticos de Carbono (PQCs). Na literatura, ainda há poucos trabalhos que incorporam PQCs em uma fase sólida, de modo a desenvolver um sensor de análise de campo com alta sensibilidade e seletividade. Diante desse panorama, essa tese resulta de uma pesquisa inovadora na área de sensores químicos, cujo objetivo geral é desenvolver plataformas de sensoriamento e um dispositivo para análise de segurança alimentar em produtos industrializados. O primeiro trabalho consistiu na síntese e caracterização de PQCs obtidos a partir de uma fonte de carbono natural (sementes da planta *Caesalpinia pulcherrima*), com posterior aplicação de métodos quimiométricos de análise multivariada para identificar cinco aditivos alimentares em conservas de azeitona. As nanopartículas obtidas foram rotuladas como FM-CD e os resultados mostraram uma alta sensibilidade da estratégia proposta, a qual detectou concentrações tão baixas quanto 252 ng mL^{-1} de benzoato de sódio. Obteve-se também uma classificação com 100% de acurácia, baseada no algoritmo de Análise Linear Discriminante (LDA). Com o primeiro trabalho concluído, a próxima etapa foi obter novos PQCs, com um rendimento quântico (RQ) mais alto para ser aplicado em um sensor de análise de campo. Assim, PQCs foram sintetizados pela rota hidrotermal a partir do ácido cítrico, ácido bórico e polietilenomina ramificada e foram denominados de B,N-Cdot. Os resultados evidenciaram que essas nanopartículas com RQ igual 44,3% conseguiram detectar os íons nitrito com alta seletividade. A próxima etapa consistiu em impregnar os B,N-Cdots em uma matriz polimérica de álcool polivinílico (PVA) para desenvolver um sensor de análise de campo de íons nitrito. O nanocompósito foi empregado juntamente ao aplicativo PhotoMetrix e foi capaz de quantificar o analito. Portanto, essa tese apresenta resultados que comprovam o grande potencial dos PQCs no campo de sensoriamento químico e no desenvolvimento de dispositivos simples que viabilizam o controle de qualidade na indústria de alimentos.

Palavras-chave: Pontos Quânticos de Carbono; sensoriamento químico; fluorescência; nanocompósito; aditivos alimentares.

ABSTRACT

Fluorescent chemical sensing platforms have been applied to detect different types of analytes, including food additives. Among its advantages, the production with low cost and high sensitivity in quality control stands out, following the maximum limits recommended by competent organizations. These sensors become more viable when they are based on OD nanostructured materials known as Carbon Quantum Dots (CQDs). In the literature, there are still few works that incorporate CQDs in a solid phase, to develop a field analysis sensor with high sensitivity and selectivity. Given this scenario, this thesis results from innovative research in the area of chemical sensors, whose general objective is to develop sensing platforms and a device for analyzing food safety in industrialized products. The first work consisted of the synthesis and characterization of CQDs obtained from a natural carbon source (seeds of the plant *Caesalpinia pulcherrima*), with subsequent application of chemometric methods of multivariate analysis to identify five food additives in canned olives. The nanoparticles obtained were labeled as FM-CDs and the results showed a high sensitivity of the proposed strategy, which detected concentrations as low as 252 ng mL^{-1} of sodium benzoate. In addition, we obtained a classification with 100% accuracy, based on the algorithm Linear Discriminant Analysis (LDA). With the first work completed, the next step was to obtain new CQDs, with a higher quantum yield (QY) to be applied in a field analysis sensor. Thus, CQDs were synthesized by the hydrothermal route from citric acid, boric acid and branched polyethyleneimine, which were named B,N-Cdot. The results showed that these nanoparticles with QY equal to 44.3% were able to detect nitrite ions with high selectivity. The next step consisted of impregnating the B,N-Cdot in polyvinyl alcohol (PVA) polymer matrix to develop a nitrite ion field analysis sensor. The nanocomposite was used together with the PhotoMetrix application and was able to quantify the analyte. Therefore, this thesis presents results that prove the great potential of CQDs in the field of chemical sensing and in the development of simple devices that enable quality control in the food industry.

Keywords: Carbon Quantum Dots; chemical sensing; fluorescence; nanocomposite; food additives.

LIST OF FIGURES

Figure 1	– Classification of the nanomaterials, according to dimensionality.....	22
Figure 2	– State of the art for scientific production involving the term "Carbon Quantum Dots", performed on the ScienceDirect website on March 18, 2022.....	23
Figure 3	– Different sensing strategies: (a) turn-off/turn-on sensing; (b) sensor array.....	24
Figure 4	– Scheme of the organization of the thesis in chapters.....	25
Figure 5	– Synthesis methods of nanostructured materials.....	28
Figure 6	– Schematic illustration of properties, syntheses and sensing applications of CQDs.....	37
Figure 7	– Sensor turn-on using fluorescence property of nanomaterials: (a) KN-CDs selectivity to Fe^{3+} ions and visualization of the fluorescent sensor in the absence and presence of the analyte, under white light and UV light (inset); (b) the linear calibration graph for $(F_0/F)/F_0$ with different concentrations of Fe^{3+} ion; (c-i) photos of these real-world foods: pork, chicken and hairtail (purchased from the supermarket nearby); (c-ii) fluorescence intensity of GQDs at 366 nm for three commercially available food extracts and water (normal and polluted); (c-iii) detection of the content of HCHO in three foods (normal and polluted) by GQDs fluorescent test paper; (d) Response of nanoprobe to different interfering ions, the concentration of As(III) was 10 ng mL^{-1} , F_0 represents the luminescence intensity before the addition of ion while F_n was the luminescence after incubated with ions.....	47

Figure 8	<p>– Examples of ratiometric sensors: (a) Variation in the fluorescence emission of the CDs–RF conjugate in the presence of different RF concentrations ($0 \mu\text{mol L}^{-1}$ to $11 \mu\text{mol L}^{-1}$). Inset: the linear relationship between the fluorescence emission ratio (I_{521}/I_{441}) of the CDs-RF conjugate and the RF concentration; (b) The detection principle of a dual-mode glucose sensor based on CQDs and ODB; (c) Fluorescence spectra of the CDs upon the addition of different concentrations of Al^{3+}; (d) relation between the concentration of Al^{3+} and the I_{500}/I_{420} value. The inset shows the linear relation in the $0.15\text{--}38.46 \mu\text{mol L}^{-1}$ range; (e) images of the CDs solutions obtained by using a smartphone under a 360 nm UV lamp; (f) G/B as a function of the Al^{3+} concentration. The inset shows the linear fit of G/B as a function of the Al^{3+} concentration.....</p>	50
Figure 9	<p>– (a) Color changes observed by the naked eye for the BCP, 4-NP and MR colorimetric sensors when exposed to formaldehyde gas (20 ppm). Colorimetric responses (ΔRGB values) of (b) BCP, (c) 4-NP, and (d) MR sensors prepared with various PEI/PSMA ratios (0–10) on exposure to 20 ppm formaldehyde gas.....</p>	54
Figure 10	<p>– Thin films containing nanomaterials: (a) flexible transparent polyethylene terephthalate film with CDs as humidity sensor; (b) Procedure of preparing CDs/PVA film with silica spheres at the surface; (c) Schematic illustration of the SPR signal before and after the analyte flow.....</p>	55
Figure 11	<p>– Exploratory data and classification methods as chemometric tools applied in sensing strategies: (a) example of score plot of PCA; (b) example of canonical factors plot of Linear Discriminant Analysis (LDA).....</p>	58
Figure 12	<p>– Sectoral graph of the percentage distribution of food additives most used by the industry.....</p>	62

Figure 13	– Illustration of the developing of sensing strategy: FM-CDs obtention and further fluorescence sensing of five different food additives using LDA method.....	71
Figure 14	– Morphological characterization of FM-CDs: (a) AFM image with topographical height profile; (b) height graph.....	72
Figure 15	– Structural characterizations of FM-CDs: (a) FTIR spectra of “flamboyant mirim” seeds powder and FM-CDs; (b) Raman spectra of FM-CDs sample.....	73
Figure 16	– Results of XPS for FM-CDs: (a) survey; (b) graphic of the percentual composition of FM-CDs; (c) C1s and (d) O1s high-resolution spectrum of FM-CDs.....	74
Figure 17	– FM-CDs spectroscopy characterizations: (a) UV-Vis absorption (purple solid line), excitation spectra (black dash line), emission spectra (blue solid line), and the right inset is the photograph of FM-CDs suspension under 365 nm excitation in comparison to natural light radiation on left inset; (b) Photoluminescence spectra with different excitation wavelengths (330 to 450 nm).....	75
Figure 18	– Fluorescence-response evaluation of FM-CDs at different experimental conditions: (a) Concentration effect of FM-CDs on fluorescence and self-quenching (inset); (b) Photobleaching experiment for 30 min; (c) Effect of ionic strength with sodium chloride; (d) Effect of acidic pH FM-CDs. All average and standard deviation values were calculated based on triplicate experiments.....	76
Figure 19	– Titration curves with tested food additives at different initial concentrations of stock solution: (a) 0.1 mol L ⁻¹ ; (b) 0.01 mol L ⁻¹ and (c) 0.001 mol L ⁻¹ . Fluorescence intensity was investigated at 435 nm using an excitation wavelength of 360 nm and normalized using I/I ₀ , where I ₀ and I denote the intensity before and after analyte addition, respectively. All	

average and standard deviation values were calculated based on triplicate experiments.....	77
Figure 20 – Sensing tests using plots of LDA in three dimensions with all additives at different concentrations in CQDs suspension under neutral pH: (a) 500 $\mu\text{mol L}^{-1}$; (b) 50 $\mu\text{mol L}^{-1}$; (c) 5 $\mu\text{mol L}^{-1}$. Each average value was calculated with six replicates and 95.0% of level of confidence. CA = citric acid; LA = lactic acid; AA = ascorbic acid; SB = sodium benzoate; PS = potassium sorbate.....	81
Figure 21 – LDA-based sensing tests with pickled olives (real sample), considering two most significant canonical factor, using three different concentrations of all additives: (a) 500 $\mu\text{mol L}^{-1}$; (b) 50 $\mu\text{mol L}^{-1}$; (c) 5 $\mu\text{mol L}^{-1}$. Each average value was calculated with six replicates and 95.0% of level of confidence. Legend: CA = citric acid; LA = lactic acid; AA = ascorbic acid; SB = sodium benzoate; PS = potassium sorbate.....	82
Figure 22 – Reaction scheme for obtaining B,N-Cdot by the hydrothermal method.....	88
Figure 23 – Dimensions of pocket microscope used for the field analysis device.....	90
Figure 24 – (a) preparation of the PVA/B,N-Cdot nanocomposite in coverslips; (b) smartphone with the Photometrix applicative installed and pocket microscope clipped to smartphone.....	91
Figure 25 – Results of spectroscopic characterizations: (a) QY of all CQDs synthesized in this work; (b) UV-Vis, excitation and emission spectra of B,N-Cdot. Inset: B,N-Cdot under white lamp (left) and UV lamp (right). Legend: Exc = excitation spectrum; Em = emission spectrum.....	93
Figure 26 – Results of structural characterizations of B,N-Cdot: (a) FTIR spectrum; (b) Raman spectrum.....	95

Figure 27	– (a) XPS survey; (b) C1s and (c) B1s high-resolution spectra of B,N-Cdot; (d) structure proposal of B,N-Cdot (hydrogen atoms have been omitted for simplification).....	97
Figure 28	– (a) XPS survey; (b) C1s; (c) N1s and (d) O1s high-resolution spectra of N-Cdot.....	98
Figure 29	– AFM images of B,N-Cdot: (a) topography; (b) phase and (c) AFM section height profile of a particle. The AFM scanning was performed over a 5 μm x 5 μm region.....	99
Figure 30	– Confocal microscopy analysis of B,N-Cdot dried film with emission at: (a) 405nm; (b) 488nm; (c) 561 nm and (d) the super positioning of the channels. (e) FLIM image with a heat-map indicating the short and long life-time decays; (f) histogram of the life-time decays frequency.....	100
Figure 31	– Fluorescence-response evaluation of B,N-Cdot at different experimental conditions: (a) concentration effect of B,N-Cdot on fluorescence and PL intensity as a function of concentration (inset); (b) effect of pH in the B,N-Cdot fluorescence intensity; (c) kinetic study of the interaction between B,N-Cdot and NO_2^- ions at concentration of 40 mmol L^{-1} . (d) fluorescence intensity in the presence of possible interferences at concentration of 40 mmol L^{-1} . All average and standard deviation values were calculated based on triplicate experiments. Legend: Glu = glucose; SA = succinic acid; LA = lactic acid; GA = glutamic acid; His = histidine; Ala = alanine; Phe = phenylalanine.....	101
Figure 32	– Titration curve of sample B,N-Cdot with different concentrations of NO_2^- ions at 298.65 K in PBS 7.4: (a) effect of the concentration of quencher on the fluorescence of the system; (b) relative fluorescence intensity as a function of NO_2^- concentration and linear range of high concentrations used for nitrite sensing (inset); (c) Photographs of the sample of B,N-Cdot in the presence of different concentrations of NO_2^- used in the construction	

	of the titration curve. All average and standard deviation values were calculated based on triplicate experiments.....	104
Figure 33	– (a) Titration curves of B,N-Cdot and NO_2^- ions at different temperatures and K_{SV} values in function of temperature (inset); (b) Graph obtained from the Van't Hoff equation. All average and standard deviation values were calculated based on triplicate experiments.....	105
Figure 34	– (a) UV-Vis absorption spectrum (Abs NO_2^-), excitation spectrum of B,N-Cdot (Exc B,N-Cdot) and emission spectrum of B,N-Cdot (Em B,N-Cdot) for evaluation of spectral overlap and confirmation of IFE; (b) quenching mechanism expected by the interaction of B,N-Cdots and NO_2^- ions.....	107
Figure 35	– Development of the field device for the analysis of NO_2^- containing a thin film of the PVA/B,N-Cdot nanocomposite: (a) UV-Vis spectrum of the obtained film and magnification of the region between 250 and 400 nm; (b) photoluminescence spectra of the film at different excitation wavelengths (300 to 400 nm with an increment of 10 nm) and image of the film under irradiation of 360 nm of a UV light (inset); (c) photograph of an analysis of NO_2^- ions using the developed field device by aid of a pocket microscope and a smartphone; (d) result of the NO_2^- analysis using analytical pattern (blue curve) and meat sample (orange curve) from the Photometrix app. This experiment was performed with the channel of colors B of the app in three replicates.....	110

LIST OF TABLES

Table 1	– Main nanomaterials used in sensors and their respective synthesis methods.....	29
Table 2	– Chemical structure of the main molecules presented in this chapter and their applications.....	33
Table 3	– Nanomaterials applied in optical sensors.....	43
Table 4	– Main features of colorimetric sensors.....	52
Table 5	– Polymeric supports used with CQDs for the development of nanocomposites or thin films.....	56
Table 6	– Summary of some works developed with sensors array and their respective information.....	60
Table 7	– List of some food additives commonly used in food formulations.....	63
Table 8	– Parameters obtained from the linearization of the Stern-Volmer Equation....	79
Table 9	– Merit figures obtained from quantification of food additives using the respective calibration curve of each analyte.....	80
Table 10	– Thermodynamic and quenching parameters for interaction between NO_2^- and B,N-Cdot at different temperatures.....	106
Table 11	– Determination of the NO_2^- concentration in meat samples using the proposed strategy.....	108
Table 12	– Comparison of proposed method with earlier reported literature toward the detection of NO_2^-	108

LIST OF ACRONYMS AND ABBREVIATIONS

4-NP	4-nitrophenol
AA	Ascorbic Acid
AFM	Atomic Force Microscopy
AgÅPs	Silver Ångstrom particles
AgNC	Silver Nanocluster
AgNP	Silver Nanoparticles
AgNW	Silver Nanowires
Ala	Alanine
ANN	Artificial Neural Networks
ANVISA	Brazilian National Health Surveillance Agency
APTES	3-aminopropyltriethoxysilane
AuNC	Gold Nanocluster
AuNP	Gold Nanoparticles
AuNR	Gold Nanorods
B,N-Cdot	CQDs doped with boron and functionalized with nitrogen
B-Cdot	CQDs doped with boron
BCP	Bromocresol Purple
<i>b</i> PEI	branched Polyethyleneimine
BSA	Bovine Serum Albumin
CA	Citric Acid
CD	Carbon Dots
Cdot	CQDs from citric acid
CG-MS	Gas Chromatography-Mass Spectrometer
CNCs@AuNP	Carbyne Nanocrystals Capped with Gold Nanoparticles
CQD	Carbon Quantum Dots
CTAB	Hexadecyl Trimethyl Ammonium Bromide
DEA	Diethylamine
EDA	Ethylenediamine
FDA	Food and Drug Administration
FLIM	Fluorescence Life-Time Imaging Microscopy
FM-CD	CQDs from flamboyant mirim

FRET	Forster Resonant Energy Transfer
FTIR	Fourier Transform Infrared Vibrational Spectroscopy
GA	Glutamic Acid
GG	Gum ghatti
Glu	Glucose
GO	Graphene Oxide
GQD	Grapheme Quantum Dots
GSH	Glutathione
h-BNQD	Boron Nitrogen Quantum Dots
HCA	Hierarchical Cluster Analysis
His	Histidine
HPLC	High Performance Liquid Chromatography
IARC	International Agency for Research on Cancer
IFE	Inner Filter Effect
KN-CD	Kiwi-derived Carbon Dots
KNN	K-Nearest Neighbors
LA	Lactic Acid
LDA	Linear Discriminant Analysis
LOD	Limit of Detection
LRET	Luminescence Resonance Energy Transfer
LSCM	Laser Scanning Confocal Microscopy
LSPR	Localized Surface Plasmon Resonance
MOF	Metal Organic Frameworks
MR	Methyl Red
N-Cdot	CQDs functionalized with nitrogen
NIR	Near-Infrared
NMR	Nuclear Magnetic Resonance
ODB	o-diaminobenzene
PBS	Phosphate Buffer Saline
PCA	Principal Component Analysis
PCSNP	Polymer-based Core-Shell Nanoparticles
PEI	Polyethylenimine
PET	Photoinduced Electron Transfer

Phe	Phenylalanine
Ph-g-CNQD	Phosphate-functionalized graphitic Carbon Nitride Quantum Dots
PL	Photoluminescence
PNP	Plasmonic Nanoparticles
PS	Potassium Sorbate
PSMA	Poly(styrene-co-maleic anhydride)
PVA	Polyvinyl Alcohol
PVP	Polyvinylpyrrolidone
QD	Quantum Dots
QY	Quantum Yield
RF	Riboflavin
rGO	Reduced Graphene Oxide
RSD	Relative Standard Deviation
SA	Succinic Acid
SB	Sodium Benzoate
SIMCA	Soft Independent Modelling of Class Analogies
SiNW	Silicon Nanowires
SP	Surface Plasmons
SPR	Surface Plasmon Resonance
SVM	Support Vector Machines
SWCNT	Single-Walled Carbon Nanotubes
TET	Tetracycline
TMD	Transition Metal Dichalcogenides
TPM	Total Polar Materials
UV-Vis	Ultraviolet-Visible
XPS	X-ray Photoelectron Spectroscopy

SUMMARY

1	INTRODUCTION AND OBJECTIVES.....	21
1.1	Introduction.....	21
1.2	Objectives.....	26
<i>1.2.1</i>	<i>General.....</i>	<i>26</i>
<i>1.2.2</i>	<i>Specifics.....</i>	<i>26</i>
2	OVERVIEW: RECENT ADVANCES IN NANOSTRUCTURED MATERIALS, CHEMICAL SENSING AND FOOD ADDITIVES.....	27
2.1	Structure, properties and synthesis of nanomaterials for sensing.....	27
<i>2.1.1</i>	<i>Zero-dimensional nanomaterials.....</i>	<i>30</i>
<i>2.1.1.1</i>	<i>Quantum Dots.....</i>	<i>30</i>
<i>2.1.1.2</i>	<i>Carbon Quantum Dots.....</i>	<i>34</i>
<i>2.1.1.3</i>	<i>Plasmonic nanoparticles.....</i>	<i>37</i>
2.2	Thermodynamic properties and kinetics parameters in chemical sensing...	39
2.3	Sensing strategies based on optical properties of nanomaterials.....	42
<i>2.3.1</i>	<i>Turn-off/turn-on sensing.....</i>	<i>45</i>
<i>2.3.2</i>	<i>Ratiometric sensors.....</i>	<i>48</i>
<i>2.3.3</i>	<i>Plasmonic sensors.....</i>	<i>51</i>
<i>2.3.4</i>	<i>Colorimetric sensors.....</i>	<i>52</i>
<i>2.3.5</i>	<i>Development of thin films for nanoprobess.....</i>	<i>54</i>
<i>2.3.6</i>	<i>Chemometric tools for sensing.....</i>	<i>57</i>
<i>2.3.7</i>	<i>Sensor array.....</i>	<i>59</i>
2.4	Sensing of food additives.....	62
3	HIGHLY SENSITIVE SENSING OF FOOD ADDITIVES BASED ON FLUORESCENT CARBON QUANTUM DOTS.....	65
3.1	Introduction.....	66
3.2	Experimental section.....	68
<i>3.2.1</i>	<i>Materials.....</i>	<i>68</i>
<i>3.2.2</i>	<i>Seeds treatment.....</i>	<i>68</i>
<i>3.2.3</i>	<i>Synthesis of CQDs.....</i>	<i>68</i>
<i>3.2.4</i>	<i>Instrumentation and characterization.....</i>	<i>69</i>
<i>3.2.5</i>	<i>FM-CDs optimization assays.....</i>	<i>70</i>

3.2.6	<i>Sensing strategy</i>	70
3.3	Results and discussion	71
3.3.1	<i>Characterization of FM-CDs</i>	71
3.3.2	<i>Spectroscopy characterization and optimization of experimental conditions</i> ...	74
3.3.3	<i>Sensing tests</i>	77
3.3.4	<i>Real Samples: identification of additives in pickled olives</i>	81
3.4	Conclusion	83
4	DOPED CARBON QUANTUM DOTS/PVA NANOCOMPOSITE AS A PLATFORM TO SENSE NITRITE IONS IN MEAT	84
4.1	Introduction	85
4.2	Experimental section	87
4.2.1	<i>Material and reagents</i>	87
4.2.2	<i>Synthesis of CQDs</i>	88
4.2.3	<i>Instrumentation and characterization of CQDs</i>	89
4.2.4	<i>Sensing experiments</i>	90
4.2.5	<i>B,N-Cdot/PVA film preparation and development of the sensor device</i>	91
4.3	Results and discussion	92
4.3.1	<i>Characterization of B,N-Cdot</i>	92
4.3.2	<i>Optimization of experimental conditions for sensing of NO₂⁻</i>	101
4.3.3	<i>Sensing of NO₂⁻ and thermodynamic assays</i>	104
4.3.4	<i>PVA/B,N-Cdot nanocomposite and field analysis device</i>	109
4.4	Conclusion	111
5	GENERAL CONCLUSIONS	112
	REFERENCES	114
	APPENDIX A – PROCEDURE PROPOSAL FOR THE USE OF THE DEVICE CONSISTING OF THE PVA/B,N-CDOT THIN FILM, IN FIELD ANALYSIS	141
	APPENDIX B – (a)-(c) UV-VIS SPECTRUM; (d)-(f) PHOTOLUMINESCENCE SPECTRUM OF CQDS SYNTHESIZED IN THIS WORK	142
	APPENDIX C – PHOTOLUMINESCENCE SPECTRA WITH DIFFERENT EXCITATION WAVELENGTHS (300 TO 340 NM) OF B,N-CDOT	143

APPENDIX D – EFFECT OF THE DOPING AND FUNCTIONALIZATION OF CQDS IN THE DETECTION OF NO_2^- IONS.....	144
APPENDIX E – FTIR OF THE B,N-CDOT PRECURSORS.....	145
APPENDIX F – NMR SPECTRA OF B,N-CDOT: (a) 1H NMR AND (b) ^{13}C NMR.....	146
APPENDIX G – HIGH-RESOLUTION SPECTRA OF B,N-CDOT: (a) N1s; (b) O1s.....	147
APPENDIX H – HISTOGRAM OF THE LIFE-TIME DECAYS FREQUENCY.....	148
APPENDIX I – (a) UV-Vis SPECTRUM AND (b) PHOTOLUMINESCENCE SPECTRE OF PVA THIN FILM USING EXCITATION WAVELENGTH OF 340 NM.....	149
APPENDIX J – SCIENTIFIC PRODUCTION RELATED TO THE THESIS.....	150

CHAPTER I

1 INTRODUCTION AND OBJECTIVES

1.1 Introduction

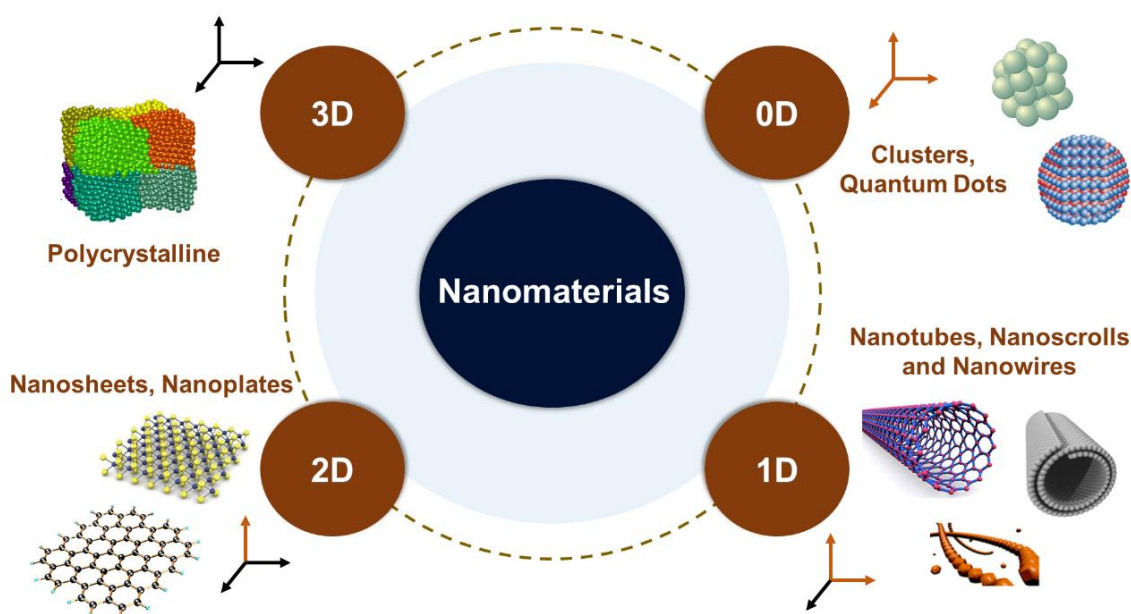
Sensors have revolutionized many sectors of the human life, due to their great ability to detect a wide range of analytes (SUI *et al.*, 2021). Sensors can be defined as device that responds to a physical stimulus and transmits a resulting impulse as a response. In this sense, chemical sensors are devices used to measure the physical and chemical properties of an analyte into a measurable signal. These sensors are usually sensitive enough to detect a single chemical or biological molecule and the magnitude of the measurable signal is proportional to the concentration of analyte (DAHMAN, [s. d.]; HANDB. NANOMATER. SENS. APPL., 2021).

For the development of sensor devices, many research groups have used nanotechnology to design new structures. In this context, nanomaterials emerge as excellent candidates for acting in chemical sensing, due to quantum dimension and surface effects that confer particular physicochemical properties (XU *et al.*, 2021). Carbon-based nanomaterials deserve a special mention, as their chemical versatility, easy-of-handling and biocompatibility allow the development of a robust sensing platform, which is resistant to factors such as temperature and ionic strength (BAPTISTA *et al.*, 2015; DE BARROS *et al.*, 2021). On the other hand, inorganic nanomaterials, such as mesoporous silica nanoparticles, iron oxide, silver and gold nanoparticles, possess several advantageous features including high rigidity, chemical inertness, uniformity, and unlimited possibilities of surface functionalization (CHEN *et al.*, 2019; SUN *et al.*, 2021). All these nanomaterials have in common their nanometric dimension.

Currently, materials with size between 1 and 100 nm in at least one dimension can be classified as nanomaterials (CALDERÓN-JIMÉNEZ *et al.*, 2017; FECHINE, 2020). There is still another classification considering the predominance of this scale as a function of the spatial dimension of the nanostructure: zero-dimensional (0D) nanomaterials, materials which the three dimensions are restricted to nanoscale and none of the dimensions are larger than 100 nm; one-dimensional (1D) nanostructures are structures in which one of the dimensions are

outside the nanoscale (one dimension larger than 100 nm); two-dimensional (2D) are structures in which two dimensions are outside the nanoscale (two dimensions larger than 100 nm) and (LI; WANG, 2020); three dimensional (3D) are not confined in the nanoscale in any dimension (three dimensions larger than 100 nm) (HU *et al.*, 2019; NIROUMAND; ZAIN, 2013; TANG; KOTOV, 2005). Figure 1 summarizes these three classes of nanomaterials and their most representative structures.

Figure 1 – Classification of the nanomaterials, according to dimensionality.



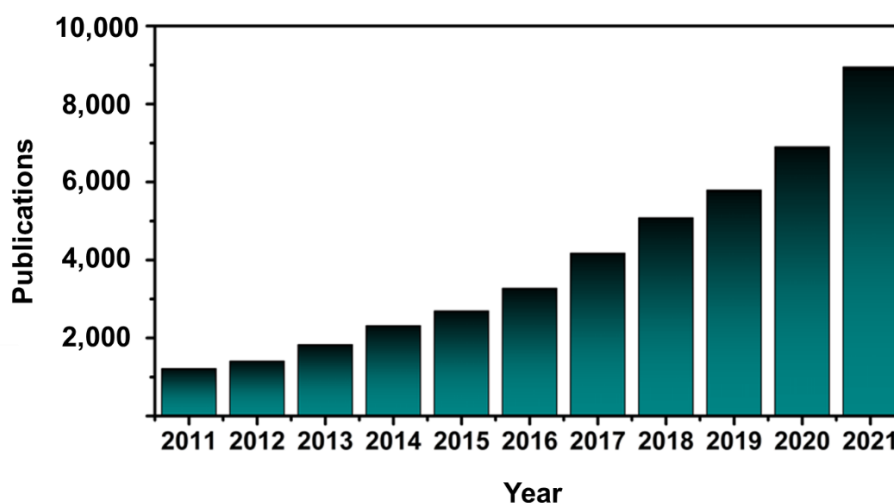
Source: Author.

Besides dimension, for the development of a chemical sensor based on nanomaterials, a transducer is required for converting the response obtained by the interaction between the target analyte and the sensing element into a measurable signal corresponding to the concentration of the analyte (AMALI *et al.*, 2021). This transducer can be understood as an instrument, which converges energy into information, resulting in a measurable signal. Some analytical tools such as spectroscopic methods can be applied for this purpose (MANOTO *et al.*, 2021). For instance, near-infrared (NIR) (LIU *et al.*, 2021), Raman (KIM *et al.*, 2021), Ultraviolet-Visible (UV-Vis) (AYAZ *et al.*, 2021) and fluorescence spectroscopies (LU *et al.*, 2021) are commonly employed techniques for developing sensing strategies. There is still the possibility of developing colorimetric sensors, in which it is possible to detect the presence of the analyte only by changing the color of the system (YU *et al.*, 2020). Thus, some authors

propose the development of thin films containing these nanomaterials (JANSI SANTHOSAM; RAVICHANDRAN; AHAMAD, 2020; KANNAN; MOUNASAMY; MADANAGURUSAMY, 2021; OMAR *et al.*, 2021). These nanocomposites can be applied as transduction signals of the phenomenon of plasmonic resonance surface on carbon nanomaterials (OMAR *et al.*, 2021; RAMDZAN *et al.*, 2021), or proving the change in the color of the system in colorimetric assays (CHI *et al.*, 2021; GONG *et al.*, 2018) and also variations in the fluorescence intensity or displacement of the band of emission of nanoprobe (DA SILVA JÚNIOR *et al.*, 2021; SHAULOFF; BHATTACHARYA; JELINEK, 2019). Given the above, a new class of carbon-based nanomaterials known as Carbon Quantum Dots (CQDs) emerges as an excellent alternative for the development of these different types of sensors.

CQDs constitute a new class of fluorescent carbon materials with a diameter less than 10 nm, accidentally discovered in 2004 during the purification process of carbon nanotubes (XU *et al.*, 2004). In recent years, CQDs can be applied in several areas, such as photocatalysis (ZHANG *et al.*, 2021), nanomedicine (WANG *et al.*, 2021), corrosion (XU *et al.*, 2021) and sensors (GAN *et al.*, 2021). In this field, it is possible to explore the fluorescence mechanism of CQDs in order to detect and quantify the analyte. Given this highlight, a search was carried out in the scientific database ScienceDirect (<http://www.sciencedirect.com>). It can be observed a gradual increase in research involving the term “Carbon Quantum Dots” in the last decade, as shown in Figure 2.

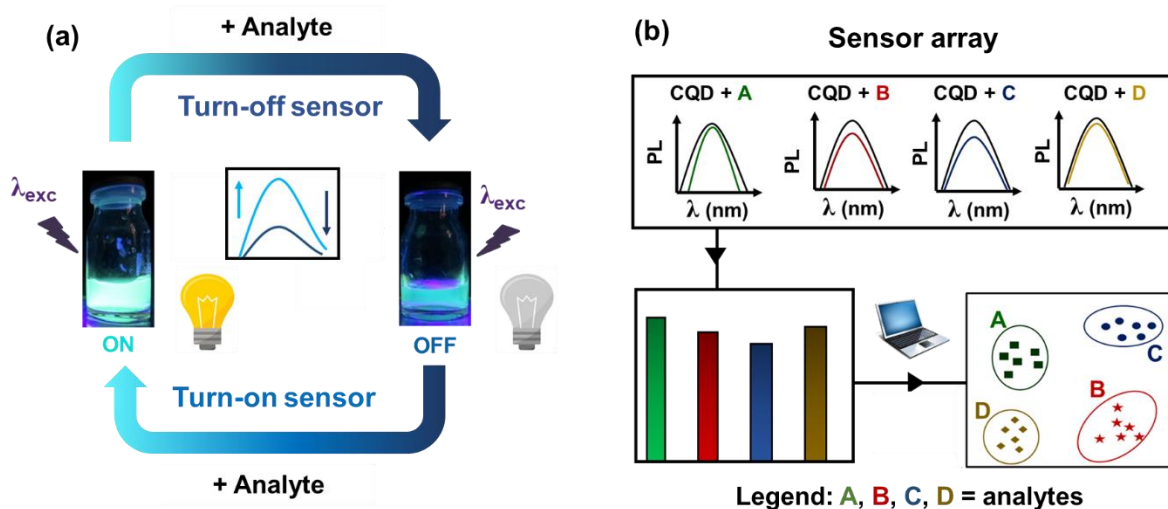
Figure 2 – State of the art for scientific production involving the term "Carbon Quantum Dots", performed on the ScienceDirect website on March 18, 2022.



Source: Author.

It is important to highlight that the search for both terms "Carbon Quantum Dots" and "Sensing" was performed. During 2021, the website registered a total of 3,631 publications containing these two terms, which is equivalent to 42.24% of the works that used CQDs in their applications. This percentage reflects the wide application of CQDs in the development of sensing strategies and chemical sensors. Generally, the design of fluorescent CQDs sensors is based on the interaction of CQDs with other materials used in sensing, such as quenchers, fluorophores and substrates. For example, when CQDs fluorescence can be quenched by the presence of metallic ions, this approach is known as turn-off sensing. Similarly, other analytes can increase the fluorescence intensity of the system. Therefore, a turn-on sensor can be developed (ZHANG; GUO, 2021). Figure 3 schematically illustrates how each of these sensors can be developed.

Figura 3 – Different sensing strategies: (a) turn-off/turn-on sensing; (b) sensor array.



Source: Author.

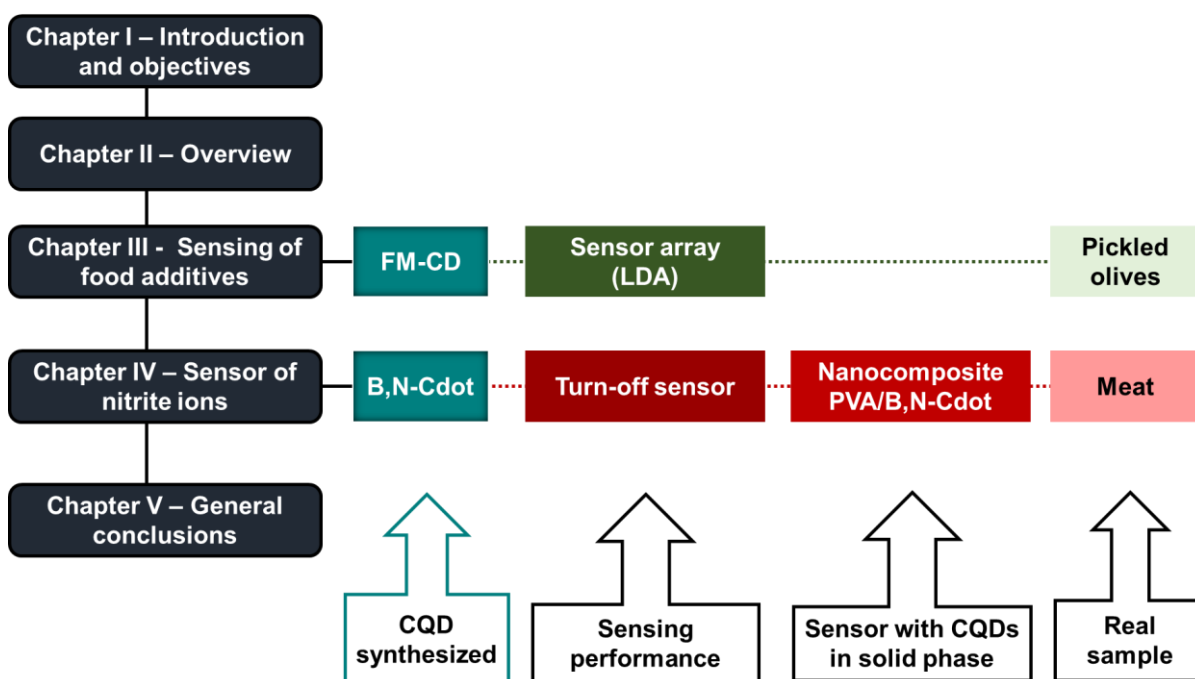
Furthermore, CQDs have been applied in the development of sensors arrays, an important analytical approach to discriminate analytes with aid of chemometric tools. Briefly, the analysis is obtained through collecting signals generated from a group of sensors, after their interaction with analytes. Hence, sufficient sensing units should be applied, and nonspecific interactions between sensors and analytes are necessary for the generation of cumulative responses (LI; ASKIM; SUSLICK, 2019).

In this work, the potential of CQDs in the sensing of food additives and nitrite ions was explored. These analytes can be found in formulations of many foods and when applied in

high concentrations can cause damage to the health of the consumer. In our research group, we have already developed works in this field. Therefore, initially, in chapter 2, an overview of the different types of nanomaterials that can be applied to sensors will be presented, with an emphasis on 0D nanomaterials and CQDs. In this same chapter, topics related to chemometric tools and food additives will be addressed in a general way.

In chapter 3, the results of the research paper entitled “*Highly sensitive sensing of food additives based on fluorescent carbon quantum dots*”, published in the Journal of Photochemistry and Photobiology A: Chemistry will be presented (CARNEIRO *et al.*, 2021). In chapter 4, the work entitled “*Doped carbon quantum dots/PVA nanocomposite as a platform to sense nitrite ions in meat*” will be presented. Finally, in the chapter 5, it will be presented the final considerations and perspectives. This section summarizes the main conclusions and highlights of the entire thesis. The described structure of the thesis is schematically illustrated in Figure 4.

Figura 4 – Scheme of the organization of the thesis in chapters.



Source: Author.

1.2 Objectives

1.2.1 General

To develop sensing strategies based on Carbon Quantum Dots fluorescence for food safety analysis in industrialized products.

1.2.2 Specifics

- a) To synthesize CQDs from natural source and doped CQDs with high quantum yield;
- b) To study the morphological characteristics and optical properties of the obtained CQDs;
- c) To use CQDs as a probe to sense food additives in pickled olive samples;
- d) To select and apply the CQDs sample with higher quantum yield to sense nitrite ions in solution;
- e) To develop a platform for sensing nitrite ions in solution, evaluating the thermodynamic parameters of the interaction between the fluorescent probe and the analyte;
- f) To obtain and apply a nanocomposite of polyvinyl alcohol (PVA) polymer with the CQDs to detect nitrite ions in meat samples;

CHAPTER II

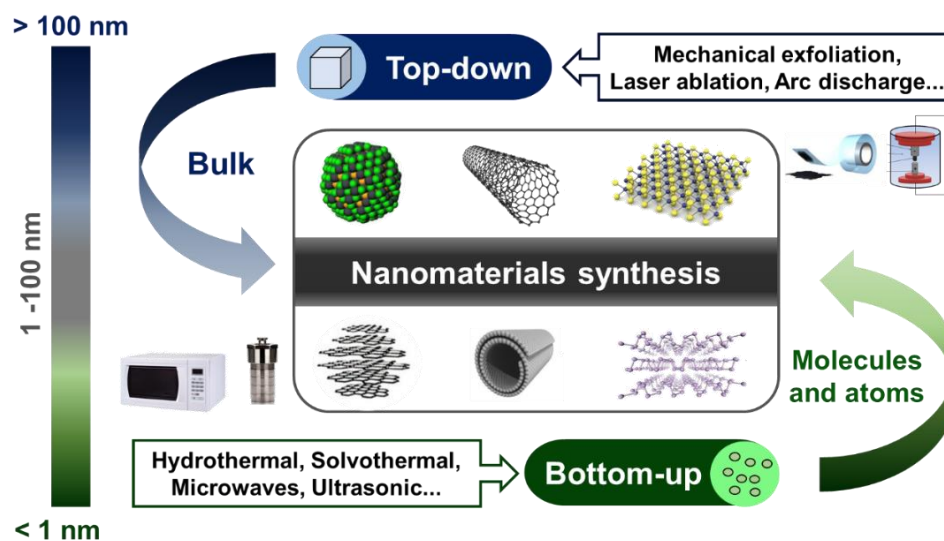
2 OVERVIEW: RECENT ADVANCES IN NANOSTRUCTURED MATERIALS, CHEMICAL SENSING AND FOOD ADDITIVES

2.1 Structure, properties and synthesis of nanomaterials for sensing

Nanomaterials are represented by a wide class of nanoparticles, nanotubes and nanosheets, whose distinct chemical structures may define special properties (quantum effect, plasmonic effect, surface charge and many others), which can be exploited for chemical sensors. The diversity of nanomaterials is mainly attributed to the variety of precursors and synthetic strategies. Different methods have been used to obtain nanomaterials and these choices influence the properties of the nanomaterials obtained. Thus, the synthetic route and precursors are chosen according to the desired property of the final product.

The synthesis of nanomaterials can be classified into two approaches: *top-down* and *bottom-up* methods. Figure 5 summarizes the main methods applied in each approach. In *top-down* methods, nanomaterials are prepared from larger precursors with bulk structures, while in *bottom-up* approaches nanomaterials are synthesized from small molecules or atoms combined (MAZARI *et al.*, 2021). In other words, the *bottom-up* method uses molecular precursors or even biological materials such as biological waste or animal and plant sub-products, which are made to chemically converge into nanoparticles. Alternatively, in a *top-down* process, a large pure structure, such as graphite for example, is fragmented into nanoparticles (HU *et al.*, 2019) (SHAMSIPUR; BARATI; KARAMI, 2017).

Figure 5 – Synthesis methods of nanostructured materials.



Source: Author.

Many techniques have been developed to synthesize nanomaterials with controlled size and shape, as well as dimensional and structure, using physical or chemical principles. For this purpose the main methods used are: i) electrochemical (LIU; MANDLER, 2020), ii) hydrothermal (CARAMAZANA *et al.*, 2018), iii) solvothermal (ABDULLAEVA *et al.*, 2017), iv) chemical vapor deposition (JIN *et al.*, 2021) and v) laser pyrolysis (MALEKZADEH *et al.*, 2020). Depending on the reaction conditions, nanomaterials with different chemical structures can have their optical and electronic properties adjustable. General characteristics such as surface area, which can be increased, and particle size, which can result in the quantum confinement effect (EDVINSSON, 2018; RAMALINGAM *et al.*, 2020; SHAJI; ZACHARIAH, 2017) can also be manipulated. In Table 1 is summarized some of the nanomaterials presented in this section and highlights the main information about synthesis methods.

Despite the wide variety of methods of obtaining, throughout this text, information about the synthesis of 0D nanomaterials will be in-depth, with an emphasis on their main properties. This approach will allow a broad understanding of the use of 0D nanomaterials, especially the nanoparticles known as CQDs, which will be applied in the sensing of food additives and nitrite ions, as described in chapters 3 and 4, respectively.

Table 1 – Main nanomaterials used in sensors and their respective synthesis methods.

Dimensionality	Nanomaterial	Synthesis method	Synthesis parameters	Precursor(s)	Reference
0D	CsPbBr ₃ QDs	Room-temperature triple-ligand	Stirring at room temperature	PbBr ₂ , Cs ₂ CO ₃	(HUANGFU; FENG, 2021)
	CdS QDs	One-pot aqueous-phase synthesis	Stirring for 4 h at room temperature	Polyethylenimine (PEI), Cd(OAc) ₂ and Na ₂ S	(DAS; RAKSHIT; DATTA, 2021)
	CQDs	Hydrothermal	180 °C for 4 h	Citric acid and neutral red	(GAO <i>et al.</i> , 2018)
	AgNPs	Thermal reduction	Not informed	AgNO ₃ solution and aqueous extract of Acacia cyanophylla.	(JALAB <i>et al.</i> , 2021)
1D	Zn ₂ GeO ₄ : Mn ²⁺ , Pr ³⁺ (ZGOMP) nanorods	Hydrothermal	220 °C for 16 h	GeO ₂ ; NaOH	(YIN <i>et al.</i> , 2021)
	Gold nanorods (AuNRs)	Seed-mediated growth	Stirring for 30 s and set overnight to obtain AuNRs	NaBH ₄ , HAuCl ₄ and Hexadecyl trimethyl ammonium bromide (CTAB)	(TAO <i>et al.</i> , 2021)
	Silicon nanowires (SiNW)	Microfabrication process	Not informed	3-aminopropyltriethoxysilane (APTES)	(D <i>et al.</i> , 2021)
	Ag nanowires (AgNWs)	Thermal reduction	130°C for 150 min	AgNO ₃ with surfactant	(ZHANG <i>et al.</i> , 2020)
	Single-walled carbon nanotubes (SWCNTs)	Chemical vapor deposition	Heating rate of 400 °C/h to 750 °C and held at this temperature for 1 h	Purified CNTs (10 mg) and yellow sulfur	(SEDELNIKOV A, 2021)
2D	Reduced graphene oxide (rGO)	Hummers' method (hydrothermal treatment)	160°C for 6 h	Graphene oxide	(CHINNATHA MBI; EUVERINK, 2021)
	MoS ₂ (TMD - Transition metal dichalcogenides)	Mechanical exfoliation	300 nm Si/SiO ₂ substrate	MoS ₂ flakes	(JIANG <i>et al.</i> , 2015)
	Carbon Nitride (g-C ₃ N ₄)	One-step polymerization of precursors	Not informed	Urea and thiourea	(ZHANG <i>et al.</i> , 2012)
	h-BN quantum dots (h-BNQDs)	Laser ablation	Laser fluence of 200 J cm ⁻² by 25 mm lens for 30 min	h-BN powders in ethanol, diethylamine (DEA), and ethylenediamine (EDA)	(NGUYEN <i>et al.</i> , 2021)

Source: Author.

2.1.1 Zero-dimensional nanomaterials

In zero-dimensional (0D) nanomaterials, all three dimensions are confined to the nanoscale (<100 nm). Common 0D nanomaterials are liposomes, polymeric nanoparticles, metallic nanoparticles, magnetic nanoparticles and quantum dots (CHAI *et al.*, 2021). The use of these nanostructures has aroused great interest from researchers, in numerous areas of knowledge, given their unique optical, electronic and surface properties (DAULBAYEV *et al.*, 2020).

2.1.1.1 Quantum Dots

One of the main groups of nanoparticles widely explored for various biomedical and industrial applications are the Quantum Dots (QDs) (RESHMA; MOHANAN, 2019). QDs have attracted strong interest among researchers in recent years due to their unique properties such as adjustable optical and electronic properties (ONYIA; IKERI; NWOBODO, 2018), exceptional photophysical properties (RESHMA; MOHANAN, 2019), high quantum yield (WANG; YU; CHEN, 2018), photostability (AN *et al.*, 2018) and a wide region of the excitation spectrum with narrow emission bands (MATEA *et al.*, 2017).

QDs are known as new-generation nanometer-sized inorganic semiconductor crystals. Generally, they are defined as nanoparticles of semiconductor material that undergo confinement in the three spatial dimensions and are generally composed of elements from groups II to VI, III to IV, or IV to VI with sizes ranging from 2 to 10 nanometers (JI *et al.*, 2014). Structurally, QDs consist of a semiconductor core, coated with a shell and a lid that allows better solubility in aqueous buffers (WANG; TANG, 2018). The particles of this nanomaterial exhibit different spectroscopic properties depending on the size, structure, and surface property. Thus, a striking feature of these materials is the dependence of their absorption and emission properties on their sizes, that is, changes in the size of nanoparticles can be responsible for changes in transition energy and, consequently, changes in optical properties (CALINK I. L. SANTOS *et al.*, 2020).

The main property of QDs is the quantum confinement, which arises when the de-Broglie wavelength associated with the electron becomes larger than the dimension of the

nanostructure and electrons are confined in one, two, or three spatial dimensions (KAUR; SINGH, 2020). This behavior increases considerably the functional properties, especially the photoluminescence, magnetic and electro-electronic properties (VOON; LIM; HO, 2018), which allow these nanostructures to be used in a wide variety of applications (KUMAR, 2021). The confinement effect is responsible for the absorption and emission, in the visible region and near regions (such as ultraviolet and near-infrared), presented by these materials (CALINK I. L. SANTOS *et al.*, 2020).

Quantum dimensional confinement can improve the optoelectronic properties of QDs, increasing carrier lifetime and increasing their photoluminescence (LIN, 2021). QDs are unique in this respect because they are less prone to deeper structural defects and tend to segregate surface defects. It was observed, for example, that confined quantum systems can increase the excitonic emission of QDs, but still, have emissions related to surface defects. As defects are on the surface, they can be easily accessed, and passivation strategies can offer opportunities to control as well as adjust these properties, particularly emission properties, greater stability, and resistivity relative to oxygen and water with the added advantage of bandgap tuning (JAIN *et al.*, 2020). Also, QDs have unique optical and electronic properties such as intense and bright fluorescence. Different types of QDs can be excited with the same wavelength of light and their narrow emission bands can be detected simultaneously for multiple assays (MATEA *et al.*, 2017). Therefore, there is a growing interest in the development of QDs for sensing applications. Sensors based on quantum dots find use in detecting ions, organic compounds (proteins, sugars, volatile substances), as well as bacteria and viruses.

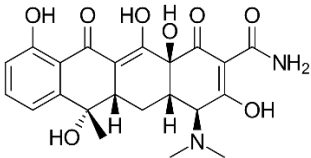
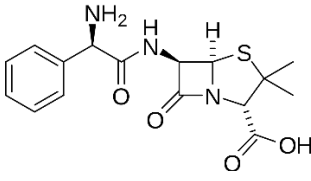
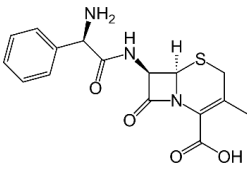
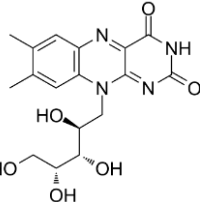
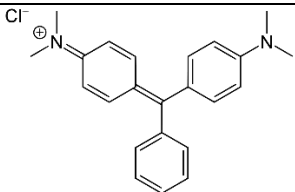
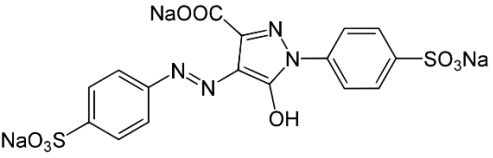
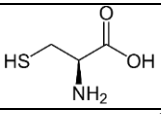
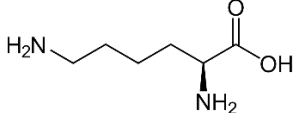
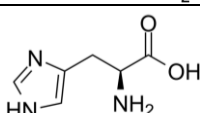
In the work by Huangfu and Feng (2021), CsPbBr₃ QDs were synthesized and used to detect various solvents with different polarities (HUANGFU; FENG, 2021). Good linear relationships between CsPbBr₃ QDs fluorescence intensity and volume of polar solvents, such as acetone, methanol, and ethanol, were separately obtained, proving the viability of perovskite quantum dots as a sensor for Total Polar Materials (TPM). CsPbBr₃ QDs were then used for the detection of TPM in edible oils. With increasing TPM content, the fluorescence intensity of the CsPbBr₃ QDs proportionally decreased without any photoluminescence peak shifts. All results indicated that CsPbBr₃ QDs could be used as an innovative fluorescent sensor for rapid TPM detection of edible oils with great practical applications.

In the work by Liang et al (2022), a dual-signal fluorescent sensor was developed with molybdenum disulfide quantum dots (MoS₂ QDs) with blue fluorescence (433 nm) and

cadmium telluride quantum dots (CdTe QDs) with fluorescence yellow (573 nm), for the detection of tetracycline (TET) in milk (LIANG *et al.*, 2022). The chemical structure of TET is presented in the Table 2 (in the next page), as are those of the other major molecules cited throughout this chapter. With the addition of TET, the authors observed the quenching of fluorescence of MoS₂/CdTe by photoinduced electron transfer (PET), and the fluorescence of CdTe QDs was quenched more obviously than MoS₂ QDs. In addition, the dual signal sensor was applied for detection of TET in milk samples with recovery of 95.53-104.22% and relative standard deviation (RSD) of less than 5%, indicating strong application potential, with excellent reproducibility and stability.

Another example of the application of QDs in sensing is the use of CdS quantum dots, coated with aqueous polyethyleneimine, in the detection of toxic metal ions suggested by Das, Rakshit e Datta (2001) (DAS; RAKSHIT; DATTA, 2021). In this work, Pb²⁺ binds strongly to the surface of the QDs, facilitating the ultra-fast transfer of electrons. As a result, a severe (~90%) photoluminescence extinction is observed. Selectivity in this detection process is controlled by the quality of the QD surface, the nature of the coating binder, and its metal ion binding properties. The engineering of these factors is crucial for the development of selective and efficient QD-based metal ion sensors.

Table 2 – Chemical structure of the main molecules presented in this chapter and their applications.

Generic classification	Molecule	Chemical structure	Samples in which the analytes can be found
	Tetracycline		
Antibiotics	Ampicillin		Milk
	Cephalexin		
Vitamin	Riboflavin		Beverages
Dyes	Malachite green		Manufactured food
	Tartrazine		
L-Amino acids	Cysteine		Biological samples
	Lysine		
	Histidine		

Source: Author.

2.1.1.2 Carbon Quantum Dots

Carbon Quantum Dots (CQDs) are a class of organic nanoparticles with features of QDs. Compared with QDs, CQDs emerge as a new type of photoluminescent nanomaterial that offers very similar attributes, such as size less than 10 nm, wavelength-dependent luminescence emission, resistance to photodegradation, ease of bioconjugation, low-cost production, colloidal stability, elemental abundance, and low environmental and biological toxicity (WANG *et al.*, 2021). The photoluminescent properties of CQDs are related to their dimension (1 and 10 nm in diameter) and in general, their chemical structure consists of an almost spherical structure formed by carbon sheets with sp^2 or sp^3 hybridization (CARNEIRO CRUZ *et al.*, 2019). According to John and colleagues, CQDs may have chromophore groups or surface defects, such as nitrogen atoms present at the edge of the nanoparticles (JOHN; NAIR; VINOD, 2021).

In general, only a carbon source is requested to obtain CQDs. Sources of heteroatoms, such as oxygen, nitrogen, or other groups enable the surface functionalization to obtain different chemical structures, with excellent photoluminescent properties. In this regard, precursors with heteroatoms (N, S, B, P, etc.) are introduced in the preparation process of the CQDs, which can efficiently regulate the state of the surface of these nanomaterials (GUO, R. *et al.*, 2021)

Among the different methods of synthesis, microwave synthesis offers advantages such as simplicity, low cost, short reaction time, and the ability to generate a variety of CQDs in a single step (MUTHUSANKAR; DEVI; GOPU, 2020). In this method, microwaves are used to improve the reaction to obtain uniform heating and, therefore, enhance chemical reactions (DE MEDEIROS *et al.*, 2019). On the other hand, thermal decomposition, also known as thermolysis, is one of the most common synthesis methods to obtain highly fluorescent CQDs (LUDMERCZKI *et al.*, 2019). This method involves the process of dehydration of the precursor molecule and includes the advantages of low economic cost, speed, and simplicity in synthesis.

On the other hand, hydrothermal synthesis is the most widely adopted method to synthesize zero-dimensional nanomaterials, such as CQDs (JIN *et al.*, 2021). The hydrothermal method is a simple and versatile method for the synthesis of nanomaterials under conditions of high temperature and pressure. It is possible to modulate the characteristics of the nanoparticles by adjusting the parameters of temperature, pressure, or concentration of the precursor (ASLAN; ESKALEN, 2021). One of the main effects of the hydrothermal treatment is the

preparation of crystals with better quality and growth, maintaining good control over their composition (KOLAHALAM *et al.*, 2019). In addition, this technique draws the attention of many scientists, considering tremendous advantages, such as low economic cost and relatively safe processing (KAUR; SINGH, 2020).

Solvothermal synthesis is another synthetic method similar to the hydrothermal method that can also be effective in the synthesis of CQDs. Both syntheses are carried out in a stainless-steel autoclave, the difference being that the precursor solution is generally not aqueous by solvothermal synthesis (MONDAY *et al.*, 2021). In the solvothermal method, by fitting certain experimental parameters, including reaction temperature, reaction time, and solvent, it is possible to precisely control the size, shape distribution, and crystallinity of the obtained nanomaterials (LU *et al.*, 2021; ŠARIĆ; DESPOTOVIĆ; ŠTEFANIĆ, 2019). Depending on the solvent used, different emission colors may exist. This is because the solvent controls the dehydration and carbonization process of the precursor, determines the particle size and the domain size of the sp^2 conjugate, thereby obtaining tunable fluorescent multicolor emission CQDs (SUN *et al.*, 2021). In the work of Ding *et al.*, 2018, for example, a series of CQDs with tunable emission from 443 to 745 nm were obtained just by setting the reaction solvents in a one-pot solvothermal path. The distinct optical characteristics of these CQDs are based on their differences in particle size and content of graphitic nitrogen and oxygen-containing functional groups, which can be modulated by controlling the dehydration and carbonization processes during solvothermal reactions.

CQDs can have a strong wavelength-dependent luminescence emission. These dependencies can be adjusted by employing different synthetic conditions (HU *et al.*, 2019). Thus, the luminescence mechanism is of great importance to guide the synthesis of CQDs with emission fluorescence. CQDs are gaining increasing importance as photoluminescent markers (DAS *et al.*, 2017). Currently, three theories seek to explain the luminescence of CQDs: quantum confinement effect, the surface state, and molecular fluorescence (LIU *et al.*, 2019). Therefore, CQDs can emit light in different regions of the visible spectrum, depending on their size (XU; LIN; CHANG, 2020), effects present on their surface caused by functional groups (DING *et al.*, 2020) and fluorescent molecules connected on the surface or interior of CQDs (SHARMA *et al.*, 2017).

The Quantum Yield (QY), a comparison parameter for the photoluminescence of CQDs, is calculated by the ratio between the number of photons absorbed and the number of

photons emitted by a material (XIE *et al.*, 2019). To calculate QY , the following Equation (1) is used:

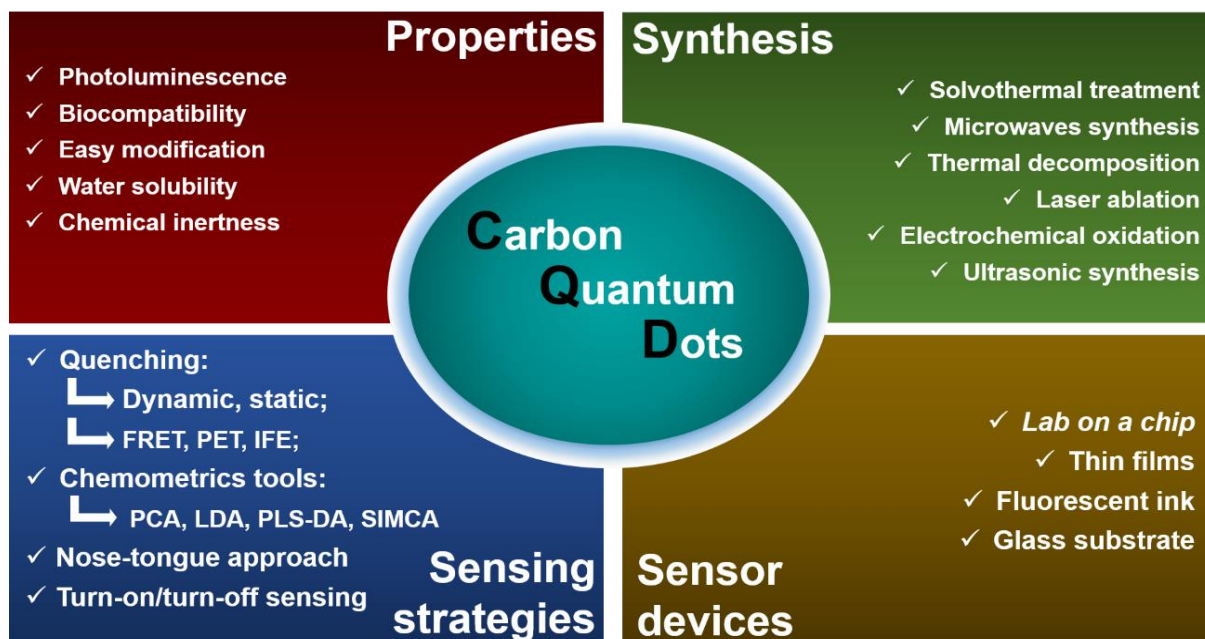
$$QY = QY_s \left(\frac{I}{I_s} \right) \left(\frac{A_s}{A} \right) \left(\frac{n}{n_s} \right)^2 \quad (1)$$

where QY refers to the quantum yield, I is the integrated emission intensity, A is the absorption intensity at the excitation wavelength, n is the refractive index of the solvent, and the subscript s is related to the values of the standard fluorescent molecule (ASLAN; ESKALEN, 2021).

The QY of the CQDs is lower when compared to QDs. However, the functionalization on the surface of the CQDs or a careful choice of precursor with specific functional groups may reflect a greater photoluminescence efficiency when there is one. Functionalization consists of organic reactions of substitution, elimination or addition, favoring the formation of functional groups in a controllable way (ALAVI; JABARI; JABBARI, 2021). With functionalization, CQDs can coordinate with some metal ions through their abundant surface functional groups, thus exerting a vital influence on the morphology and particle size of the final products. Furthermore, functionalized CQDs have good water solubility or oil solubility when introduced into different groups (GUO, R. *et al.*, 2021).

Functionalized CQDs with high fluorescence signals can act as chemical sensors. These fluorescence-based sensors have added a lot of attention to routine analysis due to their simplicity, chemical stability, and handling (CARNEIRO CRUZ *et al.*, 2019). The versatile surface modification from the presence of surface groups, good solubility in polar solvents, and extensive optical absorption across the entire visible wavelength and near-infrared regions make CQDs highly potent in sensing and sensor applications (ZULFAJRI *et al.*, 2019). Several works in the literature demonstrate the effectiveness of these nanomaterials for applications in sensing. For instance, Gao *et al.*, synthesized CQDs for detection of Au^{3+} in aqueous solution and bioimaging in cells (GAO *et al.*, 2018). Figure 6 relates these properties to synthesis methods and applications of CQDs in the sensing field.

Figure 6 – Schematic illustration of properties, syntheses and sensing applications of CQDs.



Source: (CRUZ *et al.*, 2021).

2.1.1.3 Plasmonic nanoparticles

Surface plasmons (SPs), name attributed by Stern and Ferrell in 60's years, refer to the coherent and collective oscillations of conduction electrons on the material surface under the stimulation of quantized energies, including photons, electrons and phonons (ZHOU, J. *et al.*, 2020; STERN; FERRELL, 1960). The nanoparticles that have this SP are called plasmonic nanoparticles (PNPs) and exhibit the phenomenon of Localized Surface Plasmon Resonance (LSPR), defined by the interaction of light with these nanoparticles. The theory and experimental approach adopted to explain LSPR were firstly developed for metal nanoparticles since the physical size scale is much smaller than the light wavelength used (GELLINI; FEIS, 2021). PNPs have increasingly been used for the fabrication of colorimetric sensors because of their strong LSPR extinction in the visible light region (ZHANG *et al.*, 2018). In this class, the main representatives are the gold nanoparticles (AuNPs), gold nanocluster (AuNCs), silver nanocluster (AgNCs) and the silver nanoparticles (AgNPs).

AuNPs, also known as gold colloids are the most stable metal nanoparticles and display specific properties not observed in bulk-size materials. Given this scenario, the intrinsic properties of AuNPs offer benefits to the fabrication of smart sensors (CHEN; ZHOU; ZHAO,

2018). AuNPs are the nanoparticles most preferred for sensing since it poses many desirable features which make them a potential candidate for sensing.

Regarding the synthesis method, AuNPs are obtained by numerous physico-chemical and biological routes (PRIYADARSHINI; PRADHAN, 2017). The classical Turkevich method allows the synthesis of highly stable AuNPs of around 20 nm size, wherein the nanoparticle surface is coated with citrate molecules that present a negative charge avoiding particle aggregation. The biological synthesis of nanoparticles is a safe, dynamic, and energy-efficient method of producing nanoparticles. Metabolites (proteins, fatty acids, sugars, enzymes, and phenolic compounds) found in these sources play a significant role in both the bioreduction of metallic ions to nanoparticles and their stability. AuNPs generated biologically are more stable than those generated using other methods (HAMMAMI *et al.*, 2021).

On the other hand, the most popular strategy to produce AuNPs in solution is based on the gold salts chemical reduction in presence of stabilizing molecules. This method required purification steps to separate chemical products and unreacted factors from the AuNPs, while, in pulsed laser ablation in liquid there is no need for any chemical assistance to form noble metal nanoparticles, instead it provides high purity for the prepared nanoparticles (HAMEED, 2021). In another work, Toro-González *et al* evaluated the formation of gold nanoparticles by the radiolytic synthesis in a continuous flow using a millifluidic reactor (TORO-GONZÁLEZ *et al.*, 2021). A mixture of gold ions solution, branched polyethyleneimine (*b*PEI), and ethylene glycol yielded AuNPs with a mean size of 3.4 ± 1.0 nm after irradiation with an X-ray irradiator.

A variation of AuNPs is the AuNCs, with a core size below 2 nm are also PNPs, with characteristic physical and chemical properties. The properties of AuNCs are more prominent and extremely different from their bulk counterparts (SONIA *et al.*, 2021). One of these properties is the ease of application of biomolecules for the synthesis of AuNCs. It has been reported that the cage effect of biomolecules can effectively ensure the stability of the NCs, enhance their optical properties, and reduce their possible toxicity (PANTHI; PARK, 2022). In this regard, Bovine Serum Albumin (BSA) is a well-studied biomolecule and has been applied for the synthesis of BSA templated AuNCs, which have been demonstrated as selective and sensitive sensors (LI; WEI, 2017; NASARUDDIN *et al.*, 2018).

AgNPs are a class of nanoparticles, which are mainly used for antimicrobial and anticancer therapy, and biosensors (XU, L. *et al.*, 2020). Although AuNPs remain the most studied nanoparticles due their good chemical stability and biocompatibility AgNPs offer better

results in terms of sensitivity (LOISEAU *et al.*, 2019). Recently, Wang et al have developed silver Ångstrom (Å, 1 Å = 0.1 nm) particles (AgÅPs), which exhibit better biological activity and lower toxicity compared with AgNPs (WANG *et al.*, 2019). There are several ways to produce AgNPs, but recently green chemistry has been the most used. AgNPs are also plasmonic. Jalab *et al* synthesized AgNPs by an eco-friendly, economical and more effective approach using *Acacia cyanophylla* plant extract as well as to study the effects of the preparation conditions on the size of synthesized nanoparticles and their antibacterial activity (JALAB *et al.*, 2021). Rajar *et al* obtained functionalized Ag nanoparticles with polyvinylpyrrolidone (PVP@AgNPs) by chemo-reductive methodology at ambient conditions (RAJAR *et al.*, 2021). In this work, the authors developed and examined PVP capped AgNPs for the sensing of Co^{2+} ions in aqueous solutions. AgNPs were produced by reducing the silver nitrate in sodium borohydride (NaBH_4) aqueous solution. The 0.1% of PVP was used as a capping agent and NaBH_4 was used to accelerate the reaction.

The silver-gold bimetallic nanoparticles were further oxidized to form stable silver-gold bimetallic oxide nanoparticles for the detection of Cr(III) (SHOBANA *et al.*, 2021). In this work, AgNPs were prepared using the microwave-assisted method. The saponin powder was employed to act as the capping agent and a dispersing agent during the preparation of the nanoparticle. Silver nitrate solution of 0.01 mol L^{-1} was treated with saponin powder dissolved in double-distilled water. In other work, Shehala and co-authors detected the presence of saccharin in the concentration range of $5 \times 10^{-5} \text{ mol L}^{-1}$ to $5 \times 10^{-1} \text{ mol L}^{-1}$ through the interference synthesis of gum ghatti (GG) capped silver nanoparticles (GGAgNPs) (SHEHALA *et al.*, 2021). The synthesis used sodium borohydride and GG as the reducing and capping agents respectively.

2.2 Thermodynamic properties and kinetics parameters in chemical sensing

Why does a chemical reaction take place? This is a question that can be answered from two points of view. At first, one might suggest that product formation leads to a lower energy state, regardless of the steps involved. On the other hand, a chemical reaction can occur, forming the product with the lowest energy barrier, therefore, it depends on the intermediate steps. In the first case, the product formed is thermodynamically more stable and the properties involved are a function of state. In the second case, the kinetically more favored product is formed and the parameters involved are a path function (WANG *et al.*, 2015).

In chemical sensors, the interaction of the analyte with the sensing platform causes changes in the system, which can be measured with the aid of a transducer (AMALI *et al.*, 2021). These changes can be thermodynamically or kinetically controlled and their understanding can clarify the mechanism by which the analyte interacts with the sensing platform. Herein, the main tools used in the determination of thermodynamic properties and kinetic parameters involved in chemical sensing platforms using nanomaterials will be described.

Yang and collaborators synthesized ErFeO₃ nanoparticles hydrothermally (YANG, T. T. *et al.*, 2021). The authors obtained rough nanoparticles with diameters varying from 70 to 110 nm, facilitating the adsorption and desorption of gas molecules. The results showed that ErFeO₃ nanoparticles can be used to selectively detect isopropanol in temperatures up to 330 °C. The main mechanism is based on the concentration of gas in the holes formed by the ErFeO₃ nanoparticles. In addition to nanoparticles, quantum dots are also frequently used in sensing strategies and, as in the work mentioned above, kinetic factors and thermodynamic properties of interaction are fundamental to the description of the sensing process. The main tool for determining kinetic and thermodynamic properties in these cases is the Stern-Volmer equation, shown in Equation (2):

$$\frac{I_0}{I} = 1 + K_{SV}[Q] \quad (2)$$

where I_0 is the fluorescence intensity of the fluorophore in the absence of the quencher and I is the fluorescence intensity of the fluorophore in the presence of the quencher; $K_{SV} = (k_q \cdot \tau_0)$ is the Stern-Volmer constant, given by the product of the bimolecular velocity constant (k_q) with the fluorescence lifetime of the fluorophore (τ_0); $[Q]$ is the concentration of the fluorescence quencher (GEHLEN, 2020). It is important to note that the constant K_{SV} depends on the temperature of the system and this relationship can be easily determined by integrating of the Arrhenius Equation:

$$d \ln K = - \frac{E_a}{RT^2} dT \quad (3)$$

where K is a constant analogous to K_{SV} , E_a is the activation energy, R is the Regnault's constant and T is the temperature. However, the values of I_0 and I are more commonly measured at a known concentration Q and temperature T of the quencher and then, the K_{SV} value is

determined, as in the works already reported in the literature (SA-NGUANPRANG; PHURUANGRAT; BUNKOED, 2022; ZHANG, S. R. *et al.*, 2021; ZOU *et al.*, 2022). Then, under equilibrium conditions, the enthalpy and entropy change for the fluorophore-quencher interaction can be estimated using the Van't Hoff Equation:

$$\ln K = -\frac{\Delta H}{R} \left(\frac{1}{T} \right) + \frac{\Delta S}{R} \quad (4)$$

where ΔH is the enthalpy change and ΔS is the entropy change. The variation of the Gibbs Energy ΔG can be determined using Equation (5):

$$\Delta G = \Delta H - T\Delta S \quad (5)$$

Vashisht and collaborators (VASHISHT *et al.*, 2020) used the method described above to calculate K_{SV} and the thermodynamic properties involved in the interaction of Fe(II) and Fe(III) ions and phosphate-functionalized graphitic carbon nitride quantum dots (Ph-g-CNQDs). The authors performed titrations at four different temperatures and determined ΔH , ΔS and ΔG in each of them, as well as the value of K_{SV} . It was observed that K_{SV} increased with temperature, which, according to the authors, is attributed to the increase in the rate of the bimolecular reaction k_q caused by the decrease in the E_a of the process. Furthermore, the authors reported negative ΔG values at all temperatures studied, suggesting that the interaction of the fluorophore with the quencher is a spontaneous process. Thus, the authors proposed that both Fe(II) and Fe(III) ions form a non-fluorescent complex with Ph-g-CNQDs, predominantly obtaining a static mechanism of fluorescence quenching (VASHISHT *et al.*, 2020).

Commonly the combination of advanced materials converges to obtain more responsive sensing platforms, with significant improvements in sensitivity and selectivity. Bang and colleagues (BANG *et al.*, 2021) decorated multi-walled carbon nanotubes (CNTs) with CuO/Cu₂O nanoparticles via sputtering technique to develop a 0D/1D sensing platform able to quantify H₂S gas. The authors reported that Cu₂O/CuO decorations increased the active surface area making the platform/gas interaction energy more negative and increasing the rate of adsorption of H₂S (BANG *et al.*, 2021). Liu *et al.* developed a 0D/2D nanocomposite based on CdS quantum dots and ZnO nanosheets for detection of triethylamine. The authors obtained the nanomaterial from the in-situ growth of CdS quantum dots on an ultra-thin ZnO nanosheet. The splendid 0D/2D structure showed good durability, stability and excellent selectivity in

triethylamine sensing, which the authors attribute to the large specific surface area of the nanocomposite.

2.3 Sensing strategies based on optical properties of nanomaterials

After knowing the synthesis properties and methods, in addition to the kinetic and thermodynamic factors involved in sensing with nanomaterials presented so far, the reader can perceive the richness of applications in the field of chemical analysis. Compared to other traditional methods, the use of spectroscopy techniques combined with suitable nanomaterials can meet the requirements of high precision, short detection time and analysis simplicity (CHEN, H. *et al.*, 2021).

In many cases, it is not mandatory to apply the totality of the analyzed range and then only a specific wavelength is selected, usually where there is a greater intensity of the measured signal, considering sensitivity reasons. In this case, for example, turn-off and turn-on sensors only evaluate the quenching or enhancing of fluorescence intensity, respectively (ZHANG; GUO, 2021; ZHOU, Z. *et al.*, 2020). On the other hand, it is common to find works that use all the information obtained from spectroscopic measurements to identify and quantify the analytes. In these works, multivariate analysis chemometric tools are used to develop sensor arrays (DU *et al.*, 2021; SONG *et al.*, 2021). In this section, our study will focus on the application of nanomaterials presented so far in these types of sensors, summarized in Table 3.

Table 3 – Nanomaterials applied in optical sensors.

Type	Nanomaterial sensing and dimensionality	Analyte (s)	LOD	Linear range	Reference
Turn-off/turn-on	MOFs (1D)	Fe ³⁺	77.6 $\mu\text{mol L}^{-1}$	0.0-0.05 mmol L ⁻¹	(LONG MA <i>et al.</i> , 2021)
		Cr ₂ O ₇ ²⁻	7.48 $\mu\text{mol L}^{-1}$	0.01-0.05 mmol L ⁻¹	
	Carbon Dots (0D)	Fe ³⁺ ions	0.16 $\mu\text{mol L}^{-1}$	0-5 and 5-50 $\mu\text{mol L}^{-1}$	(AN <i>et al.</i> , 2021)
		Ascorbic acid	0.32 $\mu\text{mol L}^{-1}$	0-80 $\mu\text{mol L}^{-1}$	
	Boron carbon oxynitride quantum dots (0D) and MnO ₂ nanosheets (2D)	Organophosphate pesticides	0.03 ng mL ⁻¹	0.1-250 ng mL ⁻¹	(LIU, F. <i>et al.</i> , 2021)
	Carbon dots (0D) and MnO ₂ nanosheets (2D)	H ₂ O ₂	104 nmol L ⁻¹	0.2-15 $\mu\text{mol L}^{-1}$	(TANG <i>et al.</i> , 2022)
		Glucose	113 nmol L ⁻¹	0.2-20 $\mu\text{mol L}^{-1}$	
	MoS ₂ quantum dots (0D)	Bovine serum albumin (BSA)	Not reported	10-70 nmol L ⁻¹	(SWAMINATHAN; BALASUBRAMANIAN, 2018)
	Carbon dots (0D)	Ampicillin	0.70 $\mu\text{mol L}^{-1}$	0-60 $\mu\text{mol L}^{-1}$	(FU <i>et al.</i> , 2020)
	Kiwi-derived carbon dots (0D)	Fe ³⁺ ions	0.95 $\mu\text{mol L}^{-1}$	5-25 $\mu\text{mol L}^{-1}$	(ATCHUDAN <i>et al.</i> , 2021)
	Graphene Quantum Dots (GQDs) (0D)	Formaldehyde	0.0515 $\mu\text{g mL}^{-1}$	0-3 $\mu\text{g mL}^{-1}$	(ZHANG, Y. <i>et al.</i> , 2021)
	Luminous nanorods (1D) and graphene oxide (2D)	As ³⁺ ions	0.5 ng mL ⁻¹	1-50 ng mL ⁻¹	(CHEN, Teng <i>et al.</i> , 2020)
	CdTe quantum dots (0D) and Zr-MOF (0D)	Ascorbic acid	39.5 $\mu\text{mol L}^{-1}$	200-1200 $\mu\text{mol L}^{-1}$	(CHEN, L. <i>et al.</i> , 2021)
	Al-MOF nanosheet (2D)	Malachite green	1.6 $\mu\text{g mL}^{-1}$	0.5-200 $\mu\text{g mL}^{-1}$	(YUE <i>et al.</i> , 2022)
CdTe quantum dots (0D)	Cd ²⁺ ions	1.1 $\mu\text{g L}^{-1}$	0.01-2.0 mg mL ⁻¹	(LI, W. <i>et al.</i> , 2021)	
Carbon Dots (0D)	Cephalexin	0.7 $\mu\text{mol L}^{-1}$	1-500 $\mu\text{mol L}^{-1}$	(HAO <i>et al.</i> , 2021)	

	Carbon Dots (0D)	Cu ²⁺ ions	44.63 nmol L ⁻¹	0.8–55.0 μmol L ⁻¹	(HUANG <i>et al.</i> , 2021)
	Carbon Dots (0D)	Riboflavin	0.025 μmol L ⁻¹	0 to 11 μmol L ⁻¹	(SOTOLONGO-GARCÍA <i>et al.</i> , 2021)
	CQDs (0D)	Glucose	3.00 μmol L ⁻¹	10-500 μmol L ⁻¹	(ZHAI <i>et al.</i> , 2019)
	Carbon Dots (0D)	Al ³⁺ ions	113.8 nmol L ⁻¹	0.15-38.46 μmol L ⁻¹	(WEI <i>et al.</i> , 2021)
Plasmonic	Silver deposition on gold nanostars	β-glucuronidase	0.1 U L ⁻¹	Not reported	(XIANYU <i>et al.</i> , 2021)
	ZnO nanosheets doped by AuNPs	Acetone	0.2 ppm	Not reported	(GUO, J. <i>et al.</i> , 2021)
	AgNPs (0D)	Fe ²⁺	0.54 μmol L ⁻¹	1-90 μmol L ⁻¹	(BASIRI; MEHDINIA; JABBARI, 2018)
		H ₂ O ₂	0.032 μmol L ⁻¹	0.05-7.5 μmol L ⁻¹	
	AuNPs (0D) and AgNPs (0D)	organophosphorus pesticides	9 – 44 ppm	Variable for each analyte	(DISSANAYAKE <i>et al.</i> , 2019)
Colorimetric	AuNPs (0D)	Pd(II)	4.23 μmol L ⁻¹	1-100 μmol L ⁻¹	(ANWAR <i>et al.</i> , 2018)
	Carbyne nanocrystals capped with AuNPs	Fe ²⁺ ions	1.2 μmol L ⁻¹	2.5–1000 μmol L ⁻¹	(CHEN, Tongming <i>et al.</i> , 2020)
	AgNPs (0D)	S ²⁻ ions	0.03 μmol L ⁻¹	2 to 15 μmol L ⁻¹	(ZHAO <i>et al.</i> , 2017)
	Polymer-based core-shell nanoparticles	Formaldehyde gas	0.5 ppm	Not reported	(PARK <i>et al.</i> , 2020)
Sensor array	Carbon Dots (0D) and AuNPs (0D)	Twelve proteins	50 nmol L ⁻¹	Not reported	(SUN <i>et al.</i> , 2019)
	Lanthanide-based fluorescent probes	Multiple metal ions	Variable for each analyte	Variable for each analyte	(ZHOU <i>et al.</i> , 2021)
	CQDs and AgNPs (0D)	Pesticides	Variable for each analyte	Variable for each analyte	(CARNEIRO <i>et al.</i> , 2019)
	CQDs (0D)	Food additives	Variable for each analyte	Variable for each analyte	(CARNEIRO <i>et al.</i> , 2021)

Source: Author.

2.3.1 Turn-off/turn-on sensing

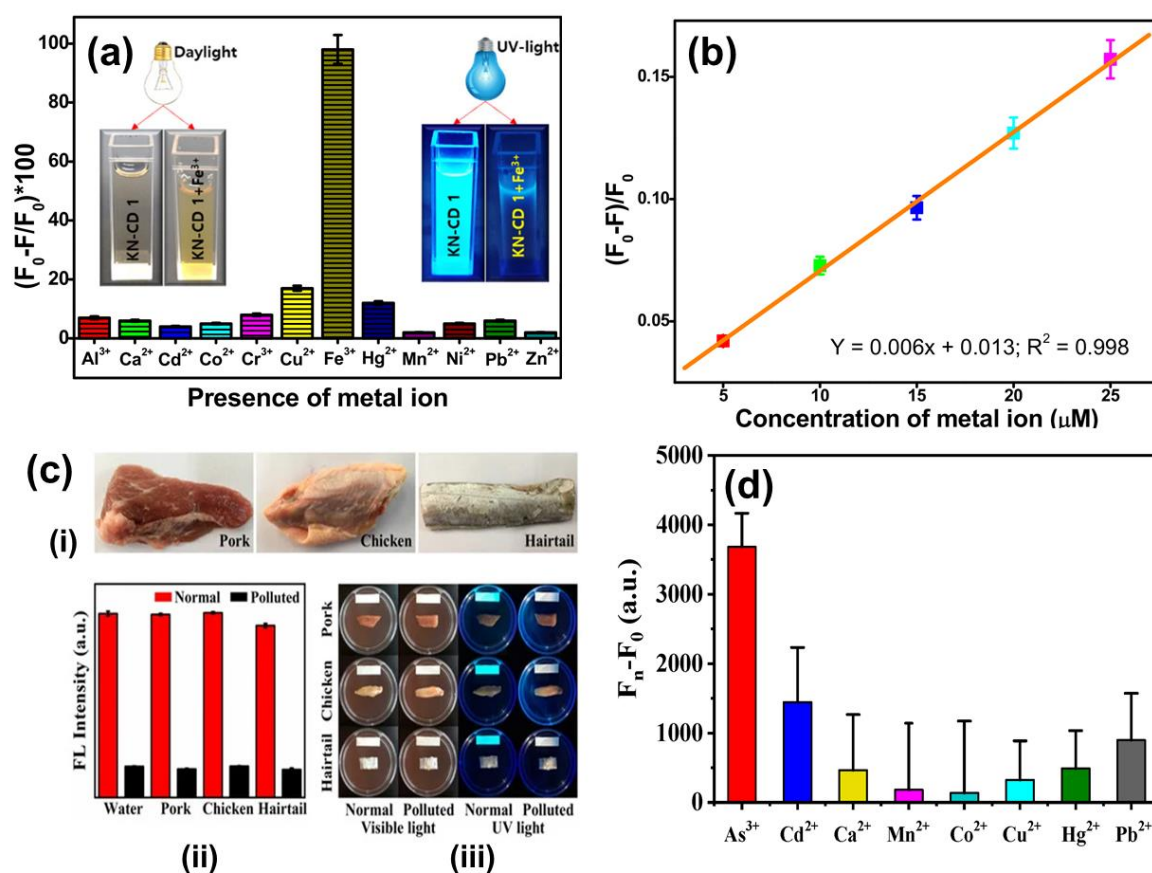
The fluorescence is a property of nanomaterials, especially 0D and 2D, which can be used for analytical purposes. This phenomenon is observed when the electrons of a molecule or nanoparticle return to the ground state, after being excited at a certain wavelength, in a relatively short time (10^{-9} to 10^{-7} s) (SINGH, 2016). Many specialized fluorescence techniques are used to understand electronic or charge transfer mechanisms, such as Forster Resonant Energy Transfer (FRET), Photoinduced Electron Transfer (PET) and inner filter effect (IFE) (ZU *et al.*, 2017). FRET is a nonradiative energy transfer phenomenon that can occur in a system having a fluorescent donor and a light-absorbing acceptor. To occur the FRET process, it is essential to overlap between the emission spectrum of the donor and the absorbance spectrum of the acceptor (NEEMA; TOMY; CYRIAC, 2020). On the other hand, several molecular turn-on sensors were reported for a variety of cations and anions based on PET, since occurred the electron transfer, forming the cation radical and the anion radical respectively (PUTHIYEDATH; BAHULAYAN, 2018; ZU *et al.*, 2017). IFE results from the absorption of the excitation or emission light by absorbers in the detection system when the absorption spectra of the absorbers overlap with the fluorescence excitation or emission spectra of fluorophores (AL-HASHIMI; OMER; RAHMAN, 2020).

Generally, one of these quenching mechanisms can explain changes in the fluorescence spectrum, suggesting a good analyte detection capacity. Then, these phenomena mentioned previously are observed in two categories of fluorescence sensors are commonly reported based on their response in the presence of the analytes: when increases the fluorescence intensity, a sensor is termed as off-on, switch-on or turn-on; in contrast, if emission is quenched due to the binding to the analyte, the sensor is termed as on-off, switch-off or turn-off (SHARMA; GHOSH, 2021). In the same system, a sensor that uses both strategies with the same nanomaterial is easily obtained. Long Ma *et al* synthesized MOFs to recognize Fe^{3+} and $\text{Cr}_2\text{O}_7^{2-}$ ions via fluorescence quenching (turn-off). In the same work, the authors managed to sense pyridine from the recovery of the fluorescence signal (LONG MA *et al.*, 2021). An *et al* applied the fluorescence signal of carbon dots synthesized from the electrolysis of o-phenylenediamine to quantify Fe^{3+} ions and ascorbic acid. In the first step, Fe^{3+} ions quenched the system's fluorescence, which increased in the presence of ascorbic acid. The limits of detection (LOD) values obtained by the authors were 0.16 and 0.32 $\mu\text{mol L}^{-1}$ for Fe^{3+} and ascorbic acid, respectively (AN *et al.*, 2021).

Swaminathan *et al* explored FRET between MoS₂ QDs and polyaniline for turn-on BSA sensing (SWAMINATHAN; BALASUBRAMANIAN, 2018). Time-resolved fluorescence measurements show the reduction of lifetime components of MoS₂ (donor) upon the increasing concentration of polyaniline (acceptor). The quenched fluorescence of MoS₂ in the presence of polyaniline was gradually recovered by the addition of BSA. Fu *et al* synthesized carbon dots through hydrothermal treatment of p-dihydroxybenzene and hydrazine hydrate (FU *et al.*, 2020). The fluorescence of carbon dots was quenched significantly and quickly upon addition of Fe³⁺ and posteriorly the quenched fluorescence of carbon dots could be selectively turned on by the addition of ampicillin, with LOD of 0.70 μmol L⁻¹. Given these results, the authors applied the system in the ampicillin detection in milk, pork, river, tap and mineral water with good average recoveries ranging from 85.4% to 101.4%. Chang *et al* used carbon dots with red emission for the fluorescent and colorimetric bimodal sensing of pH (DAN CHANG *et al.*, 2021). The nanosensor can be utilized to track MnO₄⁻ and pH fluctuations in vivo and in vitro. Besides, evident color changes of the solution under sunlight can be visualized at different pH, which is more desirable for the fluorescent and colorimetric bimodal sensing of pH.

Atchudan *et al* used leftover kiwi (*Actinidia deliciosa*) fruit peels for the synthesis of fluorescent kiwi-derived carbon dots (KN-CDs) (ATCHUDAN *et al.*, 2021). Figure 7 (a) shows the strong fluorescence of the KN-CDs selectively quenched by Fe³⁺. Quenching behavior showed a linear correlation with the concentrations of Fe³⁺ ions, within a concentration range of 5-25 μmol L⁻¹ with the detection limit of 0.95 μmol L⁻¹ (Figures 7 (b)). Zhang *et al* used grapheme quantum dots (GQDs) as a highly sensitive probe for the sensing of formaldehyde (HCHO) in an aqueous solution (ZHANG, Y. *et al.*, 2021). LOD obtained by GQDs was about 0.0515 μg mL⁻¹. In addition, the authors successfully applied it to the actual food inspection (Figure 7 (c-i)) and proved to be a selective, sensitive and visualized method to check whether the concentration of HCHO in the foods exceeds the regulatory limit. To evaluate the applicability of the GQDs fluorescence probe, the performance of GQDs in three common meat samples (pork, chicken and hairtail) was investigated. The extracts of the three foods did not quench the fluorescence of GQDs in normal samples and quenched the polluted samples (Figure 7 (c -ii)). GQDs test paper in the normal sample emits cyan fluorescence under the irradiation of an ultraviolet lamp, and the fluorescence is not quenched (Figure 7 (c-iii)). In the contaminated sample, through volatilization, HCHO is transferred from the food to the GQDs fluorescent test paper, quenching the cyan fluorescence of GQDs.

Figure 7 – Sensor turn-on using fluorescence property of nanomaterials: (a) KN-CDs selectivity to Fe^{3+} ions and visualization of the fluorescent sensor in the absence and presence of the analyte, under white light and UV light (inset); (b) the linear calibration graph for $(F_0-F)/F_0$ with different concentrations of Fe^{3+} ion; (c-i) photos of these real-world foods: pork, chicken and hairtail (purchased from the supermarket nearby); (c-ii) fluorescence intensity of GQDs at 366 nm for three commercially available food extracts and water (normal and polluted); (c-iii) detection of the content of HCHO in three foods (normal and polluted) by GQDs fluorescent test paper; (d) Response of nanoprobe to different interfering ions, the concentration of As(III) was 10 ng mL^{-1} , F_0 represents the luminescence intensity before the addition of ion while F_n was the luminescence after incubated with ions.



Source: (ATCHUDAN *et al.*, 2021; CHEN, Teng *et al.*, 2020; ZHANG, Y. *et al.*, 2021)

Chen *et al* developed a turn-on luminescence resonance energy transfer (LRET) method based on luminous nanorods that were designed for As(III) detection (CHEN, Teng *et al.*, 2020). Biotin-labelled As(III) aptamers were tagged to avidin functionalized luminous nanorods as energy donors, while graphene oxide (GO) acted as the energy acceptor. In Figure 7 (d), the authors proved a high selectivity to this species, as compared to other possible

interferents, the sensor was highly selective to As^{3+} ions. Furthermore, a good linear relationship between the luminescence intensity and concentration of As(III) was obtained in the range from 1 to 50 ng mL^{-1} , with a LOD of 0.5 ng mL^{-1} . Metal-organic frameworks (MOFs) also have been demonstrated to be desired candidates for sensing definite species owing to their tunable composition, framework structure and functionality. Dong *et al* show that cysteine (Cys) can significantly enhance the fluorescence emission of amino-functionalized MOFs suspended in water, with the ability to sense lysine (Lys), arginine (Arg) and histidine (His) in aqueous media via turn-on fluorescence emission (DONG, J. *et al.*, 2021). In other work, Alf  *et al* starting from MIL125-(Ti), a 1,4-benzene dicarboxylate (BDC)-based MOF with Ti as metallic center, mesoporous TiO_2 powders containing both anatase and rutile crystalline phases were produced (ALF  *et al.*, 2021). A challenging utilization of these porous MOF-derived Ti-based oxides is the optically-based quantitative detection of molecular oxygen (O_2) in gaseous and/or aqueous media.

2.3.2 Ratiometric sensors

With the advancement of research in sensing, the development of fluorescent sensors using the intensity ratio of two distinct emission wavelengths as the detection signal has attracted the attention of researchers due to its amazing advantages, including self-calibration and precise quantification (YANG, M. *et al.*, 2021). In addition, the ratiometric fluorescence sensors that simultaneously measured two or more fluorescence changes could efficiently avoid interference of the excitation light source and provide information with a most precision in comparison with the single fluorescence probes (LI, C. *et al.*, 2021). QDs and MOFs are some examples of nanomaterials that can be used in this type of sensor. For example, Chen *et al* developed a dual-emission sensor constructed with CdTe QDs and Zr-MOF for sensing ascorbic acid (CHEN, L. *et al.*, 2021). The authors showed that this system had appropriate sensitivity, superior selectivity and good accuracy for the detection of ascorbic acid.

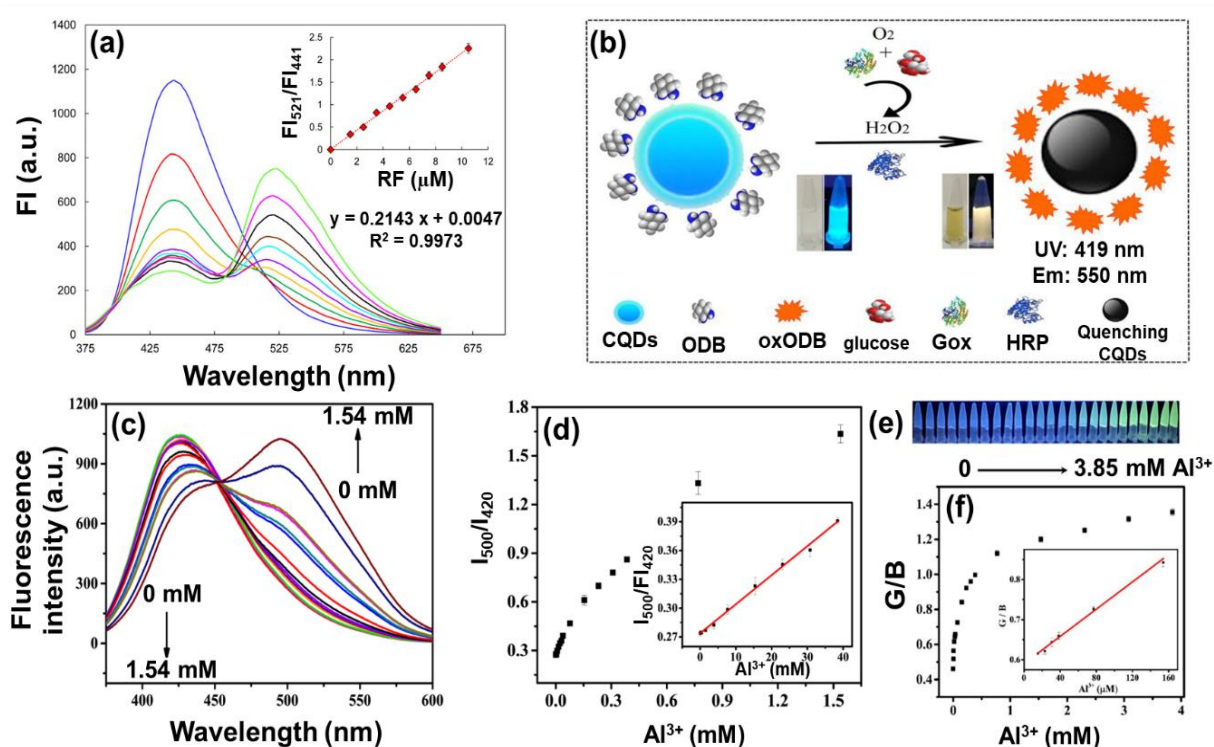
There is still a lot of applicability of this type of sensor in practical daily situations. Yue *et al* built a new portable smartphone-assisted ratiometric fluorescence sensor for intelligent and visual detection of malachite green (YUE *et al.*, 2022). A portable smartphone-assisted ratiometric fluorescent sensor was successfully designed using fluorescent Al-MOF nanosheet and rhodamine B as fluorescent probes to adjust to the requirement of dye detection.

In this same perspective, Li *et al* obtained a smartphone-integrated ratiometric fluorescence sensor for visual detection of Cd^{2+} ions (LI, W. *et al.*, 2021). The limit of $1.1 \mu\text{g L}^{-1}$ for Cd^{2+} detection is qualified for the safety inspection and a smartphone-based colorimetry assay could achieve visual assay of the analyte in oyster. Hao *et al* designed a smartphone-combined dual-emission ratiometric fluorescence probe for specifically and visibly detecting cephalixin (HAO *et al.*, 2021). In the probe, blue-emitting fluorescent CDs were synthesized and covered with a layer of silica spacer.

Sotolongo-García *et al* optimized a FRET between CDs as energy donors and riboflavin (RF) as an energy acceptor for characterizing the main parameters of interaction and sensing this analyte in beverages (SOTOLONGO-GARCÍA *et al.*, 2021). Figure 8 (a) shows the variation in fluorescence spectra of CDs–RF conjugates in the presence of various RF concentrations and the RF calibration curve (average of three repetitions), with a linear concentration range from 0 to $11 \mu\text{mol L}^{-1}$, a correlation coefficient of 0.9973, and a LOD of $0.025 \mu\text{mol L}^{-1}$ (inset). Zhai *et al* constructed a novel colorimetric and ratiometric fluorescence sensor by using CQDs and o-diaminobenzene (ODB) (ZHAI *et al.*, 2019). The detection principle is shown in Figure 8 (b). Glucose was oxidized to produce gluconic acid and hydrogen peroxide under the catalytic action of glucose oxidase. Hydrogen peroxide, as an oxidant, was able to rapidly oxidize ODB with the action of horseradish peroxidase, producing a fluorescence peak at 550 nm, and the intensity increased with glucose.

Wei *et al* obtained blue emission CDs in the one-pot solvothermal method using naringin as precursor (WEI *et al.*, 2021). Therefore, CDs were used to develop a ratiometric fluorescence sensor for the sensitive analysis of Al^{3+} with a detection limit of $113.8 \text{ nmol L}^{-1}$. As displayed in Figure 8 (c), the fluorescence of the CDs at 420 nm decreases gradually, whereas the fluorescence emission peak at 500 nm appears upon the addition of Al^{3+} . The fluorescence intensity ratio (I_{500}/I_{420}) was used to investigate the sensitivity of the CDs probe for Al^{3+} (Figure 8 (d)). On the other hand, Figure 8 (e) shows a photo that was taken by a smartphone under a 360 nm UV light. The fluorescence of the CDs- Al^{3+} solution was displaced from blue to green upon the increase in the concentration of Al^{3+} , which was available for the RGB analysis. The results show that the fluorescence intensity of B decreases gradually, whereas the fluorescence intensity of G increases. By considering the ratio between the blue channel and the green channel (G/B) as the signal, a linear trend between the concentration of Al^{3+} and the G/B value can be obtained (Figure 8 (f)).

Figure 8 – Examples of ratiometric sensors: (a) Variation in the fluorescence emission of the CDs–RF conjugate in the presence of different RF concentrations ($0 \mu\text{mol L}^{-1}$ to $11 \mu\text{mol L}^{-1}$). Inset: the linear relationship between the fluorescence emission ratio (I_{521}/I_{441}) of the CDs–RF conjugate and the RF concentration; (b) The detection principle of a dual-mode glucose sensor based on CQDs and ODB; (c) Fluorescence spectra of the CDs upon the addition of different concentrations of Al^{3+} ; (d) relation between the concentration of Al^{3+} and the I_{500}/I_{420} value. The inset shows the linear relation in the $0.15\text{--}38.46 \mu\text{mol L}^{-1}$ range; (e) images of the CDs solutions obtained by using a smartphone under a 360 nm UV lamp; (f) G/B as a function of the Al^{3+} concentration. The inset shows the linear fit of G/B as a function of the Al^{3+} concentration.



Source: (SOTOLONGO-GARCÍA *et al.*, 2021; WEI *et al.*, 2021; ZHAI *et al.*, 2019).

2.3.3 Plasmonic sensors

As mentioned in section 2, metals, such as Au, Ag, and Cu, have high charge-carrier concentration and light absorption in the visible and NIR range. Given this feature, noble metal-based nanoparticles can support the plasmonic effect (ZHOU, J. *et al.*, 2020). Plasmonic sensors have emerged as a powerful tool in chemical and biological sensing applications and noble metal nanoparticles (AuNPs and AgNPs) are especially suitable for sensing applications since they possess high extinction coefficients in the visible region (MI *et al.*, 2021). Similar to the plasmon resonance band, the aggregation profile and thus, the optical readout by UV–Vis spectroscopy depends on the size distribution, shape and dielectric environment (SANJUAN-NAVARRO *et al.*, 2021). This mechanism can then be exploited in many sensing strategies and the development of new SPR-based sensors.

Xianyu *et al* developed a sensor for naked-eye detection of the β -glucuronidase activity with silver deposition on gold nanostars to enable a plasmonic nanosensor (XIANYU *et al.*, 2021). By modulating the silver deposition on gold nanostars, the unique plasmonic property of silver-coated gold nanostars enables a significant change in the surface plasmon resonance that allows for a plasmonic readout for detecting the enzymatic activity. Gu *et al* developed an ultrasensitive acetone sensor based on holey zinc oxide nanosheets doped by AuNPs (GUO, J. *et al.*, 2021). Au doped holey ZnO nanosheets were prepared by hydrothermal method. Due to the high specific surface area, the small crystallite size of the holey ZnO nanosheets and the catalytic effect of gold nanoparticles, the sensor based on the composite shows ultra-sensitivity and selectivity to acetone (1012.6/100 ppm) and the detection limit is 0.2 ppm. Considering this excellent performance, the sensor was used in medical diagnosis.

A new strategy based on Fenton reaction coupled with AgNPs was designed by Basiri *et al* for highly sensitive colorimetric determination of Fe^{2+} , H_2O_2 and glucose (BASIRI; MEHDINIA; JABBARI, 2018). A selective sensor with a detection limit of $0.54 \mu\text{mol L}^{-1}$ was provided for Fe^{2+} measuring. On the other hand, the concentration of H_2O_2 affected both the oxidation of AgNPs and the discoloration of the solution. These conditions were used to measure H_2O_2 with a LOD as low as $0.032 \mu\text{mol L}^{-1}$. In other work, Dissanayake *et al* detected five organophosphorus pesticides (ethion, fenthion, malathion, parathion and paraoxon-ethyl) with AuNPs and AgNPs (DISSANAYAKE *et al.*, 2019). The detection can be monitored by changes in the LSPR band. Furthermore, each sensor can differentiate between the five organophosphorus pesticides and the detection is visible to the naked eye and the LOD of

AgNPs with ethion, fenthion, malathion, and parathion were 9 ppm, 11 ppm, 18 ppm, and 44 ppm, respectively. Also, Liang *et al* have developed a resonance scattering spectral detection of catalase activity using Au@Ag nanoparticle as probe and coupling catalase catalytic reaction with Fenton reaction and proofed the applicability of this technique (LIANG *et al.*, 2009).

2.3.4 Colorimetric sensors

Colorimetric sensors featuring have been designed based on the colorimetric method, since a simple and rapid technique used for detecting certain analytes by chromogenic reactions. In this type of sensor, signal changes can be detected with the naked eye or portable spectrophotometers and even the digital camera of smartphones (LIU, X. *et al.*, 2021). In the last years, the smartphone has been highlighted in works with colorimetric strategies integrated with sensors, because of their portability and ubiquitous availability.

Colorimetric sensors have attracted more and more research attention on account of their advantages, for instance, simple operation, safety, high sensitivity and suitability for high-throughput screening applications (DONG, C. *et al.*, 2021). During the past few years, colorimetric sensors have been widely used in the detection of various analytes including metal (CHAROENSUK *et al.*, 2021; DONG *et al.*, 2020), anions (MARTYANOV *et al.*, 2021; WU *et al.*, 2019) and organic contaminants (NORTON *et al.*, 2021). Some colorimetric sensors are shown in Table 4, as well as their main characteristics.

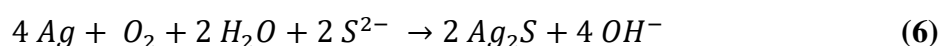
Table 4 – Main features of colorimetric sensors.

Nanomaterials employed	Principle or Mechanism	Analyte detected	LOD	Reference
AuNPs	SPR	Pd (II) ions	4.23 $\mu\text{mol L}^{-1}$	(ANWAR <i>et al.</i> , 2018)
Carbyne nanocrystals capped with gold nanoparticles (CNCs@AuNPs)	SPR	Fe ²⁺ ions	1.2 $\mu\text{mol L}^{-1}$	(CHEN, Tongming <i>et al.</i> , 2020)
AgNPs	SPR	S ²⁻ ions	0.03 $\mu\text{mol L}^{-1}$	(ZHAO <i>et al.</i> , 2017)
Polymer-based core-shell nanoparticles (PCSNPs)	Color changes by dyes	Formaldehyde gas	0.5 ppm	(PARK <i>et al.</i> , 2020)

Source: Author.

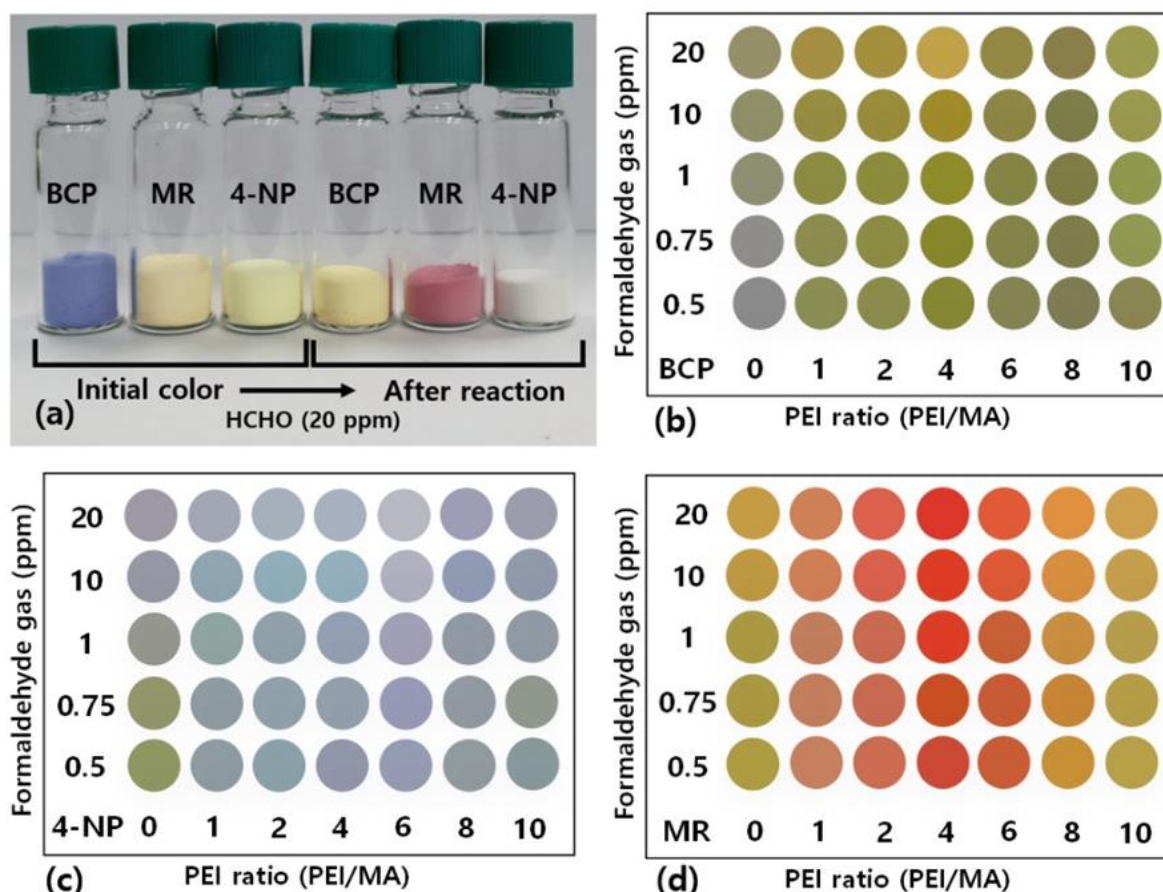
Anwar *et al* obtained AuNPs stabilized by a pyrazinium thioacetate ligand: A new colorimetric nanosensor for detection of heavy metal Pd(II) (ANWAR *et al.*, 2018). The system demonstrated a sensitive and selective spectrophotometric recognition, as well as naked eye indication for recognition of Pd(II) ions, ensuring the colorimetric analysis of Pd(II), which has a distinguished response of the aggregation-induced decrease of SPR band. The nanoprobe displayed a sensitive response to the Pd(II) ions in a wide range of concentrations and pH, with LOD as low as $4.23 \mu\text{mol L}^{-1}$. There are many works, where dual-functional nanosensors for fluorescent and colorimetric detection of metal ions are generally shown in complex organic-inorganic hybrid nanostructures. Chen *et al* fabricate fluorescent carbyne nanocrystals (inorganic nanocrystals) capped with gold nanoparticles (CNCs@AuNPs) via convenient one-step laser ablation in liquids. The authors demonstrated that, with the involvement of ferrous ions, CNCs@AuNPs show fluorescence-quenching and color-producing properties, which make them be a double-channel platform for chemical and biomedical detection (CHEN, Tongming *et al.*, 2020).

Zhao *et al* reported a method for sulfide anion detection using AgNPs, with dopamine as a reducing and protecting agent (ZHAO *et al.*, 2017). The changes in the AgNPs absorption response depend linearly on the concentration of S^{2-} in the range from 2 to $15 \mu\text{mol L}^{-1}$, with a LOD of $0.03 \mu\text{mol L}^{-1}$. A possible mechanism was proposed by the degradation of the structure of silver nanoparticles (AgNPs) due to the formation of Ag_2S , which consequently precipitated from the dispersion by the reaction between Ag^+ and S^{2-} according to Equation (6):



Park *et al* developed a colorimetric sensor based on polymer-based core-shell nanoparticles (PCSNPs), which are inexpensive, stable, and exhibit enhanced selectivity (PARK *et al.*, 2020). Spherical and uniform poly(styrene-co-maleic anhydride) (PSMA)/polyethyleneimine (PEI) core-shell nanoparticles were prepared and then impregnated with Methyl Red (MR), Bromocresol Purple (BCP), or 4-nitrophenol (4-NP) to construct colorimetric sensors for formaldehyde gas. The colorimetric sensor performance was evaluated as shown in Figure 9, when the colorimetric sensors incorporating various dyes (BCP, 4-NP, or MR) and PEI ratios were exposed to formaldehyde gas, color changes were observed.

Figure 9 – (a) Color changes observed by the naked eye for the BCP, 4-NP and MR colorimetric sensors when exposed to formaldehyde gas (20 ppm). Colorimetric responses (Δ RGB values) of (b) BCP, (c) 4-NP, and (d) MR sensors prepared with various PEI/PSMA ratios (0–10) on exposure to 20 ppm formaldehyde gas.



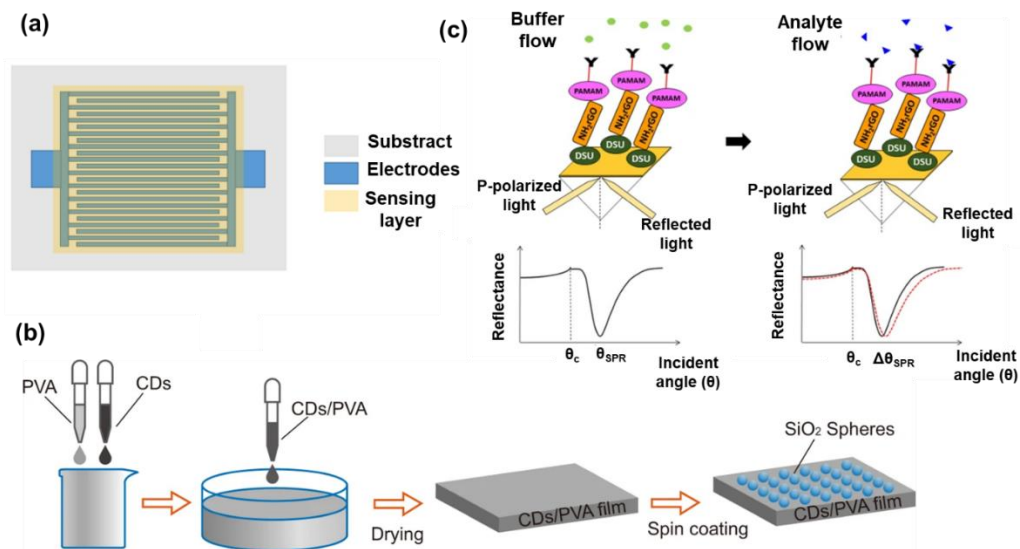
Source: (PARK *et al.*, 2020)

2.3.5 Development of thin films for nanoprobess

Thin films have been key points in the development of new sensors in different fields, from optical sensors to gas detection, using nanomaterials. Indeed, thin films are usually obtained from materials or nanomaterials. For example, Wang *et al* used N-doped carbon-dots to be embedded in polyvinylpyrrolidone (PVP) thin films (WANG *et al.*, 2018). In another work, Segkos *et al* obtained a CD-based fluorescent nanocomposite for application in thin film deposition with SiO₂ as substrates, ensuring the films were dissolution-resistant and processable (SEGKOS *et al.*, 2020). Optical lithography and O₂ plasma etching are utilized to pattern the

deposited films in the desired shapes and dimensions and a solid-state relative humidity sensor is fabricated on the SiO_2 substrate. Rivadeneyra *et al* developed based on interdigitated capacitive electrodes screen printed on a flexible transparent polyethylene terephthalate film (Figure 10 (a)) (RIVADENEYRA *et al.*, 2020). This work presented an innovative application of CDs nanoparticles as a sensing layer for relative humidity detection.

Figure 10 – Thin films containing nanomaterials: (a) flexible transparent polyethylene terephthalate film with CDs as humidity sensor; (b) Procedure of preparing CDs/PVA film with silica spheres at the surface; (c) Schematic illustration of the SPR signal before and after the analyte flow.

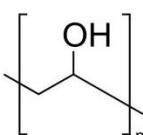
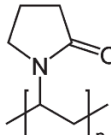
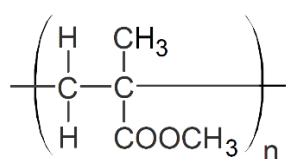
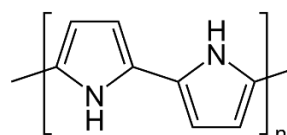
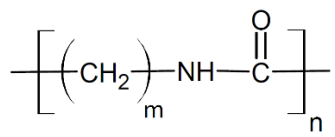


Source: (OMAR *et al.*, 2020; RIVADENEYRA *et al.*, 2020; ZHAO *et al.*, 2020).

Kwuan *et al* evaluated the dispersal of CDs in low cost, biocompatible and transparent poly(vinyl alcohol) (PVA) and polyethylene glycol (KWAN *et al.*, 2019). The nanocomposite films showed highly photoluminescent properties with the addition of CDs and the sensor showed promising results to detect tartrazine, ensuring food quality control at an analyte concentration as low as $10 \mu\text{mol L}^{-1}$. Zhao *et al* dispersed CQDs in polymer matrices to form luminescent films (ZHAO *et al.*, 2020). The authors fabricated free-standing flexible PVA films with photoluminescent CQDs embedded in them, as shown in Figure 10 (b). The simulated results show that the evanescent wave at the flat PVA/air interface can be effectively scattered out of the film.

Omar *et al* developed a sensitive detection of dengue virus type 2 E-proteins (DENV-2 E-proteins) that was performed in the range of 0.08 to 0.5 pmol L⁻¹ (OMAR *et al.*, 2020). The specificity, sensitivity, binding affinity, and selectivity of the SPR sensor were then studied. SPR measurements were conducted based on Kretschmann configuration and Figure 10 (c) is a schematic illustration representing the proposed sensor with the introduction of DENV-2 E-proteins. Results proved that the variation of the sensing layer due to different spin speeds, time incubation, and concentration provided a better interaction between the analyte and sensing layer. In the table presented in the Table 5, some other examples of polymeric supports are cited, in which CQDs can be impregnated, with their respective applications.

Table 5 – Polymeric supports used with CQDs for the development of nanocomposites or thin films.

Polymer	Chemical structure	Application	Reference
Poly(vinyl alcohol) (PVA)		Sensing of iron ion	(TANG <i>et al.</i> , 2022)
		Sensing of tartrazine	(NG HAU KWAN <i>et al.</i> , 2020)
Poly(vinylpyrrolidone) (PVP)		Sensing of hexavalent chromium	(TRUSKEWYCZ <i>et al.</i> , 2020)
Poly(methyl methacrylate)		Luminescent solar concentrators	(GONG <i>et al.</i> , 2018)
		Solar cells	(MAXIM <i>et al.</i> , 2020)
Polypyrrole		Energy storage	(MALIK <i>et al.</i> , 2020)
Polyamide		Osmotic power generation	(GAI; ZHAO; CHUNG, 2018)

Source: Author.

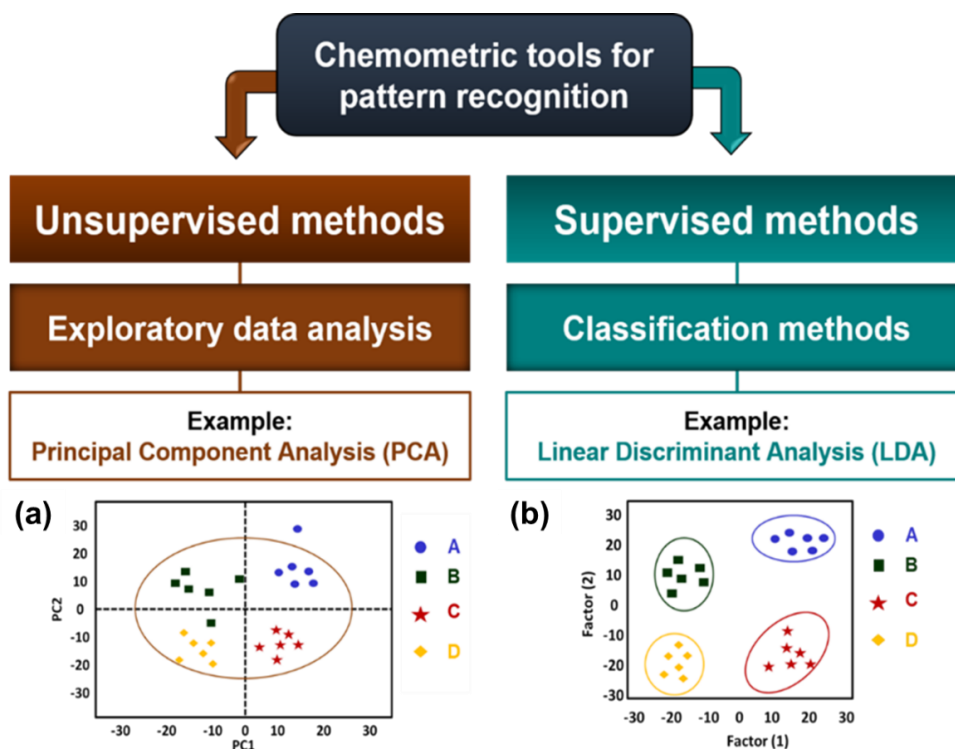
2.3.6 Chemometric tools for sensing

The search for regularities has always been a challenge, principally in chemistry. For instance, Mendeleev developed the periodic table based on empirical data, i.e. building a characteristic pattern (FERREIRA, 2015). In chemometrics, patterns can be recognized from component models. These methods aim to reduce the dimensionality of the data while retaining as much as possible information by summarizing the information in a set of low dimensional components. Component models can handle collinear data and missing values as those arising from throughput measurement techniques like nuclear magnetic resonance (NMR), Mass Spectroscopy and Fluorescence Spectroscopy (SACCENTI; CAMACHO, 2020).

Pattern recognition methods can be classified into unsupervised and supervised. Figure 11 (in the next page) lists the main methods of exploratory data analysis and classification methods. Unsupervised methods do not use any prior information about classes. They are then said to provide neutral (unguided) information that will help to understand the differentiation between analytes in a complex system. These methods are also known as multivariate statistical analysis exploratory of data. Some examples of these methods are Principal Component Analysis (PCA) and Hierarchical Cluster Analysis (HCA) (MESSAI *et al.*, 2016).

PCA is probably the most commonly used multivariate technique, in which the correlated original variables are transformed into sets of linearly uncorrelated variables called principal components. This procedure reduces the dimensionality of data with a minimum loss of information (KEERTHI VASAN; SURENDIRAN, 2016; PEARSON, 1901). In a typical PCA analysis, two results are generated, loadings and scores plots. The loading vectors describe the direction of the principal components with the original variables, whereas the score vectors describe the direction of the principal components about the observations. Therefore, the maximum amount of information is retained in the smallest number of dimensions (SUN *et al.*, 2020). These dimensions are denominated Principal Components (PCs).

Figure 11 – Exploratory data and classification methods as chemometric tools applied in sensing strategies: (a) example of score plot of PCA; (b) example of canonical factors plot of Linear Discriminant Analysis (LDA).



Source: (CRUZ *et al.*, 2021).

Supervised methods (classification methods), in turn, are defined by two sets of data called objects (inputs) and classes (target). These methods aim to discover the relationship between objects and classes, where a mathematical model is constructed. For this, in supervised methods, it is necessary to know the classes previously. This information represents the set of features that define the classification process. Linear discriminant analysis (LDA), Soft Independent Modelling of Class Analogies (SIMCA), and K-Nearest Neighbors (KNN) are examples of supervised methods of pattern recognition (MONCAYO *et al.*, 2015).

Ronald A. Fisher proposed a criterion for maximizing the separation between two or more classes of samples that became known as LDA (BELHUMEUR; HESPANHA; KRIEGMAN, 1997), which searches for a linear function of the variable in multivariate space. When the number of variables is larger than the number of observations in multi-dimensional data, the direct use of LDA is limited. In that case, we proceed with the selection of variables or use another strategy: first apply PCA for data compression to transform the original variables

into a reduced new set of variables (KUMAR *et al.*, 2014); then, LDA makes a discriminate function for each group according to the Equation (7):

$$F(G_i) = k_i + \sum_{j=1}^n w_{ij} p_{ij} \quad (7)$$

where i represents the number of groups (G), k_i is the constant of each group, n is the number of parameters used to classify a data set into a given group and w_j is the weight coefficient assigned by LDA to a selected parameter (p_i) (KUMAR *et al.*, 2014).

PCA and LDA is a grouping technique in which point groups (or clusters) are created in a multidimensional space using some kind of distance metric. Thereby, three types of metric proximity measurements are used: Euclidean, Mahalanobis and Manhattan. In Euclidian distance it is an invariant measure, but it assumes equal covariance between classes, the problem related to this distance is the dependence with the scale change, however, it still being the most used metric proximity measurement.

The Manhattan distance is a simplification of the Euclidian distance, known as the straight distance used to calculate the distance between pairs of samples. Nevertheless, Mahalanobis considers that the surfaces of each class are ellipsoids centered on the mean, and as the Mahalanobis distance is dimensionless, it is also called statistical or generalized distance. (LI; ASKIM; SUSLICK, 2019). In this work, the Mahalanobis distance will be used to build the LDA recognition patterns and thus develop the food additive sensing platform.

2.3.7 Sensor array

Array-based sensing system assembled from various cross-reactive sensors has emerged as a powerful tool for simultaneously identifying multiple analytes in a complex environment (DU *et al.*, 2021). Sensor arrays have many advantages over individual sensor elements, including accuracy, diversity, and the capacity for simultaneous detection and discrimination of a series of analytes with similar structures or properties (CHEN *et al.*, 2018). As well as colorimetric sensors, a wide range of analytes can be sensed by this method, including speciation of metallic ions (ZHAO *et al.*, 2021), antibiotics discrimination (XIE *et al.*, 2021; XU, Z. *et al.*, 2020), pesticides identification (KOUSHKESTANI *et al.*, 2021; OROUJI; ABBASI-MOAYED; HORMOZI-NEZHAD, 2019) and proteins differentiation (LIU; ZHANG; LIANG, 2021; WANG *et al.*, 2017). Table 6 summarizes the main array sensors as well as the algorithms used as statistical analysis tools.

Table 6 – Summary of some works developed with sensors array and their respective information.

Nanomaterials employed	Statistical tool	Analytes discriminated	Number of analytes detected	Reference
Carbon nanodots (CDs)-induced reversible aggregation of AuNP with glutathione GSH as a regulator	Linear Discriminant Analysis (LDA)	Pesticides	12	(SUN <i>et al.</i> , 2019)
Silver Nanoclusters (AgNC)	Principal Component Analysis (PCA)	Metal ions	7	(CAO <i>et al.</i> , 2020)
Carbon Quantum Dots (CQDs) and Silver Nanoparticles (AgNPs)	Linear Discriminant Analysis (LDA)	Pesticides	5	(CARNEIRO <i>et al.</i> , 2019)
Carbon Quantum Dots (CQDs)	Linear Discriminant Analysis (LDA)	Food additives	5	(CARNEIRO <i>et al.</i> , 2021)
Gold Nanoclusters (AuNC)	Hierarchical Cluster Analysis (HCA)	Metal ions	7	(ZHANG, X. P. <i>et al.</i> , 2021)
	Linear Discriminant Analysis (LDA)			
Carbon Quantum Dots (CQDs)	Linear Discriminant Analysis (LDA)	TETs	4	(XU, Z. <i>et al.</i> , 2020)
	Support Vector Machines (SVMs)			

Source: Author.

Sun *et al* proposed a doubled nanoplasmonic colorimetric sensor array for protein recognition based on CDs-induced reversible aggregation of AuNP with glutathione (GSH) as a regulator (SUN *et al.*, 2019). GSH was introduced into each unit containing protein samples *in situ*. The SPR absorption band of AuNP was substantially affected due to the stronger affinity between AuNP and GSH, producing another three-unit response signal. With this strategy, each sensing element can give two output signals to each target protein, which doubles the number of units from three to six without changing the three-cell configuration, resulting in greatly improved discrimination ability of proteins and identification accuracy of unknown samples. Twelve proteins at 50 nmol L⁻¹ can be well discriminated by this novel colorimetric sensor array.

Zhou *et al* developed a novel lanthanide-based sensor array for discriminating eleven metal ions (ZHOU *et al.*, 2021). In this work, three lanthanide-based fluorescent probes were developed as a novel tongue-mimic chemosensor array for rapid discrimination of multiple metal ions. The three fluorescent probes exhibit different binding affinities toward metal ions, resulting in diverse fluorescence behaviors and distinct fluorescence response patterns. The patterns can act as “fingerprints” for the identification of multiple metal ions via PCA technology.

Cao *et al* obtained four kinds of silver nanoclusters for the identification of heavy metal ions (CAO *et al.*, 2020). The sensor array was used to identify seven kinds of ions: Pb^{2+} , Fe^{3+} , Cu^{2+} , Cd^{2+} , Cr^{3+} , Co^{2+} and Ni^{2+} . The fluorescence intensity before and after the addition of the ions was used as a response signal and the vast amount of data obtained can be reduced using the PCA tool. The authors observed that it was possible to clearly separate the seven types of ions in a PCA scatter plot, in a concentration range of 15-800 $\mu\text{mol L}^{-1}$ at $\text{pH}=7$. In addition, the sensor was also able to detect the seven ions in a tap water sample, indicating their potential for practical applications in the environment (CAO *et al.*, 2020).

In addition to PCA, the LDA technique is customarily applied in a sensor array. Carneiro *et al* used CQDs obtained from the hydrothermal treatment of riboflavin and AgNPs, which efficiently quench the fluorescence of CQDs due to a FRET and the results were analyzed by LDA, obtaining different response patterns against pesticide concentrations, with a confidence level of 95% (CARNEIRO *et al.*, 2019). It was verified that in pepper extract, the sensibility of the sensing strategy was 250 ng mL^{-1} .

Zhang *et al* developed a fluorescent sensor array for the discrimination of heavy metal ions based on a single AuNC probe (ZHANG, X. P. *et al.*, 2021). The sensor was prepared using 2-mercapto-1-methylimidazole as a ligand and PVP as a dispersing agent. The fluorescence emission of PVP/MMI-AuNC was used as a response signal in the sensing of Mn^{2+} , Fe^{3+} , Ag^+ , Sn^{2+} , Fe^{2+} , Pb^{2+} and Hg^{2+} . The authors observed that the different ions produced different effects on the photoluminescence of PVP/MMI-AuNC and generated distinct fluorescent responses at 512 and 700 nm. This phenomenon provided the complete separation of the seven ions, either in the buffer solution or in water samples, using hierarchical cluster analysis (HCA) and LDA (ZHANG, X. P. *et al.*, 2021).

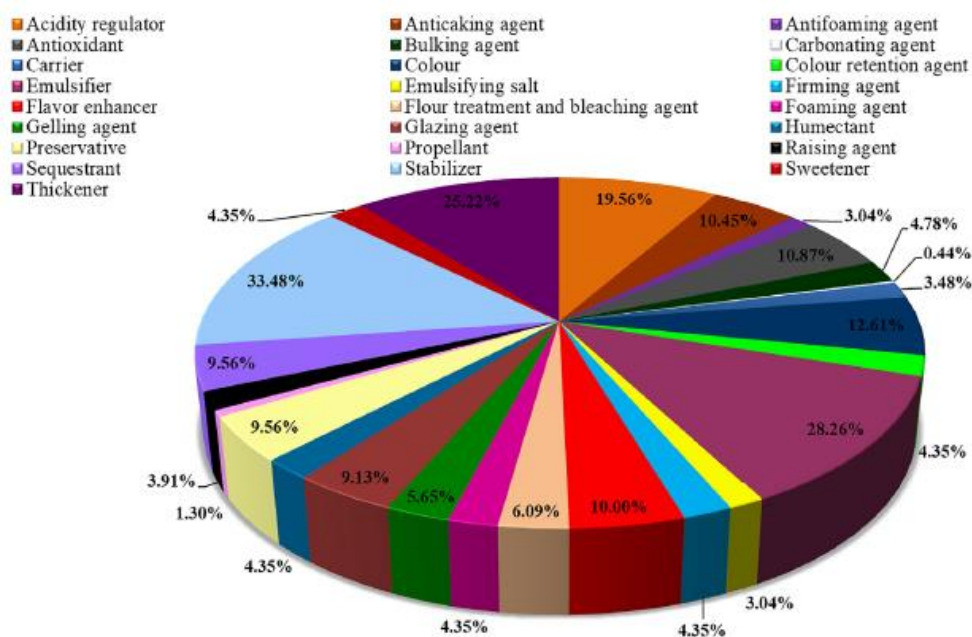
On the other hand, Support Vector Machines (SVMs) have shown better generalization performance and hence have been applied across different domains, including

sensor arrays. Unlike artificial neural networks (ANNs) which minimize the empirical risk, SVMs implement the structural risk minimization principle (GANAIE; TANVEER, 2021). Xu *et al* obtained CQDs for the determination of four TETs based on the IFE mechanism (XU, Z. *et al.*, 2020). A dual-channel fluorescence sensor array based on two CQDs was fabricated to distinguish between four TETs and a distinct fluorescence variation pattern (I/I_0) was produced when CQDs interacted with the four TETs. This pattern was analyzed by LDA and SVM. The results proved that SVM can achieve the same accurate classification and prediction as LDA, and considering its additional advantages, it can be used as an optional supplementary method for data processing, thereby expanding the data processing field.

2.4 Sensing of food additives

Food additives are natural or synthetic chemical substances used to improve the quality of manufacturing-type food, avoiding oxidation and other degradation processes (ZHANG *et al.*, 2019). According to industrial use, the food additives are classified into 25 classes, which include about 230 different compounds. Figure 12 shows a survey carried out in 2019, which shows the percentage distribution of additives most used by the food industry.

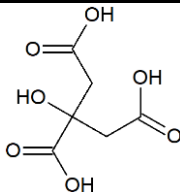
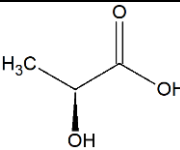
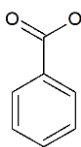
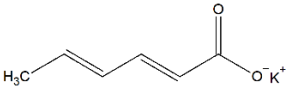
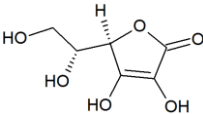
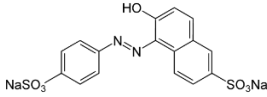
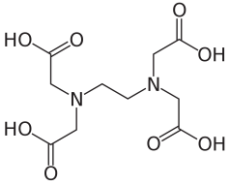
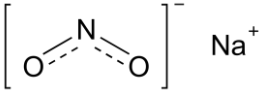
Figure 12 – Sectoral graph of the percentage distribution of food additives most used by the industry.



Source: (MARTINS; SENTANIN; DE SOUZA, 2019).

Some compounds present more than one principal action, due to their different functionalities, which are dependent on the added quantities and processing mode of the food (MARTINS; SENTANIN; DE SOUZA, 2019). The chemical structure and some information about the most common food additives are shown in Table 7.

Table 7 – List of some food additives commonly used in food formulations.

Food Additive	Classification	Chemical structure	Recommended maximum limit according to ANVISA
Citric acid	Acidity regulator		<i>Quantum satis</i>
Lactic acid	Acidity regulator		<i>Quantum satis</i>
Sodium benzoate	Antifungal agent		0.03-0.10 g/100 g
Potassium sorbate	Preservative		0.03-0.10 g/100 g
Ascorbic acid	Acidity regulator		0.03-0.10 g/100 g
Twilight yellow	Colour		0.01 g/100 g
Ethylenediaminetetraacetic acid	Sequestrant		0.01 g/100 g
Sodium nitrite	Color and flavor preservative		15 mg/100 g

Source: Author.

Given this scenario, CQDs are excellent candidates to act as fluorescent nanoprobe for the analysis of food additives. The CQDs synthesized in this work were structurally characterized and then, after optimized experimental conditions, it was proved that the fluorescence signal of these nanoparticles in the presence of analytes could be used to build a pattern recognition methodology by LDA. Thus, a sensing strategy containing a nanomaterial of low cost, easy to obtain and high chemical stability was developed and applied in the identification of food additives in canned olives and will be presented in the next chapter.

CHAPTER III¹

3 HIGHLY SENSITIVE SENSING OF FOOD ADDITIVES BASED ON FLUORESCENT CARBON QUANTUM DOTS

Abstract

A robust fluorescence-based sensing strategy was designed considering the relevance of analyzing chemical additives in industrialized food. In this study, a sensing approach was developed using fluorescent carbon quantum dots (CQDs) as a chemometric tool. CQDs were synthesized by a simple one-step hydrothermal route using the American natural seed *Caesalpinia pulcherrima*, and further characterized regarding their chemical structure. Five food additives were identified, citric acid, lactic acid, ascorbic acid, sodium benzoate and potassium sorbate, which showed a highly sensitive response with a limit of detection (LOD) as low as 252 ng mL⁻¹. The sensing platform was designed using the supervised method for recognizing patterns of linear discriminant analysis (LDA), where we could identify different concentrations of additives, after optimization of experimental parameters. Furthermore, the sensing strategy successfully identified all tested additives in a pickled olives sample with 95% of confidence, where 100% of combinations were correctly identified based on the classification matrix. Overall, the obtained results evidence the accuracy and potential of CQDs-based fluorescence sensing in the identification of food additives.

Keywords: Carbon Quantum Dots; Fluorescence; Linear Discriminant Analysis, Food additives; Pickled olives.

1. This chapter is the results of the research paper entitled “Highly sensitive sensing of food additives based on fluorescent carbon quantum dots”, published in the Journal of Photochemistry and Photobiology A: Chemistry.

3.1 Introduction

Food additives are natural or synthetic chemical substances used to improve the quality of manufacturing-type food principally regarding its taste, appearance and texture. Indeed, additives play a key role in the preservation of foodstuffs which can prevent oxidation and other degradation processes (ZHANG *et al.*, 2019a). Besides a number of food additives may be toxic, they must be necessary considering the economic view and worldwide population growth. Herein, the use of these chemical substances is monitored in order to prevent any kind of human life damage, i.e. with no risk to consumers' health (LINO; PENA, 2010; MARTINS; SENTANIN; DE SOUZA, 2019). For instance, according to the Brazilian National Health Surveillance Agency (ANVISA), depending on the type of food, some additives such as ascorbic acid, sodium benzoate and potassium sorbate can be only used at a concentration range of 0.03 - 0.1 g per 100 g of food. Other additives, such as citric and lactic acids, can be used at concentration *quantum satis*, i.e. the needed amount to obtain a desired technological effect, not affecting the identity and the genuineness of the original product. The FDA (Food and Drug Administration) also authorizes the use of sodium benzoate and potassium sorbate at a concentration of 0.1 g per 100 g of food (ASLAM *et al.*, 2017).

In this sense, several analytical methods have been reported to detect and quantify food additives, including high-performance liquid chromatography (HPLC) (MATHIYALAGAN; MANDAL; LING, 2019), gas chromatography-mass spectrometer (GC-MS) (JIMÉNEZ-SALCEDO; TENA, 2017), nuclear magnetic resonance (NMR) (HATZAKIS, 2019) and electrochemical methods (MANJUNATHA, 2018). Although, these techniques require expensive equipment, complex procedures of sample preparation, a long time of analysis and trained analysts (CAO *et al.*, 2019), providing some limitations considering their applicability. Thus, the development of advanced methods based on optical properties of nanomaterials has gained attention as a possible alternative to conventional analyses (XU *et al.*, 2020).

In recent years, the interest in optical sensors has been growing due to their sensitive properties to target analytes as a result of physical and chemical interactions (BENER; ŞEN; APAK, 2020). In this perspective, a new class of fluorescent nanomaterials, so-called carbon quantum dots (CQDs), have been used to perform different strategies in the optical sensing field (AHMED *et al.*, 2015; CARNEIRO CRUZ *et al.*, 2019; FREIRE *et al.*, 2018; MA *et al.*, 2020; POURREZA; GHOMI, 2019; YANG *et al.*, 2018). Carbon-based nanoparticles are a type of

advanced material presenting low cost and toxicity, great water dispersion, good optical properties and easy synthesis (DU *et al.*, 2020). For instance, recently, natural carbon sources have been used in the synthesis of CQDs due to their ecofriendly profile, low cost and easy access (KAZEMIFARD; ENSAFI; REZAEI, 2020), where, according to the literature, different precursors have been used for CQDs preparation, including milk (ATHIKA *et al.*, 2019), potato starch (QIANG *et al.*, 2019) and lentils (KHAN *et al.*, 2019).

Some CQDs synthetic routes have been also performed using natural carbon sources, such as microwave-assisted pyrolysis (DE MEDEIROS *et al.*, 2019), thermal combustion (ZHANG *et al.*, 2019b) and hydrothermal methods (DE YRO *et al.*, 2019). However, the hydrothermal method shows great feasibility owing to its distinct advantages, such as simple, ecofriendly, low cost and scalable. Soon, hydrothermally obtained CQDs are great candidates in a variety of applications. For example, Zhang and co-workers synthesized CQDs by hydrothermal method from dried prawn shell for determination of nitrite ions in water based on fluorescence response (ZHANG *et al.*, 2016). Besides the literature has already reported the use of these nanoparticles as a fluorescent platform to detect analytes in food (SHI *et al.*, 2019), full consideration and potential of CQDs for identification of additives as a robust fluorescence sensing strategy still unknowing. Principally, those using multivariate methods of analysis, such as linear discriminant analysis (LDA) (CHEN *et al.*, 2018b).

In this perspective, this work aims to develop a new sensing platform for the identification of food additives based on the fluorescence intensity of CQDs. Firstly, CQDs were synthesized from a carbon natural source, the edible leguminous plant well-known as “flamboyant mirim” (FM) (*Caesalpinia pulcherrima*) belonging to the Fabaceae family originated in Central America, which they were further labeled as FM-CDs. This natural carbon source is costless and easily supplied, which could provide the development of a cost-effective and eco-friendly sensing strategy. Considering optimal performance, after full spectroscopy evaluation, FM-CDs fluorescence response was analyzed by aid of LDA in the presence of five food additives (citric acid, lactic acid, ascorbic acid, potassium sorbate and sodium benzoate). Despite the health risks, it can be seen that these five food additives are routinely used in food formulations and are authorized by inspection agencies in many countries. Thus, in this work we seek to use a fluorescent probe and chemometric tools to identify them in a real food sample, such as pickled olives. Our results evidence the potential of FM-CDs to detect food additives since the applied methodology was found to afford 100% of accuracy, according to matrix of

classification. In addition, the sensing strategy was also applied in pickled olives, in order to evaluate the sensibility of the developed platform in a real sample.

3.2 Experimental section

3.2.1 Materials

The green beans of *Caelsalpinia pulcherrima* (SisGen Code: ABA588D) were collected in the city of Fortaleza, Ceará, Brazil (Latitude: 3° 49' 39.716" S; Longitude: 38° 25' 37.668" W). Sodium hydroxide (NaOH, 98.0%), hydrochloric acid (HCl, 37.0%), sodium chloride (NaCl, 97.0%), citric acid (C₆H₈O₇, 99.5%) and sorbic acid (C₆H₈O₂, 99.0%) were purchased from Dinâmica, Brazil. Potassium hydroxide (KOH, 85.0%), ascorbic acid (C₆H₈O₆, 99.0%) and sodium benzoate (C₇H₅O₂Na, 99.5%) were purchased from Vetec, Brazil, and lactic acid (C₃H₆O₃, 85.0%) from Synth, Brazil. All other reagents were analytical grade and used without previous treatment. The pickled olive sample was supplied from VALE FÉRTIL® (Brazil). Deionized water was used as solvent in all experiments.

3.2.2 Seeds treatment

After collecting in an ideal maturation point for manual removal, the beans were opened and the seeds were manually removed, which had a light brown color. The seeds were washed under running water and dried with paper towels. After drying, the seeds were crushed for three intervals of 5 minutes, and further taken to the sieving stage with a size sieve of 8x2 INOX 60 MESH/TYLER 60 opening 0.250 mm stainless steel screen. Finally, the powder of seeds was obtained.

3.2.3 Synthesis of CQDs

FM-CDs were synthesized according to conventional hydrothermal method (WANG *et al.*, 2018). Briefly, 1.0 g of pre-treated seeds powder were added in 10 mL of deionized water. After quick stirring, the mixture was transferred into a 50 mL teflon-lined autoclave. The hydrothermal reaction was performed at 180°C during 3h. Further, the autoclave was cooled down to room temperature (25 ± 2°C). In order to remove non-reactive materials, the suspension was centrifuged at 3,000 rpm for 20 min. In addition, FM-CDs sample was

dialyzed in two cycles (12 h/cycle) using a cellulose membrane (Spectra/Por®6 dialysis membrane of 1 kDa MWCO), and then 2 mL of the purified solution were freeze-drying in order to obtain FM-CDs sample.

3.2.4 Instrumentation and characterization

Atomic force microscopy (AFM) images were obtained using an Asylum MFP 3D. Topography and phase contrast of the FM-CDs were performed with an NCHR-50 silicon non-contact tip (Nano World), (less than 8 nm of radius tip, 42 N m⁻¹ of force constant, 320 kHz of resonance frequency), operating with a scan rate of 0.20 Hz. The absorption spectra of the FM-CDs were recording in the spectrophotometer UV-Vis Shimadzu model UV-2600. The fluorescence spectra of FM-CDs were obtained in the Shimadzu RF-6000 spectrofluorophotometer. All characterizations were performed at room temperature.

Fourier transform infrared vibrational spectroscopy (FTIR) was carried out using a Shimadzu FTIR spectrometer, in a scanning range of 400 to 4000 cm⁻¹. To record the FTIR spectra, a KBr pellet containing the lyophilized FM-CDs was prepared. The Raman spectrum was recorded in a range of 100 to 3000 cm⁻¹, using a Raman Horiba spectrometer. The spectral excitation was performed in a laser using the 785 nm line, with adjustable filters with effective powers of 10.7 and 151 μW with 10 accumulations of 50 s. The sample was submitted to measurement, with the aid of a coverslip, in which a concentrated suspension of FM-CDs was dripped.

X-ray photoelectron spectroscopy (XPS) was performed using a ThermoFisher Scientific model K-alpha+, using monochrome radiation from Al-ka with energy passing through the photoelectrons was 200 eV and 50 eV for the low-resolution and high-resolution scanning spectra, respectively. As a reference for connection energy, the value 284.8 eV for the C1s photoelectric line is associated with C-C and/or C-H of adventitious hydrocarbons. The previously lyophilized samples were placed on a conductive carbon tape and the spectra were recorded. The adjustment of the peaks was done using the program provided by the equipment manufacturer (Avantage), with curves mixed Gaussian / Lorentzian and background subtraction using the Smart algorithm.

3.2.5 FM-CDs optimization assays

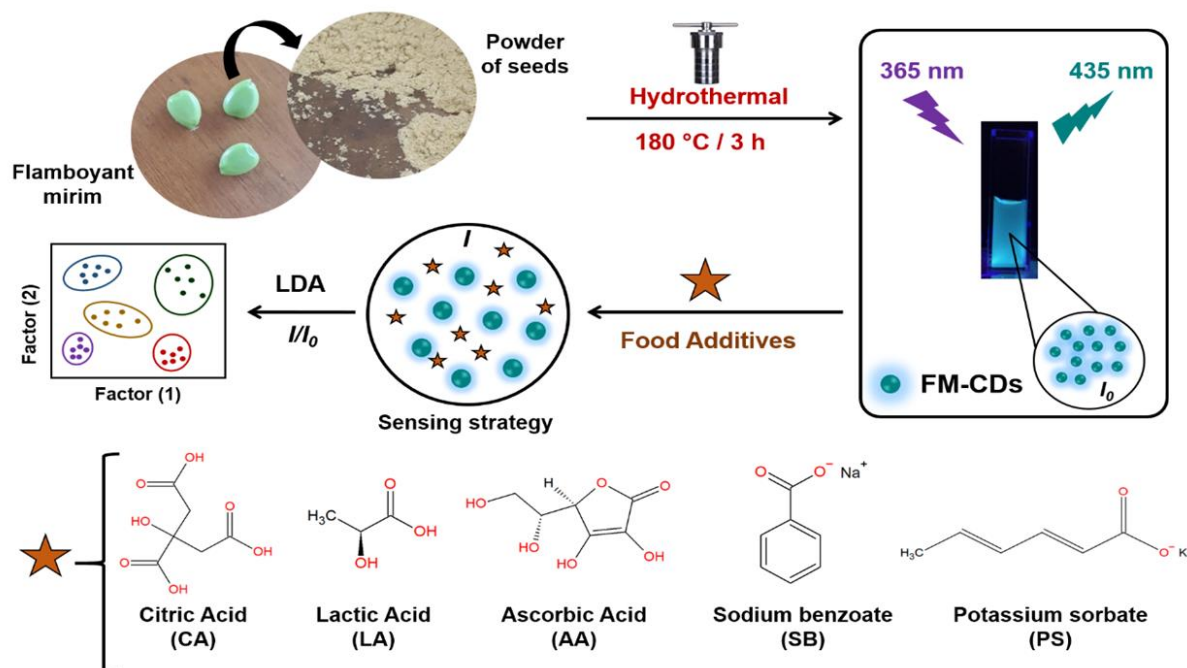
A fluorescence-based sensing strategy was developed using the FM-CDs synthesized from seeds of “flamboyant mirim”. Initially, fluorescence spectra were measured at different excitation wavelengths (330 to 450 nm). Then, the effect of FM-CD concentration, pH and ionic strength on the fluorescence intensity was evaluated at the maximum excitation wavelength (360 nm). For pH effect, solutions of HCl and NaOH at concentration 0.1 mol L⁻¹ were prepared, adjusting pH levels from 1 to 7. The study of ionic strength was performed to evaluate the intensity of fluorescence of FM-CDs in solutions of NaCl with different concentration values ranging from 1.0 x 10⁻⁵ to 1.0 mol L⁻¹. Posteriorly, FM-CDs suspension was titrated with additives in order to evaluate the sensibility of the sensing strategy.

3.2.6 Sensing strategy

The tests were conducted similarly to methodologies presented in other previous works of our group (CARNEIRO *et al.*, 2019; FREIRE *et al.*, 2018). Initially, the stock aqueous solutions of each additive were prepared at initial concentrations of 0.1, 0.01 and 0.001 mol L⁻¹, except the sorbic acid, where firstly a KOH solution was prepared at 0.1, 0.01 and 0.001 mol L⁻¹, and further used to neutralize sorbic acid, obtaining the potassium sorbate salt in aqueous solution. Then, the discrimination tests were performed in deionized water at dilution factor of 201, where 10 µL of each additive in aqueous solution were added into 2000 µL of FM-CD suspension. The first signal (I_0) was recorded, which is related to the fluorescence emission spectrum of FM-CD sample only; signal I was obtained for FM-CD sample + additive.

The values of I and I_0 were evaluated throughout the spectral range (380 at 600 nm), and the ratio between these signals is obtained by I/I_0 , which will be further used to build the LDA platform. All raw data set was then processed in SYSTAT software (version 11.0). Figure 13 shows a representative illustration of whole sensing strategy to identify food additives. The tests with samples of pickled olives were performed using 10 µL of sample fortified with the respective additives were added to 2000 µL of the FM-CD suspension. Then, the results were processed similarly to what was done with the analytical standards of the additives.

Figure 13 – Illustration of the developing of sensing strategy: FM-CDs obtention and further fluorescence sensing of five different food additives using LDA method.



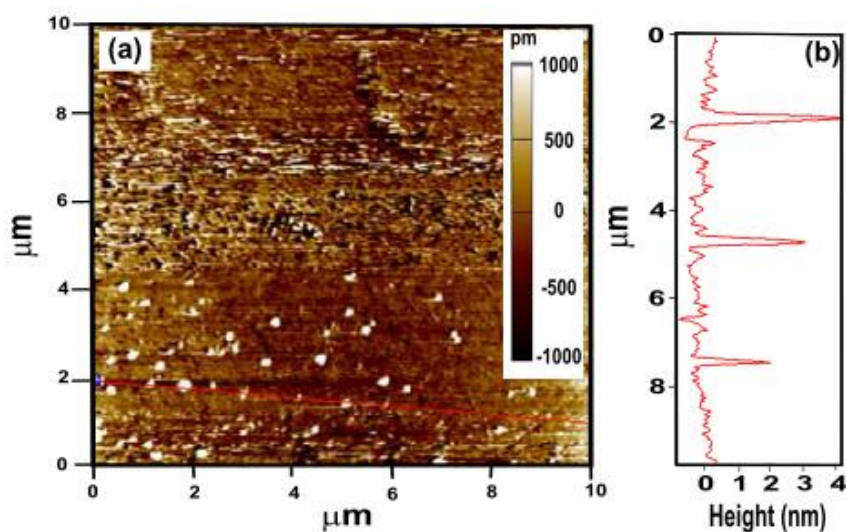
Source: (CARNEIRO *et al.*, 2021)

3.3 Results and discussion

3.3.1 Characterization of FM-CDs

Initially, the morphology of FM-CDs was characterized by AFM, and clearly a nanomaterial with quasi-spherical morphology can be observed in the AFM images in Figure 14 (a). In addition, according to the Figure 14 (b), the size range of FM-CDs was also estimated, and AFM measurements were conducted with a scanning size of 10 x 10 μm . The average thickness of FM-CDs was in the range of 0.5 - 4.0 nm, as observed in the topographical height profile, where particle size distribution values were in agreement with Ma *et al.*, (2020), which obtained CQDs by hydrothermal route using citric acid and tetraphenylborate as carbon sources.

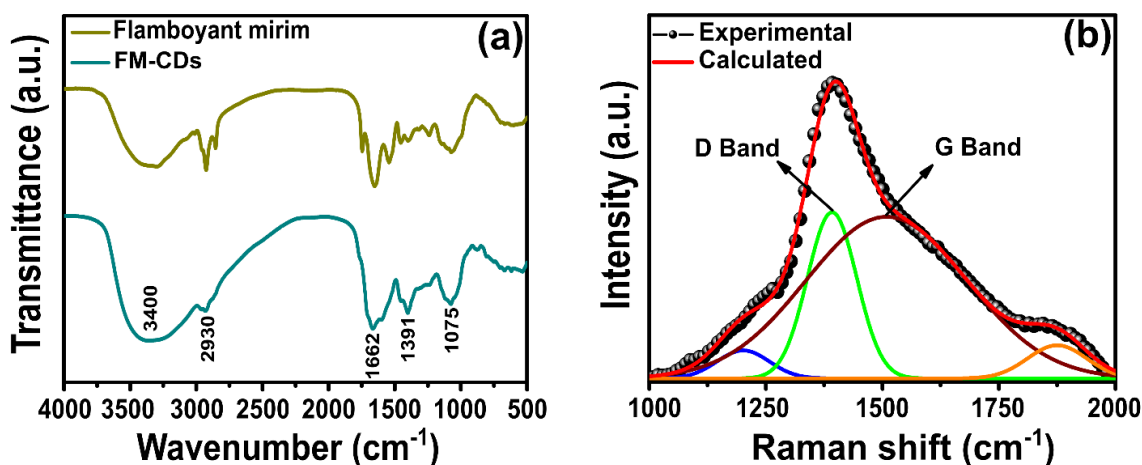
Figure 14 – Morphological characterization of FM-CDs: (a) AFM image with topographical height profile; (b) height graph.



Source: (CARNEIRO *et al.*, 2021)

FTIR and Raman spectroscopies were carried out in order to identify the surface chemistry of FM-CDs. As shown in Figure 15 (a), characteristic absorption bands of -OH stretching vibration mode are observed at 3400 and 1075 cm^{-1} . The presence of C=O and C=C bonds was confirmed by absorption at 1662 and 1391 cm^{-1} , respectively. A band of low intensity is also observed at 2930 cm^{-1} , which can be assigned to asymmetric stretching of C-H bonds in the aliphatic portion of FM-CDs surface (ALARFAJ; EL-TOHAMY; ORABY, 2018). Furthermore, it is possible to notice the clearly difference between synthesized FM-CD and its precursor spectra in Figure 15 (a). For instance, the band at 2854 cm^{-1} is only present in “Flamboyant mirim” spectrum, which can be attributed to symmetric stretching of C-H in CH_2 groups. Although C=O stretching vibration from carbonyl groups appears due to lipid component at 1740 cm^{-1} , it is not shown in FM-CD spectrum (ARAÚJO *et al.*, 2010). Indeed, the difference in spectral profiles of FM-CDs and “Flamboyant mirim” seeds powder suggests a chemical reaction route for the formation of FM-CDs.

Figure 15 – Structural characterizations of FM-CDs: (a) FTIR spectra of “flamboyant mirim” seeds powder and FM-CDs; (b) Raman spectra of FM-CDs sample.

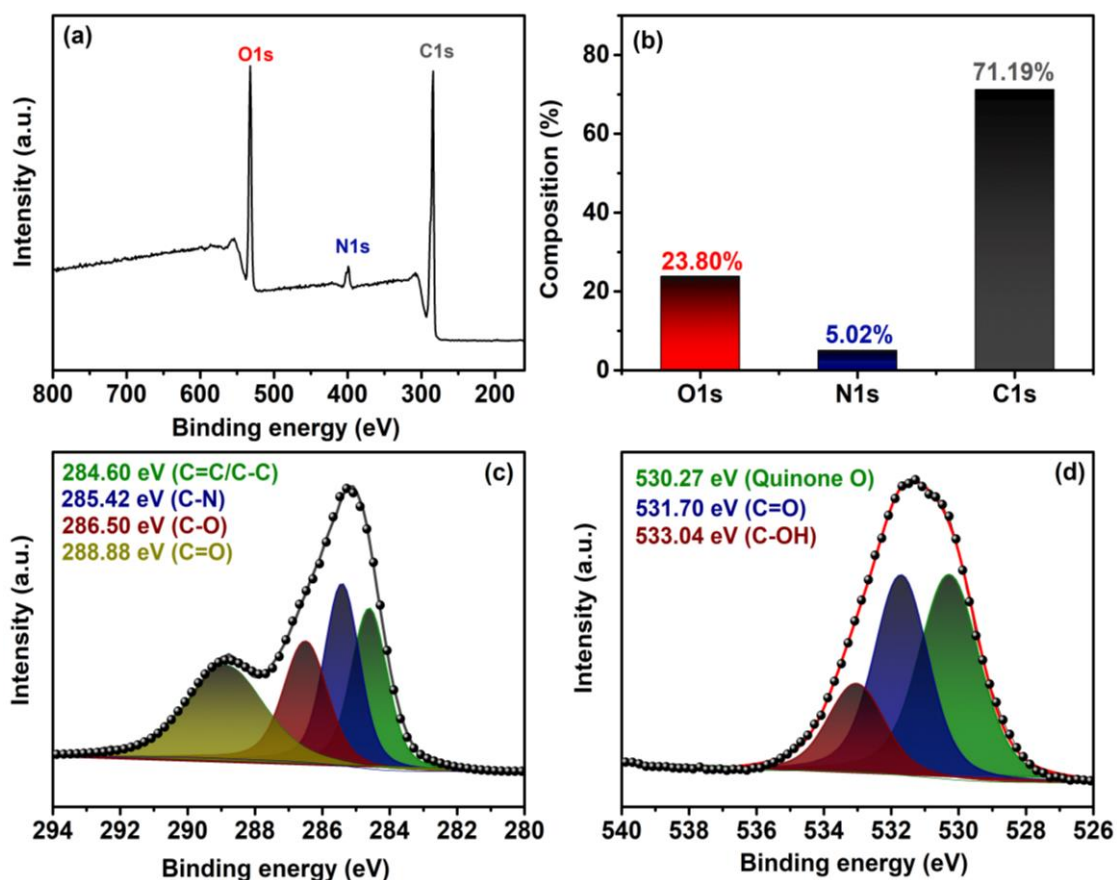


Source: (CARNEIRO *et al.*, 2021)

Raman spectrum was obtained to confirm the carbon-based structure. Moreover, a deconvolution process was also performed to a deeper chemical understanding, where it was possible to identify D and G characteristic bands of FM-CDs, as shown in Figure 15 (b). The spectrum exhibits D band at 1392 cm^{-1} and G band at 1510 cm^{-1} associated to disorder and defects in the hexagonal lattice (D band) and sp^2 domains (G band) (CHHABRA *et al.*, 2018). Furthermore, D and G bands correspond to A_{1g} symmetry photons near to K-zone boundary and E_{2g} to vibrational mode of sp^2 carbon, respectively (VASIMALAI *et al.*, 2018). In addition, the I_D/I_G intensity ratio value, used to express the extent of sp^3/sp^2 hybridization of carbon atoms was 1.03, showing the existence of vacant lattice sites of sp^3 carbon (VASIMALAI *et al.*, 2018). A similar result could be also observed by Kouloumpis and co-workers, where the value of I_D/I_G ratio was 0.95 for CQDs obtained from citric acid and urea (KOULOUMPIS *et al.*, 2017).

XPS measurements are also performed to gain structural insight into the as-produced FM-CDs. Figure 16 (a) presents the survey scan spectrum of FM-CDs and revealed three apparent binding peaks at 284, 399 and 532 eV, corresponding to the signals originated from C1s, N1s and O1s, respectively. The calculated atomic percentage of C, N and O are 71.19, 5.02 and 23.80%, respectively, as shown in Figure 16 (b).

Figure 16 – Results of XPS for FM-CDs: (a) survey; (b) graphic of the percentual composition of FM-CDs; (c) C1s and (d) O1s high-resolution spectrum of FM-CDs.



Source: Author.

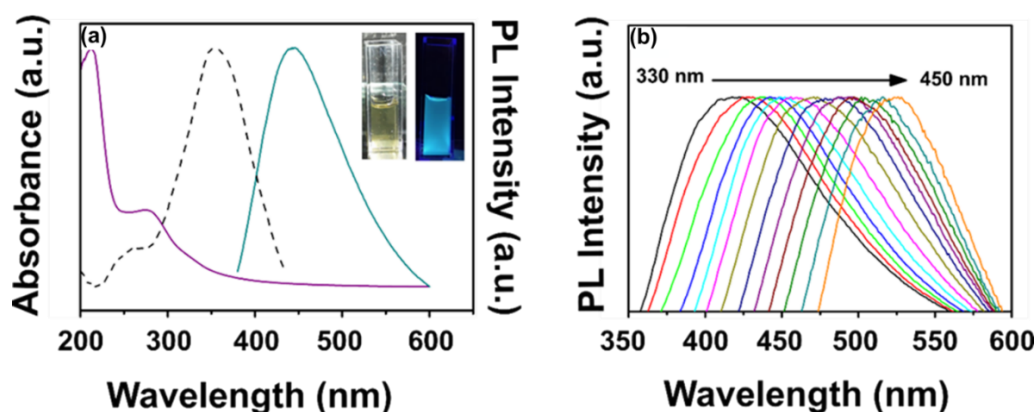
The deconvolution spectrum of C1s (Figure 16 (c)) revealed four peaks at 284.60, 285.42, 286.6 and 287.9 eV, corresponding to the C-C/C-H, C-N, C-O and C=O groups, respectively (DING *et al.*, 2017; HOU *et al.*, 2014; VEDAMALAI *et al.*, 2014). The broad high-resolution XPS spectrum of O1s, as seen in Figure 16 (d), is split into three peaks centered at 530.27, 531.7 and 533.04 eV, corresponding to O from quinone, C=O and C-OH bonds, respectively (HUANG *et al.*, 2014; QU *et al.*, 2015; WEI *et al.*, 2019). The results from XPS and FTIR are in good agreement.

3.3.2 Spectroscopy characterization and optimization of experimental conditions

In Figure 17 (a) is shown UV-Vis absorption spectra of FM-CDs sample, which was carried out to study the optical features of FM-CDs mainly governed through electron

transitions of band gaps (CHEN *et al.*, 2018a). According to literature, the absorption band around 212 nm can be attributed to the π - π^* transitions of aromatic sp^2 domains, whereas at 276 nm is related to the transitions n - π^* of C=O (ADINARAYANA AVINASH CHUNDURI *et al.*, 2017). This result is also supported by FM-CD FTIR spectrum. In Figure 17 (a) is also shown that maximum excitation and maximum fluorescence wavelengths are around 360 and 435 nm, respectively.

Figure 17 – FM-CDs spectroscopy characterizations: (a) UV-Vis absorption (purple solid line), excitation spectra (black dash line), emission spectra (blue solid line), and the right inset is the photograph of FM-CDs suspension under 365 nm excitation in comparison to natural light radiation on left inset; (b) Photoluminescence spectra with different excitation wavelengths (330 to 450 nm).



Source: (CARNEIRO *et al.*, 2021)

Moreover, FM-CDs suspension showed a very strong blue color light under UV lamp radiation (365 nm), as shown in the inset of Figure 17 (a). In Figure 17 (b), it is possible to observe that the displacement of maximum emission bands is dependent of excitation wavelength (330 to 450 nm), shifting from 420 to 525 nm, which can be related to particle size polydispersity and distribution of different surface states. This can be attributed to the presence of emissive sites of different functional groups on nanoparticles surface, mainly carbonyls, carboxyl and hydroxyls, confirmed by UV-Vis and FTIR spectrum (JIN *et al.*, 2017).

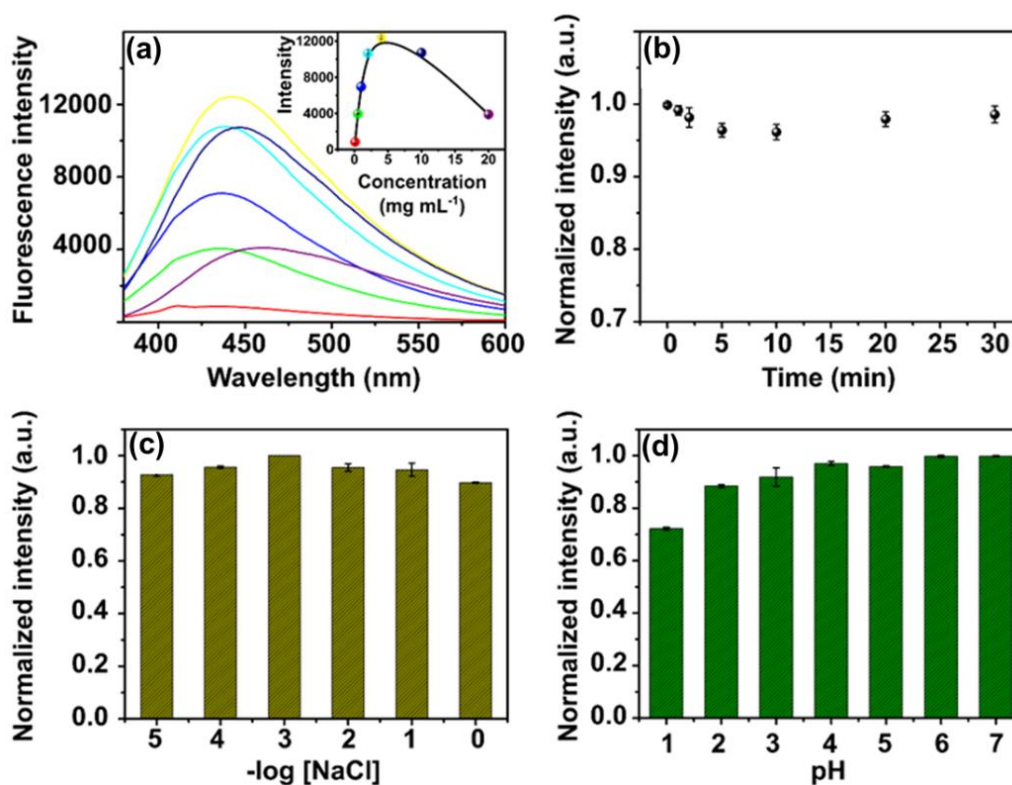
Before developing of sensing strategy, FM-CDs fluorescence at best performance must be achieved. Considering food application, it is extremely important to verify possible fluorescence variations under different chemical environments. Therefore, the concentration effect of FM-CDs is displayed in Figure 18 (a). It is possible to observe that the fluorescence intensity increases with FM-CDs concentration until 5 mg mL⁻¹. Although, the increasing in

FM-CDs concentration results in an aggregation process, which can negatively affect the fluorescence intensity. Indeed, the aggregation of nanoparticles is expected, which induces the decrease in surface area, where also decreases functional groups on FM-CDs surface, consequently decreasing their fluorescence intensity. The inset in Figure 18 (a) clearly evidences the self-quenching process, found at a concentration above 5 mg mL^{-1} . However, for sensing tests, the chosen concentration was 1 mg mL^{-1} , since fluorescence intensity was already enough to be detected within the linearity.

Figure 18 (b) presents the fluorescence intensity as a function of time, demonstrating minor 5% photobleaching during 30 min. It can be inferred that the sample dilution time does not affect the fluorescence intensity. Then, all measurements were taken after 1 min of each briefly prepared solution. However, the NaCl concentration affects the fluorescence intensity of FM-CDs, as shown in Figure 18 (c). Thereby, in the ionic strength tests, NaCl solutions were used at a concentration range from 1.0×10^{-5} to 1.0 mol L^{-1} , and after $1.0 \times 10^{-3} \text{ mol L}^{-1}$, the increase of salt concentration decreased the fluorescence intensity. This suppression could be related to the aggregation of FM-CDs into solution. Indeed, with fewer available surface traps, a partial reduction on fluorescence intensity of FM-CDs was observed.

The pH studies presented in Figure 18 (d) were performed aiming the further use of FM-CDs in real samples, such as picked olives, which presents acid medium. At low pH values, carboxylate groups on FM-CDs surface are protonated, resulting in a decrease on fluorescence of nanoparticles. Indeed, primarily, the aggregation by lowering pH occurs because of the decreasing of electrostatic repulsion, which increases van der Waals interactions, and possible π - π bond interactions (LI; CHEN; XING, 2017). Once nanoparticles are aggregated, their surface area decreases, consequently, decreasing the amount of carbonyl and carboxyl groups on FM-CDs surface (BAYATI *et al.*, 2018). Thus, the further sensing tests with standard solutions of food additives were performed without any addition of NaCl under neutral pH.

Figure 18 – Fluorescence-response evaluation of FM-CDs at different experimental conditions: (a) Concentration effect of FM-CDs on fluorescence and self-quenching (inset); (b) Photobleaching experiment for 30 min; (c) Effect of ionic strength with sodium chloride; (d) Effect of acidic pH FM-CDs. All average and standard deviation values were calculated based on triplicate experiments.



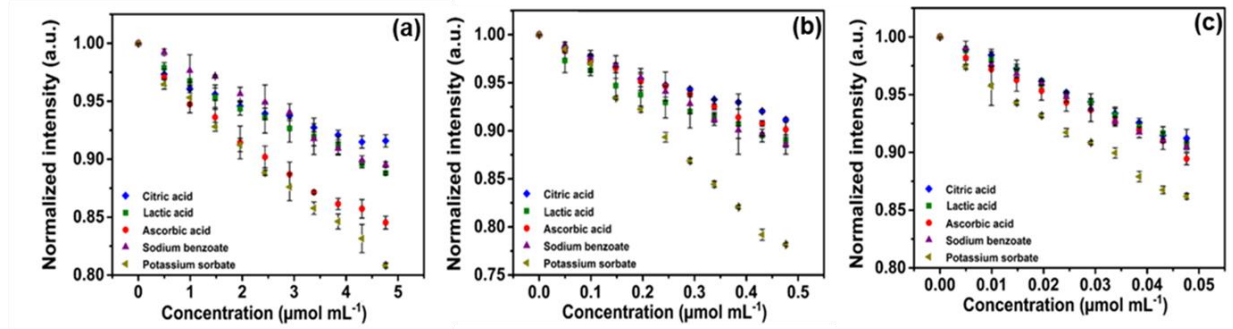
Source: (CARNEIRO *et al.*, 2021)

3.3.3 Sensing tests

In order to investigate the potential of FM-CDs towards the sensing in food safety field, five food additives were analyzed (citric acid, lactic acid, ascorbic acid, sodium benzoate and potassium sorbate). In this regard, under optimum conditions, the analytes were added to FM-CDs suspension 1 mg mL⁻¹. Figure 19 (a), (b) and (c) display the titrations of each food additive at three initial different concentrations, 0.1, 0.01 and 0.001 mol L⁻¹, respectively. After considering dilution factor (201x) into FM-CDs suspension, the analytes presented initial concentrations of 500 μmol L⁻¹, 50 μmol L⁻¹ and 5 μmol L⁻¹, respectively. The relative fluorescence intensity ratio I/I_0 and additive concentration range were investigated as dependent and independent variables, respectively.

Figure 19 – Titration curves with tested food additives at different initial concentrations of stock solution: (a) 0.1 mol L⁻¹; (b) 0.01 mol L⁻¹ and (c) 0.001 mol L⁻¹. Fluorescence intensity was investigated at 435 nm using an excitation wavelength of 360 nm and normalized using I/I_0 ,

where I_0 and I denote the intensity before and after analyte addition, respectively. All average and standard deviation values were calculated based on triplicate experiments.



Source: (CARNEIRO *et al.*, 2021)

According to the Figure 19 (a), (b) and (c) for each analyzed concentration range, the increasing of concentration of analytes results in the decrease in relative fluorescence intensity (I/I_0 ratio), promoted by the quenching of FM-CDs fluorescence with additive addition. Besides, it was also possible to observe a deviation of linearity at high additive concentration, which suggests that static and dynamic mechanisms may govern sensing chemical interactions, resulting in quenching of fluorescence (LAKOWICZ, 2006). Before real sample analysis, it is mandatory to elucidate which mechanism defines the interactions between FM-CDs and analytes. That said, parameters involved in the quenching process must be determined, which was studied using the adapted Stern-Volmer Equation:

$$\frac{I_0}{I} = 1 + K_{SV} [A]^n \quad (8)$$

Where I_0/I denotes the relative intensity of fluorescence: I_0 is the signal obtained from FM-CDs only and I is the signal obtained from the interaction between FM-CDs and food additives; K_{SV} is the Stern-Volmer quenching constant; $[A]$ is the molar concentration of the additive; n is the number of active sites which effectively interact with FM-CDs. These parameters can be achieved from linearized Equation (8), where the experimental data was fitted to Equation (9).

$$\log\left(\frac{I_0 - I}{I}\right) = \log K_{SV} + n \log[A] \quad (9)$$

According to Equation (9), when the linearization of the modified Stern-Volmer equation is applied, the number of bond sites is numerically equal to the angular coefficient of the linearized curve. The parameters K and n , as well as the linear determination coefficients obtained in this work, are shown in Table 8.

Table 8 – Parameters obtained from the linearization of the Stern-Volmer Equation.

Additive	Initial concentration (mol L ⁻¹)	K _{sv} (L mol ⁻¹)	n	R ²
Citric acid	0.1	0.03929	0.55874	0.9814
	0.01	0.17516	0.82450	0.9720
	0.001	2.19392	1.01445	0.9972
Lactic acid	0.1	0.03499	0.77874	0.9932
	0.01	0.20120	0.69260	0.9951
	0.001	2.85871	1.0858	0.9976
Ascorbic acid	0.1	0.05600	0.78962	0.9986
	0.01	0.19848	0.82836	0.9956
	0.001	1.82890	0.92600	0.9647
Sodium benzoate	0.1	0.01857	1.20008	0.9939
	0.01	0.30247	1.13940	0.9934
	0.001	2.39657	1.01509	0.9951
Potassium sorbate	0.1	0.05554	0.92323	0.9941
	0.01	0.69220	1.21731	0.9954
	0.001	2.11529	0.85112	0.9908

Source: (CARNEIRO *et al.*, 2021)

Clearly, K_{SV} values decrease for a higher initial concentration of additives. As a consequence, higher amount of analyte will result in an increasing in the fluorescence quenching rate. Additionally, only citric acid, lactic acid and sodium benzoate, at a concentration of 0.001 mol L⁻¹, showed n values close to 1, as seen in Table 8, indicating a static mechanism interaction, where fluorescence quenching occurs due to association between fluorescent species and the quencher. This interaction results in a non-fluorescent complex, reducing the relative fluorescence intensity of the system. However, for other analytes at different concentrations, n values were different from 1, suggesting a dynamic mechanism. In dynamic quenching, the fluorophore (FM-CDs) and quencher molecules (additive) collide with each other and thus the energy of the fluorophore decreases (BOZKURT; GUL, 2019). In this mechanism, the FM-CDs are in the excited state and return back to their ground-state as a result of the collision between the fluorophore and quencher by the mechanism of charge transfer or energy transfer.

Table 9 – Merit figures obtained from quantification of food additives using the respective calibration curve of each analyte.

Additive	Equation	Linear Range ($\mu\text{mol mL}^{-1}$)	R ²	LOD (nmol mL^{-1})	LOD (ng mL^{-1})	LOD ($\text{g } 100\text{g}^{-1}$)
Citric acid	$I_0/I = 0.9984 + 2.1185 [C]$	0.004975-0.047619	0.9962	1.486	285.490	0.0286
Lactic acid	$I_0/I = 0.9997 + 2.1543 [C]$	0.004975-0.047619	0.9974	2.880	259.430	0.0260
Ascorbic acid	$I_0/I = 1.0040 + 2.2674 [C]$	0.004975-0.047619	0.9922	8.452	1488.566	0.149
Sodium benzoate	$I_0/I = 0.9997 + 2.2843 [C]$	0.004975-0.047619	0.9975	1.752	252.481	0.0253
Potassium sorbate	$I_0/I = 1.0080 + 3.2745 [C]$	0.004975-0.047619	0.9923	3.929	590.214	0.0592

Source: Author.

After quenching mechanism evaluation, the quantification of the analytes was carried out by other linearization of titration curves. In order to measure the sensibility of quantification, food additives at a lower concentration of 0.001 mol L^{-1} was selected. I_0/I ratio values were used as a function of additive concentration in order to obtain a better linearity and further calculate the limit of detection (LOD), as shown in Table 9, where is also presenting line equations and linear range values for each tested additive. From that, we found a $R^2 > 0.99$ for all analyzed linear ranges.

For determination of *LOD*, a curve of fluorescence recovery *versus* concentration of analyte was plotted and fitted with a straight line, where was calculated by Equation (10):

$$LOD = \frac{3.3 SD}{b} \quad (10)$$

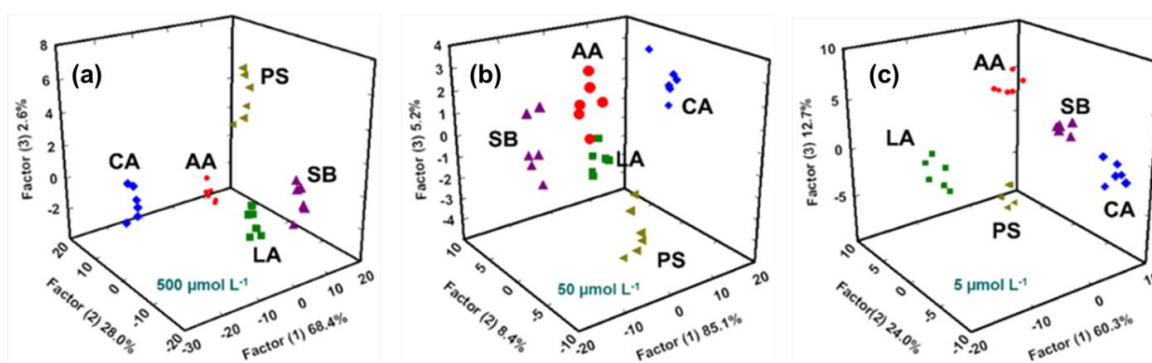
Where *SD* is the standard deviation of ordinate intercept and *b* is the slope of regression line (SHRIVASTAVA; GUPTA, 2011). All obtained *LOD* values were as low as the concentration of 252 ng mL^{-1} (or $0.0260 \text{ g}/100 \text{ g}$) for sodium benzoate, which indicates a great sensibility of the adopted sensing strategy. Values between 200 and 300 ng mL^{-1} were obtained for lactic acid and citric acid. The highest value was 1488 ng mL^{-1} (or $0.149 \text{ g}/100 \text{ g}$) for ascorbic acid. These distinct values can be attributed due to different interactions between additive molecules and functional groups on the surface of FM-CDs. For example, ascorbic acid has a five-membered ring containing an oxygen atom, which is a quite distinct chemical structure in comparison to

citric acid and lactic acid molecules. In addition, these molecules, as well as sodium benzoate, are smaller and also present carboxyl groups in their chemical structures, indicating that the FM-CDs-based sensing platform does not only show great sensibility, but can be also a versatile strategy in the identification and quantification of a wide variety of chemical additives

3.3.4 Real Samples: identification of additives in pickled olives

After developing a robust sensing platform, we firstly applied LDA sensing strategy against standard solutions of each food additive, to further analysis in real sample. Briefly, as expected, the interaction between FM-CDs and additive molecules results in quite different fluorescent intensities. These values were evaluated by I/I_0 ratio, considering all analyzed spectral range (380 at 600 nm), and then the generated patterns were recognized by LDA. The results were expressed considering three most significant canonical factors as shown in Figure 20. Clusters LDA separation is based on the standard distance of Mahalanobis: the larger the distance between aggregates, the lower the probability of a wrong identification of analytes (LE *et al.*, 2017).

Figure 20 – Sensing tests using plots of LDA in three dimensions with all additives at different concentrations in FM-CDs suspension under neutral pH: (a) $500 \mu\text{mol L}^{-1}$; (b) $50 \mu\text{mol L}^{-1}$; (c) $5 \mu\text{mol L}^{-1}$. Each average value was calculated with six replicates and 95.0% of level of confidence. CA = citric acid; LA = lactic acid; AA = ascorbic acid; SB = sodium benzoate; PS = potassium sorbate.



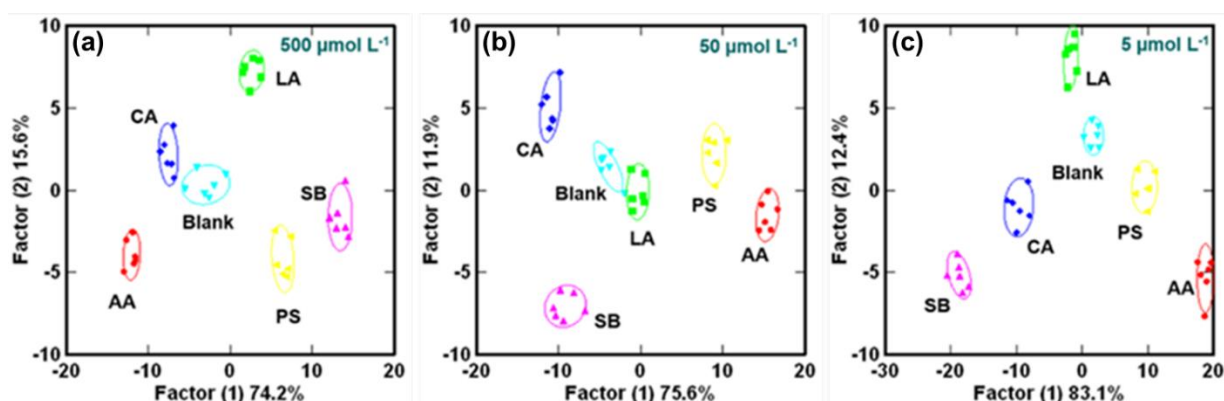
Source: (CARNEIRO *et al.*, 2021)

It is clearly observed that the sensing strategy greatly identified all tested analytes, since pooled points of each respective additive is well-separated from each other, considering

a 95% of confidence level. By analyzing full set of data (one binding event \times five additives \times six replicates), three canonical factors were generated for each concentration, 500, 50 and 5 $\mu\text{mol L}^{-1}$. Then, these values were used to generate a 3D-LDA plot, and explain the variance of data. For concentrations of 500, 50 and 5 $\mu\text{mol L}^{-1}$, the values of the three canonical factors were 99.0%, 98.7% and 97.0%, respectively. The results obtained were already expected since the lower concentration, the more canonical factors will be needed to explain the differentiation of additives.

The same procedure was performed using a pickled olives sample. Firstly, pickled olives, without any additive previously addition, were added in FM-CDs suspension, labeled as blank sample. Then, each additive was intentionally added, separately, to the pickled olives sample containing FM-CDs at concentrations of 500, 50 and 5 $\mu\text{mol L}^{-1}$. In Figure 21 is shown the score plot obtained by LDA algorithm to analyze the fluorescence response pattern for all five additives at three different concentrations.

Figure 21 – LDA-based sensing tests with pickled olives (real sample), considering two most significant canonical factor, using three different concentrations of all additives: (a) 500 $\mu\text{mol L}^{-1}$; (b) 50 $\mu\text{mol L}^{-1}$; (c) 5 $\mu\text{mol L}^{-1}$. Each average value was calculated with six replicates and 95.0% of level of confidence. Legend: CA = citric acid; LA = lactic acid; AA = ascorbic acid; SB = sodium benzoate; PS = potassium sorbate.



Source: (CARNEIRO *et al.*, 2021)

As observed in Figure 21 (a) and (c), at 500 and 5 $\mu\text{mol L}^{-1}$, respectively, no overlapping among all ellipses was detected, considering 95% of confidence level, indicating a great differentiation of all tested analytes using the proposed sensing strategy. As shown in

Figure 21 (b), besides at $50 \mu\text{mol L}^{-1}$ the overlapping was not notice, the blank sample cluster was too close to lactic acid, indicating that the pickled olive sample might have a concentration of lactic acid similar to $50 \mu\text{mol L}^{-1}$. In this regard, considering both tested food additives and pickled olives sample, the sensing strategy detected values below the range considered to be safe by ANVISA. Therefore, considering lower recommended limits of additives usage, the herein developed sensing strategy displays a potential application as a robust sensing platform for identification and also motorization of additives in a wide variety of products within food industries.

3.4 Conclusion

In summary, we have presented an easy and simple sensing strategy of food additives in pickled olives using FM-CDs obtained from seeds of *Caesalpinia pulcherrima*. The FM-CDs exhibited high fluorescence at 435 nm and could be used as a novel fluorescent probe for detection of five food additives (citric acid, lactic acid, ascorbic acid, sodium benzoate and potassium sorbate), *via* static or dynamic quenching mechanism. The proposed sensing strategy, FM-CDs together with LDA algorithms, was able to greatly differentiate all tested additives, which were also identified in a real sample of pickled olives. Furthermore, the sensing platform successfully differentiates the five additives with 100% of accuracy, showing potential to might be applied on manufactured food quality control. In addition, it is really important to mention the excellent sensing performance of FM-CDs from natural source, which could provide different binding events with all tested additive molecules.

CHAPTER IV²

4 DOPED CARBON QUANTUM DOTS/PVA NANOCOMPOSITE AS A PLATFORM TO SENSE NITRITE IONS IN MEAT

Abstract

A sensor device based on doped-Carbon Quantum Dots is proposed for detection of nitrite ions in meat products by fluorescence quenching. Firstly, for the sensing platform, carbon quantum dots doped with boron and functionalized with nitrogen (B,N-Cdot) are synthesized with a high quantum yield of 44.3% through one-step hydrothermal route, using citric acid, boric acid and branched polyethyleneimine (*b*PEI) as sources of carbon, boron and nitrogen, respectively. After standard investigation of the chemical structure and fluorescent properties, the B,N-Cdot aqueous suspension showed highly selective for NO_2^- ions in a linear range from 20 to 50 mmol L^{-1} , under optimum conditions at pH 7.4 and excitation wavelength of 340 nm. Furthermore, B,N-Cdots were able to successfully detect NO_2^- in a real meat sample, with a recovery percentage of 91.43 to 103.90% within the analyzed range. Herein, we developed a B,N-Cdot/PVA nanocomposite film with emission in the blue region under excitation wavelength of 360 nm, and, then, a first-assay detection of nitrite ions in meat product was tested by aid of a smartphone applicative. The results evidence a potential application of the sensor device, containing a highly fluorescent probe, in the development of an advanced, faster and costless strategy of NO_2^- ions detection.

Keywords: Carbon Quantum Dots; Sensor device; Nanocomposite; Fluorescent sensing; Nitrite; Meat.

2. This chapter is the result of the research paper entitled “Doped carbon quantum dots/PVA nanocomposite as a platform to sense nitrite ions in meat.” submitted in the journal ACS Applied Materials & Interfaces.

4.1 Introduction

Nitrite ion (NO_2^-) is an inorganic compound usually present in drinking water and industrialized foods (ZHU *et al.*, 2021). As an additive, it is commonly used in meat products since reduces the growth of bacteria and ensures the conservation of meat color and flavor (FLORES; TOLDRÁ, 2021; YUE *et al.*, 2020). For instance, sodium nitrite (NaNO_2) has been reported as the only substance capable of inactivating *Clostridium botulinum*, which secretes lethal paralytic neurotoxins (KIM *et al.*, 2021). On the other hand, NO_2^- reacts with amines and amides in the living body to form N-nitrosamines, increasing cancer risks and deformities (JIGYASA; PRATIBHA; RAJPUT, 2020; LI, L. *et al.*, 2021).

Therefore, in 2015, the International Agency for Research on Cancer (IARC) classified processed meats containing NaNO_2 in formulation as Group 1 carcinogens, since some cancer-types have been related to the consumption of nitrite ions (KARWOWSKA; KONONIUK, 2020). In agreement, the Brazilian National Health Surveillance Agency (ANVISA) accepts only a maximum concentration of 0.015 g of NO_2^- per 100 g of meat product. Additionally, it is also worth to mention that the European regulation established a maximum concentration of 0.5 mg L⁻¹ (LETE *et al.*, 2020). Besides all regulations worldwide, many meat product manufacturers use nitrite above allowed concentration, since can increase the conservation status of the meat. Therefore, it is extremely relevant to develop simple and effective methodologies to detect the concentration of NO_2^- ions, providing an easy analysis for both manufacturer and consumer. Indeed, for a rigorous industrial quality control, also propose a field analysis device, which the consumer will be able to check the safety of the purchased meat.

Several methodologies have been reported to analyze NO_2^- , including chromatography (MURRAY *et al.*, 2020), chemiluminescence (HAN; CHEN, 2019), spectrophotometry (MAŠIĆ *et al.*, 2015) and electrochemical methods (VILIAN *et al.*, 2021), however most techniques are expensive and time-consuming, involving complexed pathways that need the overuse of organic solvents. Thereby, scientific community has constantly searching for alternative methodologies in order to enhance greenness profile of analysis, as well as developing cost-effectiveness, robust and fast sensing platform strategies (JANA *et al.*, 2019). Advanced methods based on optical properties of nanomaterials are suitable alternatives to conventional analyses (XU *et al.*, 2020).

For instance, some sense devices have been developed to analyze NO_2^- . Moo and co-authors proposed a method based on an optical fiber to determine nitrite species in water

(MOO *et al.*, 2016). Indeed, optical properties can be explored at nanoscale materials since the sensing can be tailored with high selectivity, sensitivity and ranging of detection. Additionally, fluorescent systems including metal nanoclusters (XU *et al.*, 2015), semiconductor silicon quantum dots (WEI *et al.*, 2021), metal-organic framework materials (TAPANGPAN *et al.*, 2020) and carbon-based nanomaterials (LI *et al.*, 2020) have been investigated for nitrite detection.

Carbon Quantum Dots (CQDs) have been highlighted as one of the most important carbon-based fluorescent zero-dimensional nanomaterial. CQDs have become very popular due to their unique physicochemical behavior, including low toxicity, chemical resistance, water-solubility, tunable emission, broad absorption range, and photostability (JANA *et al.*, 2019; ZAN *et al.*, 2018). These properties allow the application of CQDs in bioimaging (ATCHUDAN *et al.*, 2021), photocatalysis (LI, G. *et al.*, 2021), light-emitting diodes (MOHANRAJ *et al.*, 2021) and chemical sensors (GAN *et al.*, 2021). In this field, the literature is rich in presenting sensing strategies applying CQDs in the detection of proteins (CARNEIRO CRUZ *et al.*, 2019; FREIRE *et al.*, 2018), pesticides (CARNEIRO *et al.*, 2019; LIANG *et al.*, 2021), metals (WU *et al.*, 2019) and ions such as NO_2^- (LIU *et al.*, 2019).

However, as-presented CQDs show low quantum yield (QY) values, which can decrease their sensibility. In order to overcome these drawbacks, some works reported surface-modified CQDs with nitrogen (ALI *et al.*, 2020), phosphorous (VENKATESWARA RAJU *et al.*, 2020), sulfur (MAGDY *et al.*, 2021) and boron (MA *et al.*, 2020), which could enhance CQDs quantum yield (QY). It is still possible to use more than one heteroatom or to use both in a very low concentration, i.e., to obtain doped CQDs. All these processes exhibit the advantage of developing selective platforms to identify different species, including NO_2^- ions, with high specificity, even considering complex matrixes, such as meat products.

Herein, this work proposed a sense device of nitrite ions based on modified CQDs, where, firstly, we synthesized CQDs by hydrothermal method using citric acid, boric acid and branched polyethyleneimine (*bPEI*), as sources of carbon, boron and nitrogen, respectively. The carbon nanoparticles, doped with boron and functionalized with nitrogen (B,N-Cdot), obtained a QY of 44.3%, allowing to propose an economically attractive, simply operable, easily prepared, and highly efficient sensor for NO_2^- sensing in meat. With these features, the sensor will be able to reach a large public, facilitating the monitoring of NO_2^- ions in meat.

After purification processes, the chemical structure of B,N-Cdot was investigated, confirming both doping and functionalizing modifications. Then, the NO_2^- sensing platform was proposed, firstly at colloidal suspension, showing excellent results of recovery percentage, up

to 100.76% in a meat sample and a detection range concentration of 20 to 50 mmol L⁻¹. Furthermore, the B,N-Cdots were incorporated into a polyvinyl alcohol (PVA/B,N-Cdot) thin film, which presented high fluorescence, with an emission wavelength around 430 nm. In front of excellent optical properties of the PVA/B,N-Cdot film, we developed a sensor containing the nanocomposite for the detection of NO₂⁻ ions in a concentration range from 10 to 50 mmol L⁻¹. Indeed, a free applicative, Photometrix, was used as a tool to facilitate the analysis, where fluorescence signals were registered at different NO₂⁻ concentrations, developing an easy-to-handle sensor with a fast detection response.

4.2 Experimental section

4.2.1 Material and reagents

The chemicals polyvinyl alcohol (PVA, 95.0%), sodium hydroxide (NaOH, 98.0%), sodium nitrate (NaNO₃, 99.0%), iron (II) sulfate (FeSO₄·7H₂O, 99.0%) and anhydrous zinc nitrate (Zn(NO₃)₂, 96.0%) were purchased from Dinamica. Monobasic potassium phosphate (KH₂PO₄, 98.0-100.5%) was purchased from Merck. Hydrochloric acid (HCl, 36.5-38.0%), anhydrous lithium chloride (LiCl, 98.0%) and lactic acid (C₃H₆O₃, 85.0%) were purchased from Synth. Sodium nitrite (NaNO₂, 99.0%), quinine sulfate ((C₂₀H₂₄N₂O₂)₂·H₂SO₄·2H₂O, 99.0-101.0%), sulfuric acid (H₂SO₄, 95.5%) sodium sulfate anhydrous (Na₂SO₄, 99.0-101.0%), monobasic sodium phosphate (NaH₂PO₄, 99.0%), dibasic sodium phosphate (Na₂HPO₄·12H₂O, 99.0%), sodium chloride (NaCl, 99.0%), potassium nitrate (KNO₃, 99.0%), barium chloride (BaCl₂·2H₂O, 99.0%), manganese chloride (MnCl₂·4H₂O, 98.0%), anhydrous glucose (C₆H₁₂O₆, 99.5%), succinic acid (C₄H₆O₄, 99.0%) and glutamic acid (C₅H₉NO₄, 99.0%) were purchased from Vetec. Alanine (C₃H₇NO₂, 99.0%) and calcium nitrate (Ca(NO₃)₂, 99.0%) were purchased from Sigma-Aldrich. Sodium fluoride (NaF) was purchased from EEL. Histidine (C₆H₉N₃O₂) was purchased from Inlab. Phenylalanine (C₉H₁₁NO₂) was purchased from Lab Confiança.

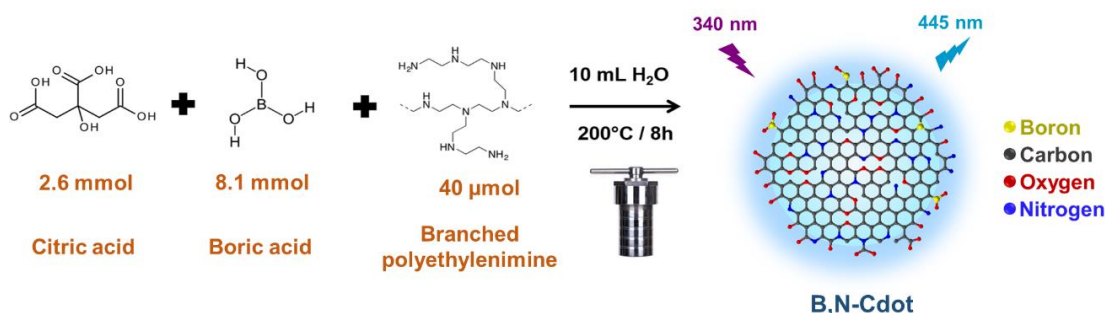
Citric acid (C₆H₈O₇, Vetec, 99.5%), boric acid (H₃BO₃, Dinamica, 99.5%) and *branched* polyethyleneimine (*b*PEI, Sigma-Aldrich, 25,000 g mol⁻¹) were used to prepare the CQDs. All chemicals were of analytical reagent grade without previous treatment and purchased in Brazil. Distilled water (conductivity = 11.51 μS cm⁻¹) was used during the experiments. Phosphate buffer solution (PBS) was prepared by mixing 100 mL of stock solutions of 0.025 mol L⁻¹ NaH₂PO₄ and 100 mL of stock solutions of 0.039 mol L⁻¹

$\text{Na}_2\text{HPO}_4 \cdot 12\text{H}_2\text{O}$. After mixing, the PBS solution had its pH adjusted with dilute aqueous solutions of HCl and NaOH until the pH of the solution was equal to 7.4. A cellulose membrane Spectra/Por®6 dialysis membrane of 1 kDa MWCO was used for dialysis.

4.2.2 Synthesis of CQDs

CQDs were synthesized according to the conventional hydrothermal method (BANO *et al.*, 2019; GUO *et al.*, 2017). In order to evaluate the effect of both boron doping and nitrogen functionalization on CQDs QY, four different nanoparticles were synthesized: Cdot, B-Cdot, N-Cdot and B,N-Cdot. In all syntheses, citric acid, boric acid and bPEI were used as carbon, boron and nitrogen source, respectively. Depending on the synthesis, 2.6, 8.1 and 0.04 mmol of citric acid, boric acid and bPEI, respectively, were solubilized in 10 mL of distilled water until complete dissolution. Each solution was transferred to a 50 mL Teflon-lined autoclave and heated up to 200 °C for 8 h. Further, the autoclave was cooled down to room temperature ($25 \pm 2^\circ\text{C}$). Then, each sample was dialyzed in two cycles (12 h/cycle) against distilled water and a suspension was freeze-dried and for structural characterizations and its concentration was determined (1.07 mg g^{-1}). The remaining CQDs solutions were stored at 4°C for further sensing experiments and PVA-film preparation, according cashing method described in section 4.2.5. Figure 22 illustrates the expected chemical reaction for obtaining B,N-Cdot. The quantum yield (QY) of the as-synthesized CQDs was measured based on a procedure described previously (LI *et al.*, 2019) and a solution of quinine sulfate in H_2SO_4 0.1 mol L^{-1} (QY_R of 54% at 360 nm, $\eta = 1.33$) was used as a reference.

Figure 22 – Reaction scheme for obtaining B,N-Cdot by the hydrothermal method.



Source: Author.

4.2.3 Instrumentation and characterization of CQDs

The absorption spectra were recorded in the spectrophotometer UV-Vis Shimadzu UV-2600. The fluorescence spectra were obtained in the Shimadzu RF-6000 spectrofluorophotometer. The Fourier transform infrared (FTIR) spectrum was recorded by using a scanning range of 400 to 4000 cm^{-1} . The Raman spectrum was recorded in a range of 500 to 2500 cm^{-1} , using a Horiba Raman spectrometer. The spectral excitation was performed using a laser line of 785 nm, with adjustable filters and adequate powers of 10.7 and 151 μW with 10 accumulations of 50 s. ^1H and ^{13}C NMR spectra were obtained on a Bruker Avance DRX-500 spectrometer, using D_2O as solvent for solubilization of the freeze-dried material previously.

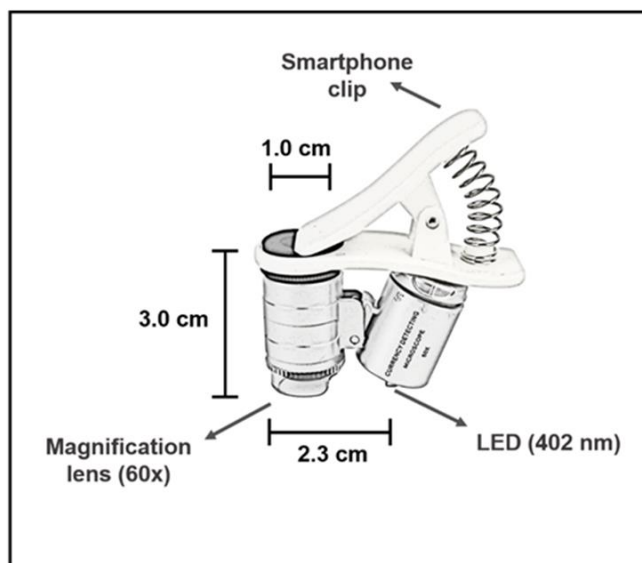
X-ray photoelectron spectroscopy (XPS) was performed using a ThermoFisher Scientific model K-alpha+, using monochrome radiation from Al- $k\alpha$ with pass energy of 200 eV and 50 eV for the survey and high-resolution scanning spectra, respectively. The spot size was 400 μm . The pressure in the analysis chamber was approximately 10^{-7} Pa. Peak fitting was done using the program provided by the equipment manufacturer (Avantage), with mixed Gaussian/Lorentzian curves and background subtraction using the Smart algorithm.

Atomic force microscopy (AFM) images were obtained using an Asylum MFP 3D. Topography and phase contrast of the B,N-Cdot were performed with an NCHR-50 silicon non-contact tip (Nano World), (less than 8 nm of radius tip, 42 N/m of force constant, 320 kHz of resonance frequency), operating with a scan rate of 0.20 Hz. Laser Scanning Confocal Microscopy (LSCM) was performed to obtain the confocal images. A confocal microscope (Zeiss - LSM 780) coupled to an Axio Examiner.Z1 (Carls Zeiss) with 20 x objective (EC Plan-Neofluar – NA 0.5) and an internal Zeiss detector was used. To investigate the fluorescence life-time decay, a Fluorescence Life-Time Imaging Microscopy (FLIM) was applied. The analysis was carried out in a dried film mounted with an air immersion objective and a rate of 10^4 - 10^5 counts/s. To acquire life-time decay, we used a Becker and Hickl set with a resolution of 200 ps. A pulsed 405nm laser was used with 80MHz repetition rate.

For the development of the field analysis device, the following items were required: coverslips with prepared nanocomposite, pocket microscope and a smartphone with the Photometrix applicative installed. To record the fluorescence emitted by the nanocomposite, a Universal Clip Type LED Microscope n° 9595W1 (imported from China) was used. This accessory is equipped with a 60x magnification objective lens and ultraviolet LEDs with an

emission source in 402 nm. The dimensions are shown in the Figure 23. The smartphone used was an LG K9 with a digital camera of 8MP. The app PhotoMetrix PRO version 1.1.23 was used. This app offers multiple color channels for univariate analysis, where the calibration curve was built from the treatment of the obtained data from B color channel.

Figure 23 – Dimensions of pocket microscope used for the field analysis device.



Source: Author.

4.2.4 Sensing experiments

Before starting the sensing, the experimental conditions that would lead to the best fluorescence response of the system were evaluated. Thus, the fluorescence intensity was evaluated, varying the concentration of B,N-Cdot from 0.1 to 20 $\mu\text{g mL}^{-1}$, the pH between 3.2 and 7.5 and the contact time between B,N-Cdot and NO_2^- ions between 1 and 40 min. Furthermore, in order to investigate the selectivity of sensing strategy, fluorescence intensity of B,N-Cdot in the presence of possible interferences was measured, including anions, cations and biomolecules. The concentration of all species was maintained at 40 mmol L^{-1} .

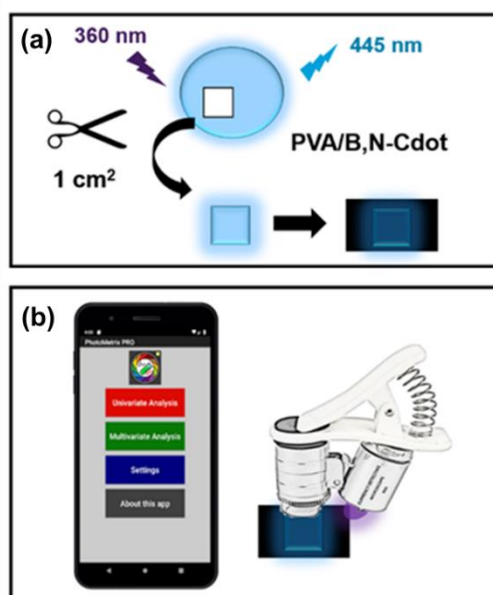
After optimization of the experimental conditions, the sensing was performed, following a well-established assay (HUO *et al.*, 2021) Briefly, 500 μL of prepared B,N-Cdot ($5.0 \mu\text{g mL}^{-1}$) were transferred to a quartz cuvette, and aliquots of NaNO_2 stock solution (concentrations of 0.1, 0.01 and 0.001 mol L^{-1}) and PBS solution pH 7.4 were added, resulting in a final volume of 2 mL for all samples and obtaining a NO_2^- range varying from 0.00 to 50.00

(mmol L^{-1}). The emission spectra were recorded after 2 min of incubation at 340 nm excitation and the PL intensity at 435 nm was used for NO_2^- quantification. Posteriorly, tests with real samples were carried out with meat purchased from the local market (Brazil). The meat exudate blood was diluted 300-fold in distilled water and then different concentrations of NaNO_2 solutions were spiked for the recovery tests.

4.2.5 B,N-Cdot/PVA film preparation and development of the sensor device

To obtain the B,N-Cdot/PVA nanocomposite in a film-form, a mass of 0.5 ± 0.01 g of PVA was initially weighed and solubilized in 10 mL of an aqueous suspension of B,N-Cdot (1.07 mg g^{-1}). Then, the mixture remained under constant magnetic stirring for 10 h at a temperature of $30 \pm 2^\circ\text{C}$ and after was transferred to two glass Petri dishes with a diameter of 5 cm, for drying for approximately 36 h. Furthermore, the film was cutted off in standard squares of 1 cm^2 area to be applied in the device tests to sense nitrite ions in meat. Figure 24 schematically illustrates how the film was cut and added to the coverslip.

Figure 24 – (a) preparation of the PVA/B,N-Cdot nanocomposite in coverslips; (b) smartphone with the Photometrix applicative installed and pocket microscope clipped to smartphone.



Source: Author.

Firstly, for the sensing of NO_2^- in meat, the following materials were used: B,N-Cdot/PVA nanocomposite film, microscope glass slides and black adhesive tapes. The analysis compartment consists of a piece of PVA/B,N-Cdot film stuck on the black adhesive tape in the coverslips in a dark environment. Figure 24 (b) shows the items needed for analysis. Thus, 1 drop of the sample (aqueous solutions of NaNO_2 in the concentration range of 10 to 50 mmol L^{-1} and meat samples diluted 300-fold in distilled water and fortified with NaNO_2 in same concentration range) was added to this compartment, which was hermetically closed, when the tape is fixed again on the coverslip, as illustrated in Appendix A. After 1 min, the images in the device were recorded in triplicate by the aid of a pocket microscope and with the camera of the smartphone.

With the assistance of the Photometrix applicative, the calibration curve was obtained. To obtain the calibration curve, each coverslip containing the respective sample at different concentrations (10, 20, 30, 40 e 50 mmol L^{-1}) of the analyte had its fluorescence signal recorded through the smartphone camera. Further, the app converted the captured images to color channels, where the fluorescence signals were measured. These signals are analogous to the intensity obtained by a spectrophotometer and were used in the construction of the calibration curve. The data were measured considering the color channel related to quenching of the intensity of blue color emission, and then the values were normalized. Photometrix was developed for univariate and multivariate analysis, using color channels from the colorimetric analysis (HELPER *et al.*, 2016). In this work, we adapted the application's routine to use the high-intensity fluorescence signals emitted by the B,N-Cdots impregnated in the polymeric matrix.

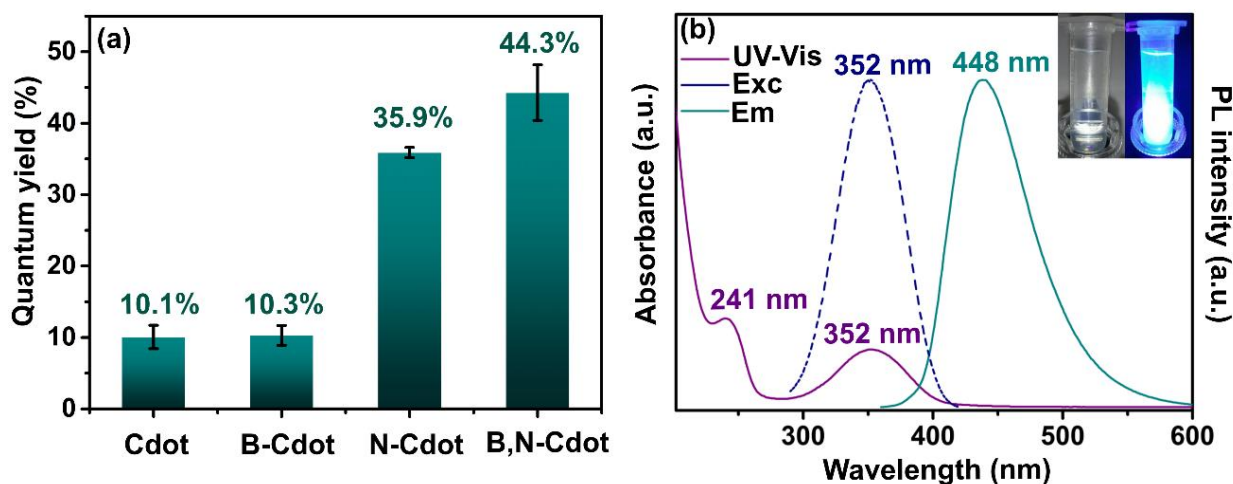
4.3 Results and discussion

4.3.1 Characterization of B,N-Cdot

Initially, four different samples of CQDs, labeled as Cdot, B-Cdot, N-Cdot and B,N-Cdot, were synthesized using distinct compounds as precursors, also combining their simultaneous addition, in order to investigate the effects of the heteroatoms in the CQDs regarding QY response. Figure 25 (a) shows that the doping of CQDs with boron and the functionalization with nitrogen significantly increased the QY values. Indeed, this increment is even higher when the precursors citric acid, boric acid and bPEI are added simultaneously, leading to a synergistic effect with a high QY value of 44.3%, as seen for the sample B,N-Cdot.

Comparatively, Jiang *et al.* also synthesized CQDs doped with boron and nitrogen, obtaining a QY value of around 19.6% using p-aminosalicylic acid, boric acid and ethylene glycol as precursors (JIANG, X. *et al.*, 2019). On the other hand, Dong *et al.* synthesized CQDs functionalized with amine groups, using citric acid and bPEI, obtaining a QY value close to 40.0%, slightly higher than that obtained in this work for the sample N-CDot, 35.9% (DONG *et al.*, 2012). Therefore, it can be inferred that the addition of an amino-rich polymer functionalizing CQDs may promote a higher QY, as observed in this work.

Figure 25 – Results of spectroscopic characterizations: (a) QY of all CQDs synthesized in this work; (b) UV-Vis, excitation and emission spectra of B,N-CDot. Inset: B,N-CDot under white lamp (left) and UV lamp (right). Legend: Exc = excitation spectrum; Em = emission spectrum.



Source: Author.

The optical properties of synthesized CQDs were investigated through UV–visible absorption and photoluminescence spectroscopy. Appendix B (a), (b) and (c) show the UV-Vis spectra of the Cdot, B-Cdot and N-Cdot samples, respectively. Cdot and B-Cdot have a characteristic peak near 240 nm, related to the π - π^* transition, whereas N-Cdot also presented a well-defined peak at 356 nm, attributed to the n - π^* transitions (WU *et al.*, 2017). As shown in Figure 25 (b), B,N-Cdot spectrum presents absorption peaks at 241 and 352 nm. The first peak is related to the transitions π - π^* corresponding to sp^2 -type carbon bonds (VAZ *et al.*, 2017). The other peak is associated with n - π^* transition of $-C=O$, $C-N$, or $-C-OH$ bonds which may be related to carboxyl ($-COOH$) or amine ($-NH_2$) groups on the surface of nanoparticles, respectively (TADESSE *et al.*, 2018). The excitation spectrum obtained by monitoring the green emission at 448 nm is consistent with the result presented in the absorption

spectrum. Under 340 nm excitation, the B,N-Cdot presents an emission at 448 nm. Moreover, this sample is transparent under bright light irradiation, but has a high blue fluorescence under a 365 nm UV lamp irradiation (Figure 25 (b), inset).

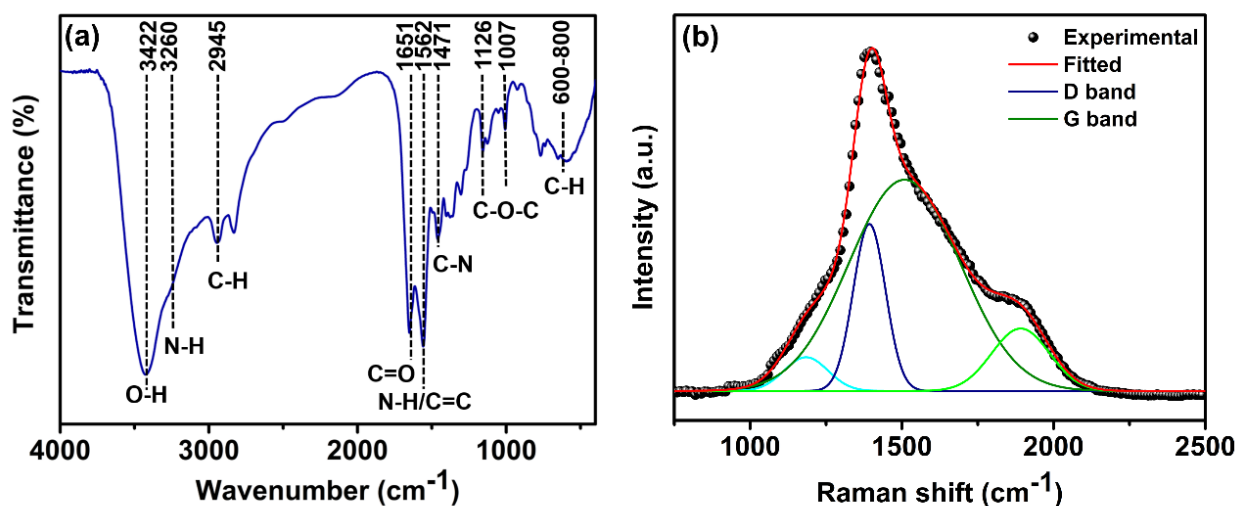
To deeper explore the optical properties of the as-prepared CQDs, we carried out a detailed PL study by changing excitation wavelengths ranging from 300 to 400 nm. The results are shown in Appendix B (d) and (e). For the Cdot and B-Cdot samples, an excitation-dependent behavior was observed, with a characteristic bathochromic shift phenomenon, due to their surface defects or surface light-emitting sites (JIANG, X. *et al.*, 2019; LI *et al.*, 2014). This also could be explained based on the presence of different-sized nanoparticles in the surface energy traps of CQDs. Smaller-sized nanoparticles were excited at a lower excitation wavelength, whereas larger-sized nanoparticles were excited at a higher excitation wavelength (KAUR *et al.*, 2020). However, N-Cdot and B,N-Cdot showed an independent excitation behavior, as seen in Appendix B (f) and Appendix C, with maximum excitation wavelengths at 350 and 340 nm, respectively. In both cases, this excitation-independent property is observed due to a narrow size distribution of the particles and a less number of defects on the surface of nanoparticles (MONDAL; GHORAI; SAHA, 2018). Then, the sample B,N-Cdot showed an independent behavior of excitation between 300 and 340 nm, with an emission peak at 448 nm.

Thereby, in order to optimize the sensing experiments, it was observed that at 340 nm the highest emission intensity was achieved, which it was chosen as the excitation wavelength for all further experiments. The fluorescence of each of these samples was tested in the absence and presence of NO_2^- ions, the target analyte of this work. Appendix D shows this result, where it is evident that doping does not affect the amount of NO_2^- ions to be detected. However, due to the highest QY value and PL property independent of the excitation, the sample B,N-Cdot was selected for structural characterization and further sensing tests.

Information regarding the surface functional groups of B,N-Cdot was obtained by FTIR. The spectrum is presented in Figure 26 (a), which shows bands at 3422, 3260 and 1651 cm^{-1} corresponding to stretching vibration of $-\text{O}-\text{H}$ (hydroxyl) or $-\text{N}-\text{H}$ (amine) and $-\text{C}=\text{O}$ (carboxyl), respectively (DING; WEI; XIONG, 2014; KURDEKAR *et al.*, 2016; SONG *et al.*, 2019). The band located at 1562 cm^{-1} can be attributed to the angular deformation of $-\text{N}-\text{H}$ (KURDEKAR *et al.*, 2016) or stretching vibration of $-\text{C}=\text{C}$ (DING; WEI; XIONG, 2014), and the presence of $-\text{C}-\text{H}$ bonds from aromatic rings is confirmed by the bands ranging from 800 to 600 cm^{-1} (COSTA *et al.*, 2018). Further, the band located at 2945 cm^{-1} is related to $-\text{C}-\text{H}$ stretching of alkyl groups of the graphitic portion of CQDs (RAO *et al.*, 2018) and the band at 1471 cm^{-1} is ascribed to $-\text{C}-\text{N}$ from amide groups (JIANG *et al.*, 2012). Absorption bands at

1126 and 1007 cm^{-1} can be assigned to the asymmetric and symmetric stretching vibrations of the $-\text{C}-\text{O}-\text{C}$ group, respectively (AF *et al.*, 2019; FAN *et al.*, 2015). Additionally, as shown in Appendix E, the spectra of each precursor and their physical mixture were also analyzed. Clearly, it was observed differences between these spectra and B,N-Cdot spectrum, showing that the chemical reaction was performed and new chemical bonds appeared in the structure of the B,N-Cdot nanoparticles.

Figure 26 – Results of structural characterizations of B,N-Cdot: (a) FTIR spectrum; (b) Raman spectrum.



Source: Author.

Raman spectrum of B,N-Cdot provides information regarding crystallinity of the nanoparticles. Figure 26 (b) illustrates the two peaks with the highest intensity, obtained from the deconvolution spectrum at 1385 cm^{-1} and 1510 cm^{-1} , assigned to the D and G bands, respectively (CARNEIRO *et al.*, 2021). The intensity ratio I_D/I_G of the Raman D (disorder) and G (crystalline) carbon bands are often used to determine the quality of graphene sheets or carbon nanotubes (RECKMEIER *et al.*, 2016). Herein, the ratio was 0.80, which evidences the presence of fewer defects in the carbon core of the synthesized B,N-Cdots (EDISON *et al.*, 2016). Therefore, Raman result suggests that the nanoparticles have a graphitic structure confirming an excitation-independent behavior observed by PL spectrum, and which is related to a crystalline structure with fewer surface defects.

Additionally, a NMR spectroscopic study was also performed considering B,N-Cdot chemical structure. Appendix F (a) and (b) show the ^1H and ^{13}C NMR spectra,

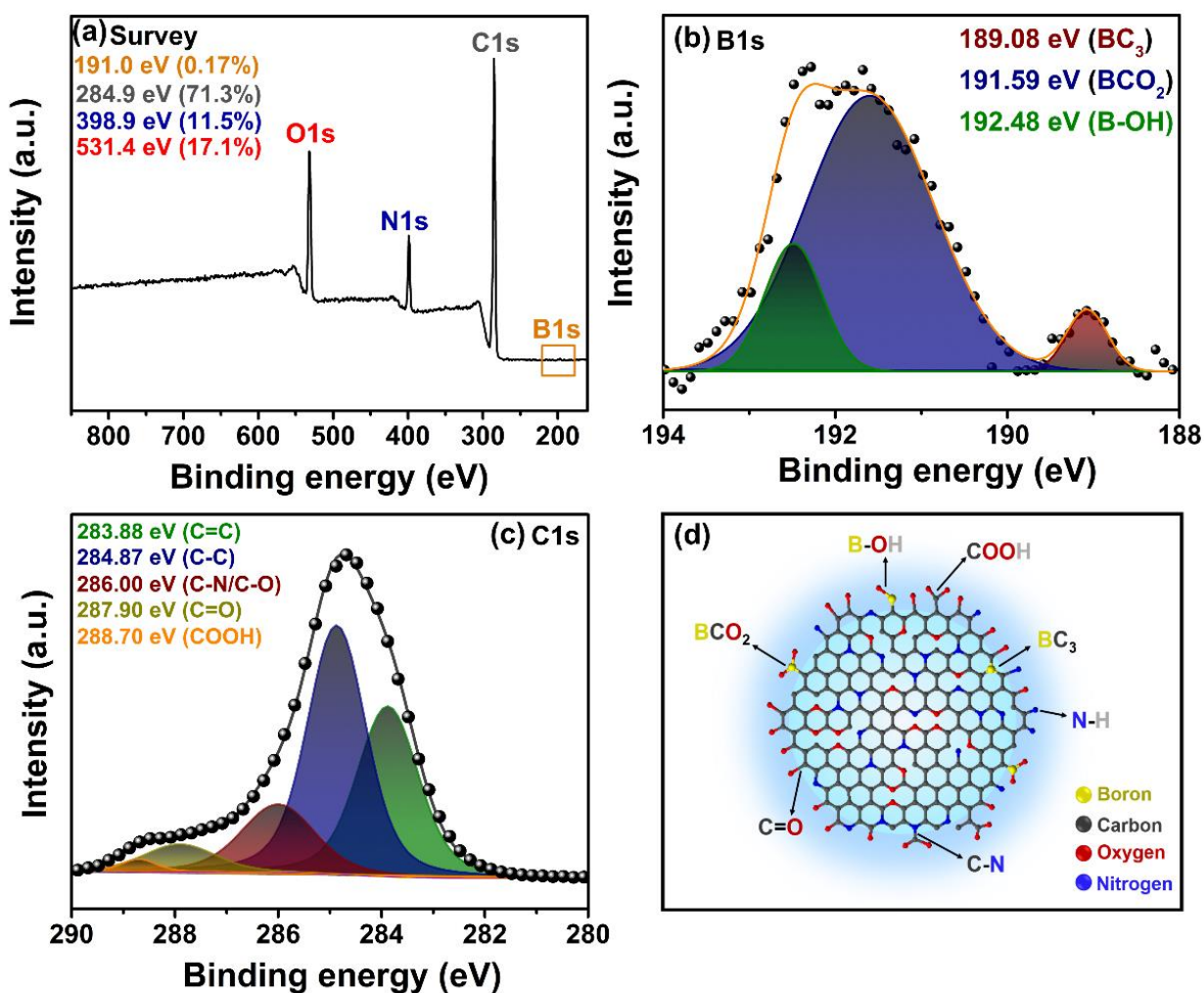
respectively. In accordance to FTIR results, the ^1H NMR showed δ_{H} of carbon dot type-structure: peaks around 0.95 – 3.17 ppm are characteristic of sp^3 C-H protons; 3.37 – 6.17 ppm can be related to sp^3 C-H protons alpha to hydroxyl, carbonyl, ether and amino groups; and a peak at 8.48 ppm can be related to sp^2 C-H protons from aromatic groups. Indeed, according to ^{13}C NMR spectrum in Appendix F(b), the sp^2 graphitic carbon network in the B,N-Cdot is also confirmed through appearance of peaks at 111.96 and 128.66 ppm related to sp^2 carbons of C=C from aromatic rings. In the ^{13}C NMR spectrum is also observed peaks around 48.95 – 85.50 ppm that are characteristic of aliphatic sp^3 and sp^2 carbons of hydroxyl and ether groups, and peaks around 180.23 – 189.90 ppm can be related to carbons of C=O from carboxylic acid groups (HUANG *et al.*, 2019).

XPS measurements were also performed to analyze additional structural insight into B,N-Cdot nanoparticles, principally regarding the doping with boron. Figure 27 (a) presents the survey scan spectrum of B,N-Cdot, which revealed four apparent binding peaks at 191.0, 284.9, 398.9 and 531.4 eV, corresponding to the signals originated from B1s, C1s, N1s and O1s, respectively. The calculated atomic percentage of B, C, N and O are 0.17, 71.3, 11.5 and 17.1%, respectively, confirming the doping of boron and functionalization with nitrogen on the nanoparticles. The lower boron content can be explained by the difficulty in doping the CQDs framework with this element, since it presents an electron deficiency, and an incompatibility, considering Pauling electronegativity values, of 2.04 for boron in comparison to 2.55 for carbon (MA *et al.*, 2020). Due to low boron concentration, a magnification was performed in the region between 186 and 195 eV. After noise smoothing, the high-resolution spectrum B1s was analyzed. In Figure 27 (b), the peaks identified at 189.08, 191.59 and 192.48 eV can be related to BC_3 , BCO_2 and B-OH bonds, respectively (JIA *et al.*, 2021; MA *et al.*, 2020).

As shown in Figure 27 (c), the deconvolution spectrum of C1s revealed five peaks at 283.88, 284.87, 286.00, 287.90 and 288.70 eV, corresponding to the C=C (sp^2 , graphitic), C-C (aliphatic), C-N/C-O, C=O and COOH groups, respectively (DING *et al.*, 2016; LU *et al.*, 2016; STEFANAKIS *et al.*, 2014). Moreover, the high-resolution XPS spectrum of N1s (Appendix G(a)) also exhibited three prominent peaks at 399.72, 400.58 and 401.88 eV, revealing the presence of the C-N-C, N-C₃ and N-H bonds, respectively (HOU *et al.*, 2014). The broad high-resolution XPS spectrum of O1s, as seen in Appendix G(b), is split into three peaks centered at 530.18, 531.53 and 532.81 eV, corresponding to C=O, C-O and B-O bonds, respectively (JANA *et al.*, 2019). This result is in good agreement with FTIR, Raman and NMR spectroscopy. Based on these results, we proposed the chemical structure of B,N-Cdot

illustrated in Figure 27 (d), in order to further evaluate the interaction mechanism with NO_2^- ions.

Figure 27 – (a) XPS survey; (b) C1s and (c) B1s high-resolution spectra of B,N-Cdot; (d) structure proposal of B,N-Cdot (hydrogen atoms have been omitted for simplification).

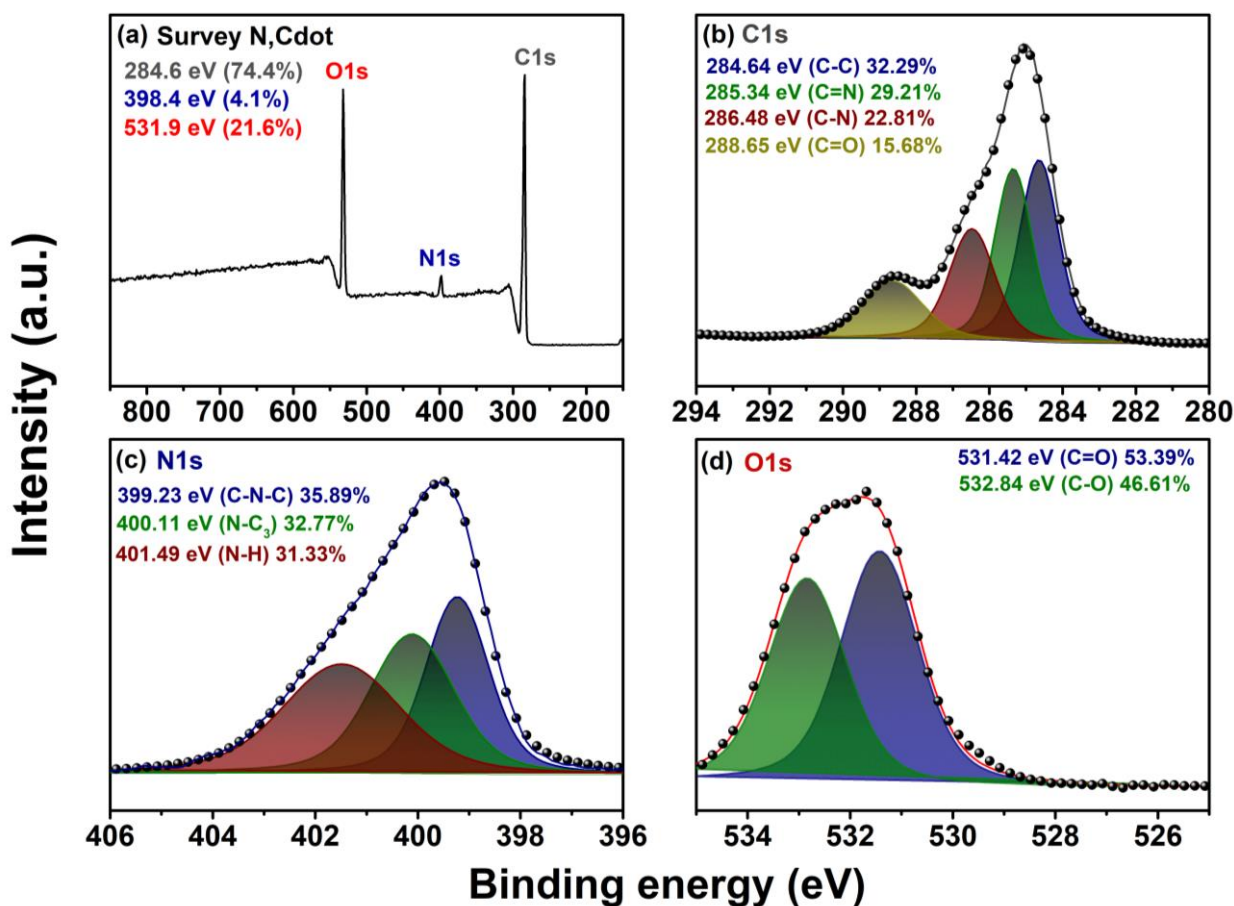


Source: Author.

In order to compare the surface defects of the B,N-Cdot with the N-Cdot, the XPS spectrum of this sample also was recorded and is shown in Figure 28. Comparing with Figure 27 (a), we can easily see in Figure 28 (a) an decrease in the nitrogen content in B,N-Cdot, suggesting that the reaction of citric acid with *b*PEI was favored in the presence of boric acid. Furthermore, according to the C1s high-resolution spectra, the B,N-Cdot presents a greater amount of carbon atoms with sp^3 hybridization (60.45%), while Figure 28 (b) reveals 55.10%

to the N-Cdot sample. Furthermore, Figures 28 (c) and (d) show other chemical bonds present in the N-Cdot structure.

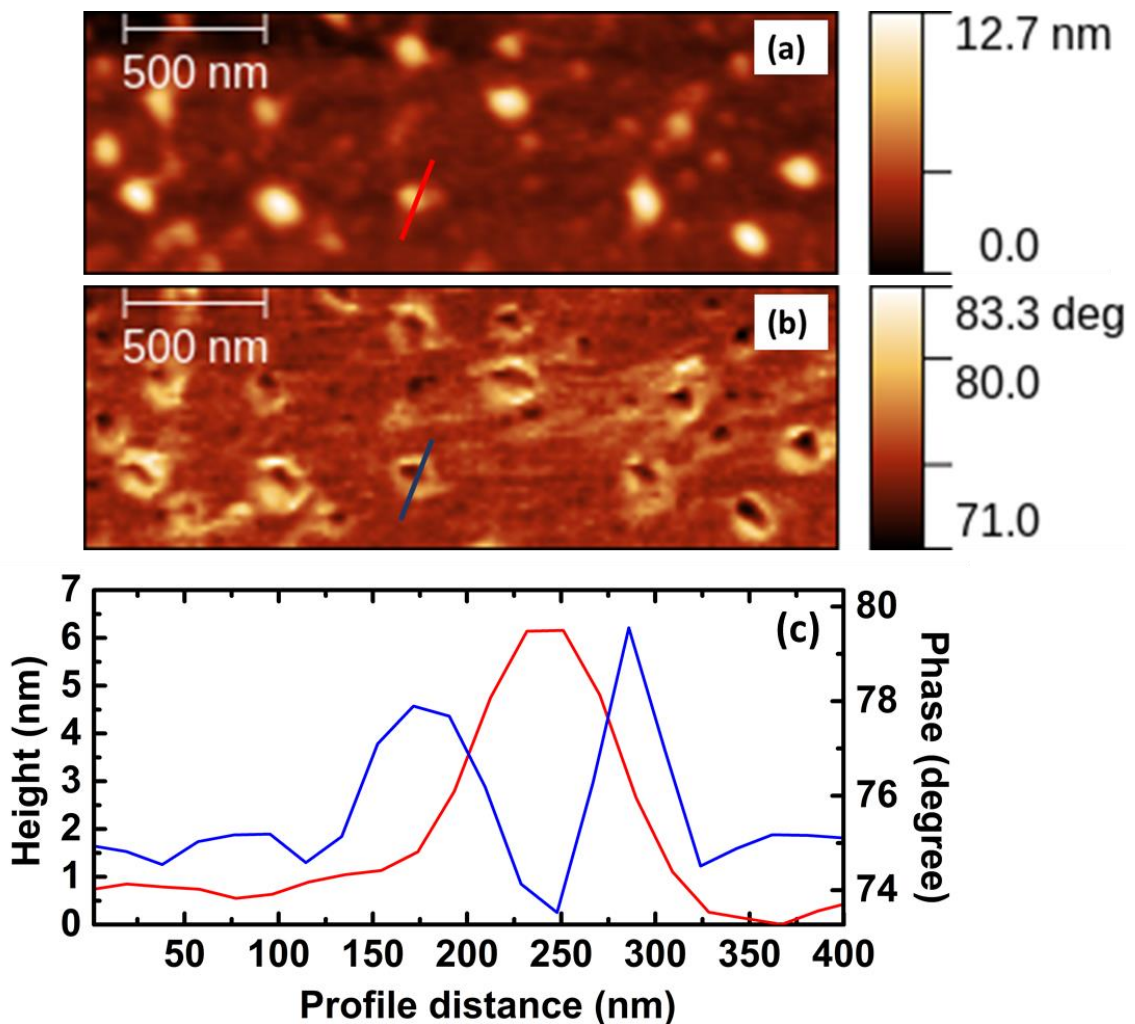
Figure 28 – (a) XPS survey; (b) C1s; (c) N1s and (d) O1s high-resolution spectra of N-Cdot.



Source: Author.

The morphology of B,N-Cdot was analyzed by Atomic Force Microscopy (AFM) operating in a tapping mode configuration. Clearly, a core-shell nanostructure is identified through the AFM topography image presented in Figure 29 (a). As expected, this type-structure is observed since the polymer *b*PEI was used as precursor. Thereby, it can be inferred that the core is composed by carbon atoms, whereas the shell can be rich in amine groups. In addition, a nanomaterial with quasi-spherical morphology can be observed in the AFM phase image in Figure 29 (b). In the topographical height profile (Figure 29 (c)), a particle size value around 4.0-6.0 nm was identified, which is similar to other studies using *b*PEI as CQDs precursor (GUO *et al.*, 2019; ZHANG *et al.*, 2017).

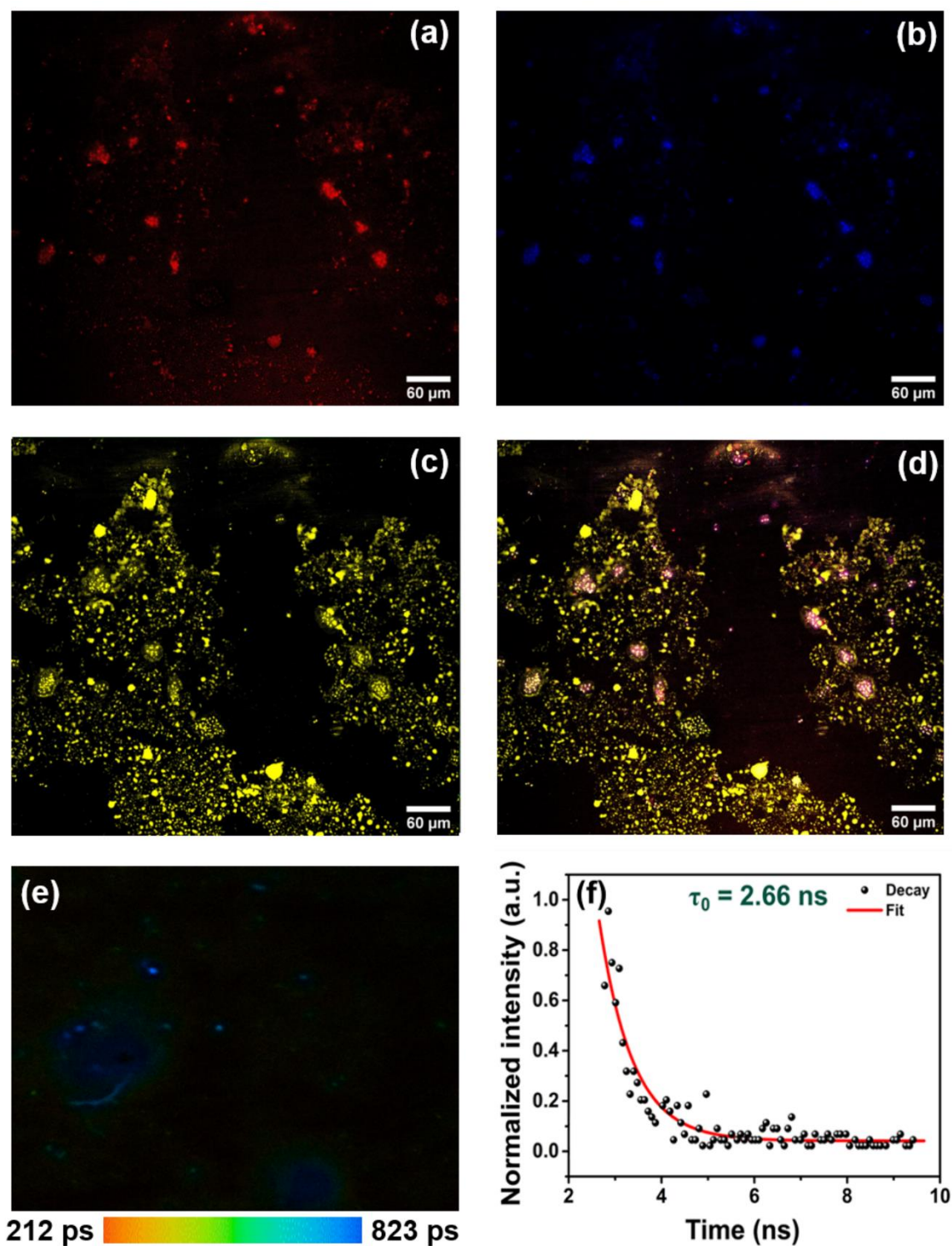
Figure 29 – AFM images of B,N-Cdot: (a) topography; (b) phase and (c) AFM section height profile of a particle. The AFM scanning was performed over a 5 μm x 5 μm region.



Source: Author.

LSCM images were obtained for different emissions of B,N-Cdot excited at 405, 488 and 561 nm, as shown in Figure 30 (a), (b) and (c), respectively. The color of each channel is given by the excitation wavelength. The brightness of each channel was chosen to smallest maximum that color saturation and the smallest minimum that extract the noisy background. The merge of the recorded images was applied as shown in Figure 30 (d). However, for the overlay of the channels, we ensure a maximum contrast, choosing the colors blue, yellow and red, making it easier to visualize what features appear or do not appear in each channel. The scale of the confocal images is visualized in 60 μm , so the aggregates of B,N-Cdot are evidenced. Clearly, the existence of spherical aggregates is confirmed by this technique in good agreement with AFM results.

Figure 30 – Confocal microscopy analysis of B,N-Cdot dried film with emission at: (a) 405nm; (b) 488nm; (c) 561 nm and (d) the super positioning of the channels. (e) FLIM image with a heat-map indicating the short and long life-time decays; (f) histogram of the life-time decays frequency.



Source: Author.

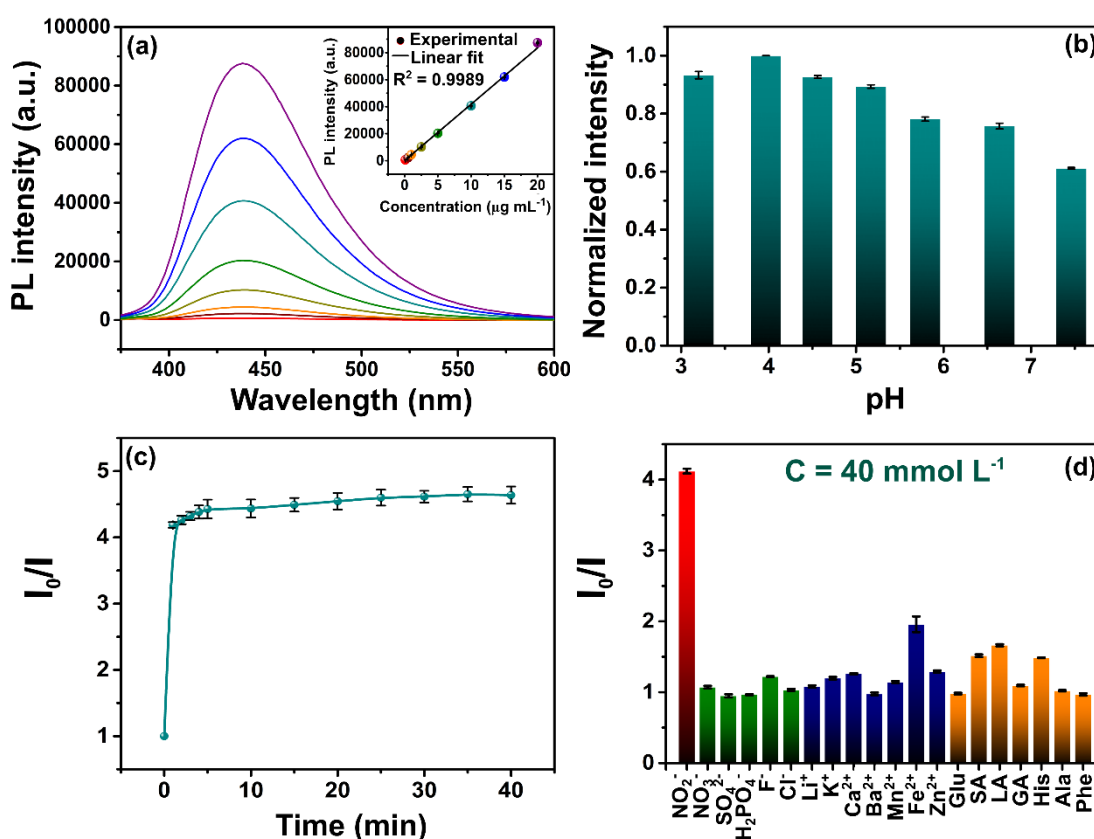
FLIM measurements were performed with 405 nm excitation to obtain the fluorescence life-time in 40 μm scale. Figure 30 (e) shows the heat-map indicating the short and long life-time decays ranging from 212 to 823 ps. A histogram of the life-time decays frequency scanned in this range is presented in Appendix H. From this result, we estimate the life-time value for B,N-Cdot sample, which can be further used to calculate K_Q and other thermodynamic parameters. As shown in Figure 30 (f), we obtained the value of 2.66 ns for the life-time with the experimental points and the fitted exponential decay curve. Comparatively, Ma and co-workers obtained boron-doped CQDs with a life-time value of 4 ns (MA *et al.*, 2020). Other studies revealed that CQDs functionalized with nitrogen had a life-time in this range (HU; LI; JIN, 2017; LI *et al.*, 2016). The shorter B,N-Cdot life-time value can be explained by the radiative recombination of excitons that give rise to fluorescence in nitrogen-functionalized CQDs (YANG *et al.*, 2014). Thus, the value obtained by the FLIM measurements will be used later to elucidate the mechanism of interaction between B,N-Cdot and NO_2^- ions.

4.3.2 Optimization of experimental conditions for sensing of NO_2^-

After spectroscopic and structural characterizations, the fluorescence properties of B,N-Cdot were evaluated, as well as the best experimental conditions. In order to determine the optimal amount of the fluorescent probe in the NO_2^- sensing, the fluorescence intensity of the system at different concentrations of the B,N-Cdot was evaluated. Thus, Figure 31 (a) shows that as the concentration of B,N-Cdot increases, the fluorescence intensity also increases. The determination coefficient obtained was 0.9989, proving the linearity of the analyzed range. Also, the self-quenching effect was not observed, which could directly affect the sensing strategy, which would provide a decrease in the fluorescence intensity of the system by nanoparticles aggregation. Considering the determined ideal concentration range, the value of $5.0 \mu\text{g mL}^{-1}$ was chosen for all further tests. As seen in the inset of Figure 31 (a), this point is within the linear range and a high fluorescence intensity can be clearly observed. Therefore, using this concentration of B,N-Cdot, a slightly change in fluorescence intensity can be visually observed after the addition of NO_2^- ions.

Figure 31 – Fluorescence-response evaluation of B,N-Cdot at different experimental conditions: (a) concentration effect of B,N-Cdot on fluorescence and PL intensity as a function of concentration (inset); (b) effect of pH in the B,N-Cdot fluorescence intensity; (c) kinetic

study of the interaction between B,N-Cdot and NO_2^- ions at concentration of 40 mmol L^{-1} ; (d) fluorescence intensity in presence of possible interferences at concentration of 40 mmol L^{-1} . All average and standard deviation values were calculated based on triplicate experiments. Legend: Glu = glucose; SA = succinic acid; LA = lactic acid; GA = glutamic acid; His = histidine; Ala = alanine; Phe = phenylalanine.



Source: Author.

The pH of the medium is also another relevant parameter to be evaluated, since meat generally has a slightly acidic pH. Thus, the effect of acidic pH on the fluorescence intensity of B,N-Cdot was investigated. The results are shown in Figure 31 (b). As the pH of the medium becomes more acidic, there is an increase in the fluorescence intensity of the B,N-Cdot until pH 4.0. This can be explained by the protonation of the amine and carboxyl groups present on the surface of the nanoparticle. As a consequence, an increase of the electrostatic repulsion is expected, exposing the surface defects, and rising the intensity of fluorescence. Indeed, at acidic pH, ~ 3.0 , there is a slight decrease in fluorescence intensity, which suggests that the amine groups are fully protonated and a particle aggregation process takes place. Dong and collaborators observed similar behavior analyzing the PL response as a function of pH

(DONG *et al.*, 2012). Therefore, considering PL response with pH, a PBS buffer solution of pH 7.4 was used to avoid any possible variation of pH level. Additionally, PBS buffer can mimic the physiological medium, which it is characteristic of meat products. In this type of product, NO_2^- ions can be added to improve quality. However, abusive concentrations need to be easily detected in order to prevent any harm to consumer's health.

The kinetic study of the interaction between B,N-Cdot and NO_2^- ions demonstrates that the analyte rapidly quenches the fluorescence of the probe, since there is a quick decrease in the value of the PL intensity, I in relation to initial I_0 , evidenced by the increase in the I_0/I ratio. Thus, the PL intensity achieves a stable status within 2.5 min, as shown in Figure 31 (c). In this assay, the concentration of 40 mmol L^{-1} of NO_2^- was used, and the equilibrium state was quickly reached, around 2 min. A shorter equilibrium time is generally favorable for detection in a real sample of meat, in order to obtain a fast result and without any additional effects in PL intensity. Perhaps, in this work, the equilibrium time for quenching was slightly shorter than that obtained by Zhang *et al* (ZHANG *et al.*, 2016), which observed a stable time of interaction between NO_2^- ions and nitrogen-functionalized CQDs around 5 min. Herein, all measurements were performed after 2 min quenching in subsequent experiments. Over this time of interaction, a variation in the fluorescence intensity was no longer observed, proving that an interaction between the nanoparticles and the analyte has already occurred, and evidencing a system saturation.

To determine the selectivity of the B,N-Cdot in the detection of NO_2^- , an evaluation of the changing in fluorescence intensity in the presence of other species was also performed. Figure 31 (d) shows the tests for possible interferents, such as anions (green bars), cations (blue bars) and biomolecules (orange bars). These species were selected considering the nature of the fresh meat. Given the obtained results, it can be inferred that only Fe^{2+} ions and biomolecules, SA, LA and His, affect the fluorescence intensity. However, the concentration of all species was maintained at 40 mmol L^{-1} , as this value already show a high quenching of B,N-Cdot fluorescence in presence of NO_2^- ions. This means that, in practice, the four species are interfering due to their high concentration, which has been extrapolated in order to stress the system and verify the maximum selectivity.

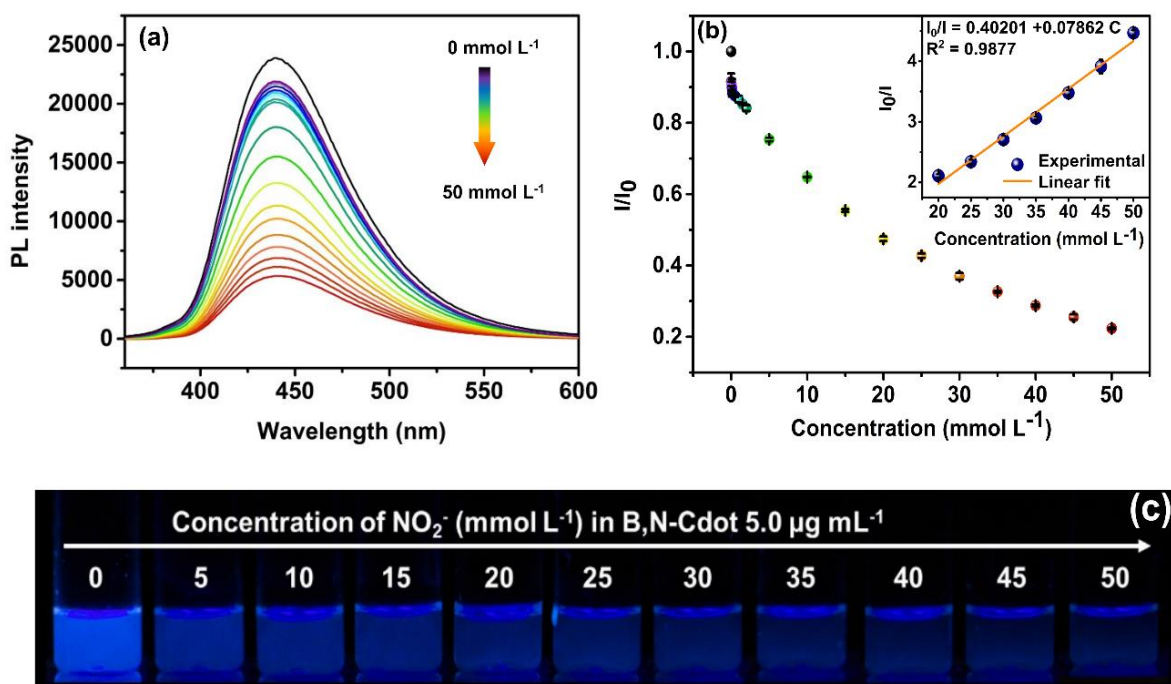
Another relevant point, it is the fluorescence response showed negligible interference for other ions, including NO_3^- , which presents a chemical structure similar to nitrite. The striking difference between the species is the delocalization of the electronic cloud of nitrite ions. This resonance profile of NO_2^- provides a stronger chemical interaction with

boron-doped nanoparticle regions, stabilizing these electron-deficient regions and explaining the high selectivity of the sensing strategy (JANA *et al.*, 2019).

4.3.3 Sensing of NO_2^- and thermodynamic assays

After knowing the intrinsic properties of B,N-Cdot and optimizing the experimental conditions of the system, the sensing tests were performed. Initially, a titration curve was built using different concentrations of the analytical standard of NaNO_2 in PBS at pH 7.4. As displayed in Figure 32 (a), the PL intensity of the B,N-Cdot around 435 nm decreased gradually with the increasing of NO_2^- concentration (0–50 mmol L^{-1}).

Figure 32 – Titration curve of sample B,N-Cdot with different concentrations of NO_2^- ions at 298.65 K in PBS 7.4: (a) effect of the concentration of quencher on the fluorescence of the system; (b) relative fluorescence intensity as a function of NO_2^- concentration and linear range of high concentrations used for nitrite sensing (inset); (c) Photographs of the sample of B,N-Cdot in the presence of different concentrations of NO_2^- used in the construction of the titration curve. All average and standard deviation values were calculated based on triplicate experiments.

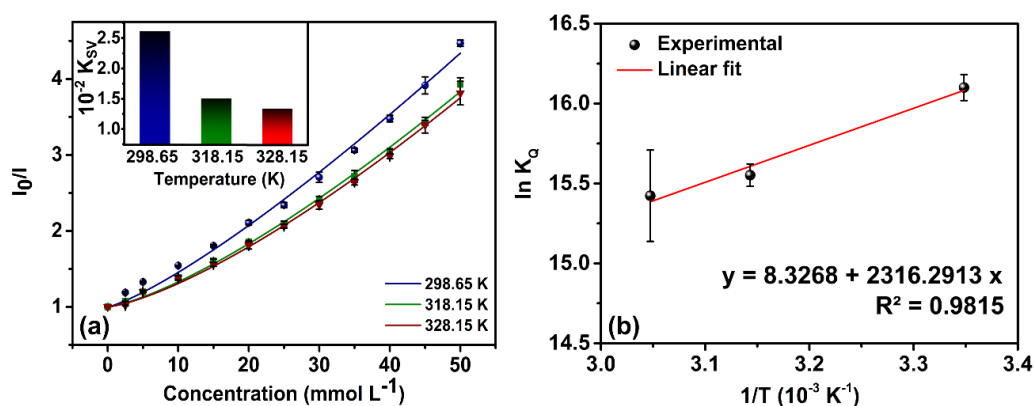


Source: Author.

A detailed relationship between fluorescence quenching level (I/I_0) and the concentration of quencher was shown in Figure 32 (b). Clearly, it is possible to visualize the system saturation at concentrations of NO_2^- above 30 mmol L^{-1} , where the I/I_0 ratio tend to become constant. As indicated in the inset of Figure 32 (b), a linear correlation graph ($R^2 = 0.9877$) was obtained between I_0/I and NO_2^- concentration in the studied range. Figure 32 (c) shows the visualization of the fluorescence quenching of B,N-Cdot in the presence of NO_2^- ions under UV light. It is possible to observe the potential of platform sense for field analysis, since the presence of the analyte can be detected macroscopically.

The mechanism of the proposed sensing system was carefully studied and the experimental data were adjusted to the Stern-Volmer mathematical model. This study was carried out under three temperatures, 298.65, 318.15 and 328.15 K, to determine the thermodynamic parameters of the interaction process between B,N-Cdot and NO_2^- ions. According to Figure 33 (a) the increase of temperature from 298.65 to 328.15 K causes a decrease in the K_{SV} value, may inferring that the quenching of B,N-Cdots by NO_2^- ions is initiated by a non-fluorescent complex formation, and a static quenching mechanism takes place as the dominant mechanism due to adsorption of the ions on the B,N-Cdot surface. (GHALI, 2010).

Figure 33 – (a) Titration curves of B,N-Cdot and NO_2^- ions at different temperatures and K_{SV} values in function of temperature (inset); (b) Graph obtained from the Van't Hoff equation. All average and standard deviation values were calculated based on triplicate experiments.



Source: Author.

According to Figure 33 (a), all values showed an excellent fit to the Stern-Volmer equation since $R^2 > 0.99$ under three different temperatures. Using the life-time value of 2.66

ns, obtained from the FLIM measurements, the K_Q values were calculated. Table 10 shows that calculated ΔG° values were obtained, -39.9, -41.1 and -42.1 kJ mol⁻¹, for the temperatures of 298.65, 318.15 and 328.15 K, respectively. Negative ΔG° values mean that the process of interaction between B,N-Cdot and NO₂⁻ ions is spontaneous. In addition, Figure 33 (b) shows that these thermodynamic results could be well adjusted to the Van't Hoff equation ($R^2 > 0.98$). The slope extracted from linear regression is equal to $-\Delta H^\circ/R$ and the intercept is $\Delta S^\circ/R$. In this perspective, the values obtained for ΔH° and ΔS° were -19.2 kJ mol⁻¹ and 69.2 J K⁻¹ mol⁻¹, respectively. It is also observed that the ΔH° value is negative, showing that the interaction process is exothermic, with the release of energy from the system. Regarding ΔS° value, it was observed that there is an increase in the entropy of the system, which is the result of a greater degree of disorganization of the species after mixing. In fluorescence systems, positive entropy variation is frequently taken as evidence of electrostatic interaction (BARBERO *et al.*, 2009).

Table 10 – Thermodynamic and quenching parameters for interaction between NO₂⁻ and B,N-Cdot at different temperatures.

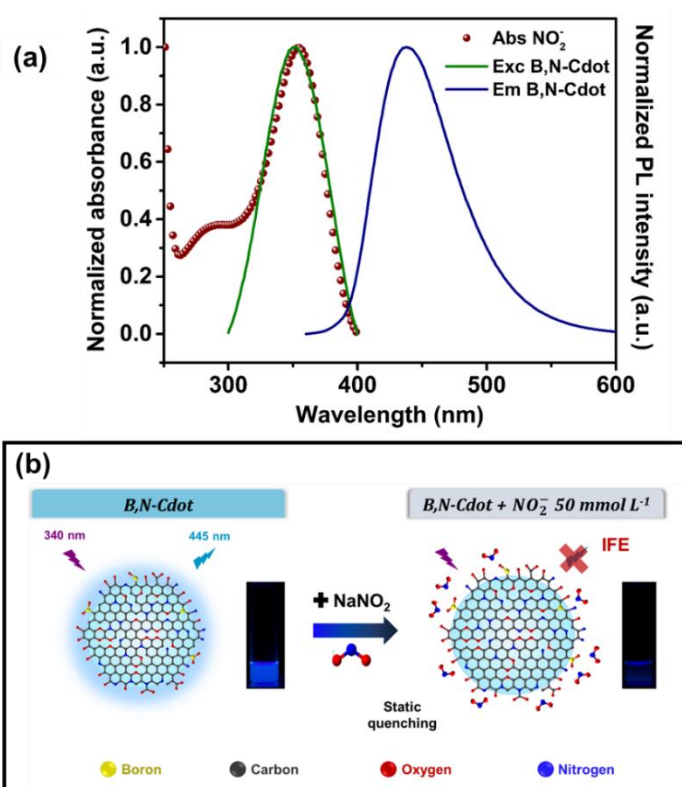
Parameter	Temperature (K)		
	298.65	318.15	328.15
n	1.2398 ± 0.0223	1.3379 ± 0.0202	1.3636 ± 0.0709
K_Q (10 ⁶)	9.8452 ± 0.8237	5.6867 ± 0.3986	5.1316 ± 1.5104
ΔG° (kJ mol ⁻¹)	-39.9097 ± 0.2028	-41.1366 ± 0.1855	-42.0781 ± 0.7787
ΔH° (kJ mol ⁻¹)		-19.2576 ± 4.2151	
ΔS° (J K ⁻¹ mol ⁻¹)		69.2290 ± 14.2679	

Source: Author.

Besides static quenching, the inner filter effect (IFE) is a mechanism most commonly found in the literature when studying the interaction of CQDs with NO₂⁻ ions (LIU *et al.*, 2019; SUN *et al.*, 2021). IFE is related to an apparent attenuation of the fluorescence due to the absorption of the emitted radiation by species present in the detection system (LIU *et al.*, 2019). IFE-based fluorescent assay happens efficiently only when the absorption peak of the absorber has a complementary overlap with the excitation and/or emission bands of the fluorophore, as shown in Figure 34 (a). Therefore, in this work, the overall fluorescence quenching mechanism of B,N-Cdot by NO₂⁻ is a combination of static quenching and IFE. In view of the chemical structure obtained for the B,N-Cdot and of the proposed mechanism,

Figure 34 (b) illustrates fluorescence quenching, when a concentration of 50 mmol L⁻¹ of NO₂⁻ is added to the suspension of nanoparticles.

Figure 34 – (a) UV-Vis absorption spectrum (Abs NO₂⁻), excitation spectrum of B,N-Cdot (Exc B,N-Cdot) and emission spectrum of B,N-Cdot (Em B,N-Cdot) for evaluation of spectral overlap and confirmation of IFE; (b) quenching mechanism expected by the interaction of B,N-Cdots and NO₂⁻ ions.



Source: Author.

After verifying the power of detection of analytical patterns of NO₂⁻ by B,N-Cdot and investigating the mechanism of interaction of the nanoprobe with the analyte, the sensing was applied to meat samples. In this type of sample, the NO₂⁻ ion can be found in concentrations above those permitted by ANVISA (0.015 g per 100 g of product), when this additive is used in order to preserve the meat for long periods. Thus, the collected chilled blood sample was diluted 300-folds with distilled water. Further, the diluted samples were analyzed after spiking with standard concentrations of NO₂⁻ (20, 30, 40 and 50 mmol L⁻¹) and recovery experiments were performed. The recoveries were found to range from 91.4 to 104%, and relative standard deviation (RSD) values were less than 0.90% (Table 11), indicating that the B,N-Cdots could be applied in detecting NO₂⁻ in meat samples.

Table 11 – Determination of the NO_2^- concentration in meat samples using the proposed strategy.

Spiked (mmol L ⁻¹)	Found (mmol L ⁻¹)	Recovery (% n = 3)	RSD (n = 3)
50.0	48.76	97.5	0.49
40.0	41.56	104	0.90
30.0	27.43	91.4	0.16
20.0	20.15	101	0.57

Source: Author.

As presented, in the developed sensing platform, a high concentration range was used, to allow the detection of NO_2^- in real samples. For instance, the fluorescent probe can detect very high concentrations of the analyte, which can be used to mask the quality of the meat. In this perspective, Table 12 summarizes the highest concentration detected the linear range and the QY of the synthesized CQD, when compared with other works in the literature.

Table 12 – Comparison of the proposed method with earlier reported literature toward the detection of NO_2^- .

Fluorescent probe	Precursor (s)	Concentration highest detected (mmol L ⁻¹)	Linear range (μmol L ⁻¹)	QY (%)	Reference
P,N-doped CQDs	Ascorbic acid, phosphoric acid and PEI	0.400	2 – 100	3.80	(JIANG, Y. <i>et al.</i> , 2019)
N-doped CQDs	p-phenylenediamine and citric acid	0.100	8 – 100	4.80	(JIA <i>et al.</i> , 2019)
N-doped CQDs	Chitosan	0.500	1 – 500	35.0	(SUN <i>et al.</i> , 2021)
CQDs	Folic acid and nicotinic acid	0.800	8 – 800	11.8	(GAN <i>et al.</i> , 2020)
B,N-doped CQD (B,N-Cdot)	Citric acid, Boric acid and bPEI	50.0	20000 – 50000	44.3	This work

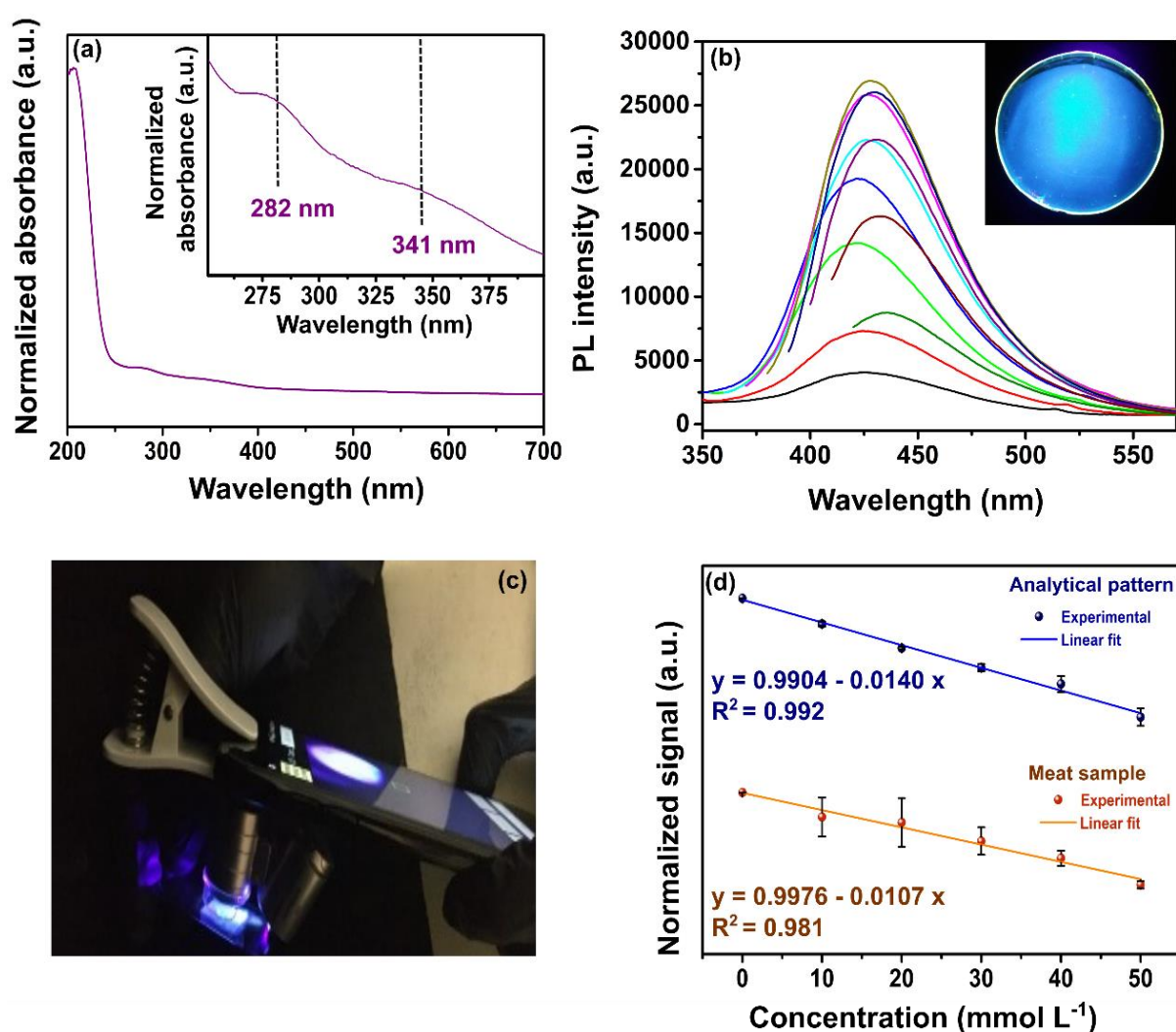
Source: Author.

4.3.4 PVA/B,N-Cdot nanocomposite and field analysis device

After the development of the sensing platform, a proposal for sensing the NO_2^- ions were developed for field analysis. Therefore, a B,N-Cdot-based nanocomposite was prepared using PVA film as polymeric matrix and an aqueous suspension of CQDs with a concentration of 1.07 mg g^{-1} . The UV-Vis spectrum of the as-prepared film was measured as shown in Figure 35 (a). In comparison to the CQD suspension, the absorption features of B,N-Cdot in the solid-state slightly changed. It was observed that the band at 241 nm was shifted to 206 nm, and bands in the regions of 280 and 340 nm were observed with a lower absorption intensity, due to the effect of the polymer matrix, contributing to the aggregation of the nanoparticles in the solid phase. With a lower exposure of the functional groups present on the surface of B,N-Cdot, it is expected a lower intensity of absorption in the dot films. Then, an accurate investigation of this region was carried out, as shown in the inset of the Figure 35 (a). The bands located at 282 and 341 nm were assigned to the $\pi \rightarrow \pi^*$ and $n \rightarrow \pi^*$ B,N-Cdot transitions, respectively, similar to those found in aqueous suspension (CARVALHO *et al.*, 2019). In Appendix I(a), the absorption spectrum of the PVA film is observed and it is verified that these bands are not present. Therefore, we can confirm that the optical properties of B,N-Cdot were maintained in the nanocomposite.

The next step was the recording of the fluorescence spectra. In Figure 35 (b), it is possible to observe that the film has a small bathochromic displacement (425-436 nm), considering the excitation range from 300 to 400 nm, as compared to the suspension of B,N-Cdot. A possible explanation for this phenomenon is the contribution of the hydroxyl functional group (-OH) of PVA to the electrophilic nature of B,N-Cdot. Since CQDs have a conjugated π electron structure, the electron donor group provides a stronger interaction, raising the energy level of the HOMO orbital and producing a narrow and small optical gap (EL-SHAMY; ZAYIED, 2020) However, even with the displacement of the emission peak, it was observed that the fluorescence intensity remains high up to 400 nm. This result is consistent with the inset of the Figure 35 (b), where it is clearly observed a high light emission in the blue region when the film is excited at a wavelength of 360 nm. Furthermore, it is important to highlight that the fluorescence spectrum PVA, as measured in excitation wavelength of 340 nm, showed a negligible fluorescence intensity, in comparison to nanocomposite, as shown in Appendix I(b).

Figure 35 – Development of the field device for the analysis of NO_2^- containing a thin film of the PVA/B,N-Cdot nanocomposite: (a) UV-Vis spectrum of the obtained film and magnification of the region between 250 and 400 nm; (b) photoluminescence spectra of the film at different excitation wavelengths (300 to 400 nm with an increment of 10 nm) and image of the film under irradiation of 360 nm of a UV light (inset); (c) photograph of an analysis of NO_2^- ions using the developed field device by aid of a pocket microscope and a smartphone; (d) result of the NO_2^- analysis using analytical pattern (blue curve) and meat sample (orange curve) from the Photometrix app. This experiment was performed with the channel of colors B of the app in three replicates.



Source: Author.

Considering the fluorescence response and the detection of nitrite ions for the PVA/B,N-Cdot nanocomposite, we proposed a device containing the thin film. The high quantum yield of the sample facilitated this process and with the aid of a glass substrate, a

pocket microscope and the Photometrix app, we propose the strategy presented in Figure 35 (c) for analysis of the NO_2^- ions. Considering all fixed distances and a square piece of the nanocomposite previously prepared with an area of 1 cm^2 , the fluorescence signals were recorded by the smartphone camera. Subsequently, the Photometrix app allowed the construction of the calibration curve shown in Figure 35 (d), using the NaNO_2 analytical standard and the same procedure with the meat sample, diluted 300-folds with distilled water. Further, the diluted sample was analyzed after spiking with the standard concentration of NO_2^- (10, 20, 30, 40 and 50 mmol L^{-1}). A single drop was taken from each stock solution and added to the device. The quenching of fluorescence occurs in both cases in a similar way that was observed in aqueous suspension. There is clearly a linear relationship between the normalized signal and the concentration of the analyte since the values of $R^2 = 0.992$ for the curve with analytical pattern and $R^2 = 0.981$ for the curve of the real sample were obtained. Given these results, we can infer that the developed device has a high potential to be used in meat analysis, in order to verify the abusive addition of NO_2^- ions as a conserving of the meat color.

4.4 Conclusion

We have successfully reported a new NO_2^- ion sensing platform based on boron and nitrogen CQDs fluorescence quenching mechanism. This work also explains in detail how to construct a simple, low-cost device with the aid of a polymeric PVA matrix with B,N-Cdots. However, to reach this level of practicality, we did a screening of possibilities for the synthesis of CQDs, from which we were able to conclude that doping with boron and functionalizing with nitrogen resulted in nanoparticles with a higher quantum yield, 44.2%. Then, the results of structural characterization helped to explain the interaction mechanism of B,N-Cdot with NO_2^- ions. Nevertheless, the sensing strategy proved that there is a high selectivity to the analyte studied and that it could be applied in the determination of high concentrations of NO_2^- ions in meat samples with a recovery of 100.76% at the concentration of 20 mmol L^{-1} of the analyte. This result proved the high detection power of the fluorescent probe in view of the quantification of NO_2^- ions in a range above that allowed in the legislation. Thereby, it was proposed to develop a sensor based on PVA/B,N-Cdot nanocomposite. The results also showed a high efficiency in the detection of high concentrations of NO_2^- ions in the solid phase. Therefore, a field analysis device has been developed, which could be used as a suitable alternative to conventional analysis methods.

CHAPTER V

5 GENERAL CONCLUSIONS

The development of nanomaterials is a target of nanotechnology and fantastic benefits to humanity can be achieved when investigating the properties of advanced materials, such as CQDs. Encouraged by the great advances in this field, the present thesis lists the results obtained in the search for new alternatives to sensing food additives. Therefore, in this work, CQDs were a fundamental part of the development of chemical sensors, which had the chemometric tools of multivariate analysis and the optical signals of fluorescence as coadjuvants for sensors array and turn-off sensing, respectively. Furthermore, a sensor more practical were developed, from the incorporation of CQDs in a thin film of PVA, constituting a potentially applicable nanocomposite in field analysis.

About the first work, involving the synthesis and characterization of CQDs from natural sources to sense different types of food additives, fulfilling the specific objectives a), b) and c), we can conclude that:

- FM-CDs were successfully synthesized by the hydrothermal method, using a natural source of a seed popularly known as “flamboyant mirim”;
- These carbon nanoparticles were structurally characterized and a particle size in the range of 0.5 - 4.0 nm was observed, which together with the functional groups present on the surface explain their characteristic fluorescence;
- The fluorescence signal of FM-CDs was altered in the presence of the tested food additives (citric acid, lactic acid, ascorbic acid, sodium benzoate and potassium sorbate), after optimized experimental conditions (FM-CD concentration = 1 mg mL⁻¹ and neutral pH);
- It was built a sensing platform using LDA chemometric tools and the strategy proved to be highly sensitive, with a LOD value equal to 252 ng mL⁻¹ was obtained for the sodium benzoate additive. In view of this exceptional result, the strategy was applied to a real sample of preserved olives and the classification matrix showed 100% accuracy in classifying the analytes, considering only two canonical factors.

In the second work, on the synthesis of CQDs with high QY to develop a field analysis sensor, fulfilling the specific objectives d), e) and f), we reach the following conclusions:

- B,N-Cdot proved to be an excellent alternative for sensing NO_2^- ions in meat;
- To fully exploit the potential of CQDs as a sensor, four hydrothermal syntheses were performed to select the sample with the highest QY. In this sense, B,N-Cdot was the selected sample with a QY equal to 44.3%;
- After structurally characterizing the nanoparticles and optimizing the experimental conditions (B,N-Cdot concentration = $5.0 \mu\text{g mL}^{-1}$, pH = 7.4 interaction time = 2 min), sensing was carried out;
- B,N-Cdot was highly selective for NO_2^- ions, according to the proposed interference test. Thus, the mixture of BNCdot with the analytical standard of NO_2^- in PBS resulted in a static quenching, via IFE mechanism, enabling the development of a turn-off sensor;
- In view of the previous conclusion, it was possible to migrate the strategy to the solid phase and a PVA/B,N-Cdot nanocomposite was obtained. This thin film has been successfully applied to detect nitrite ions in real meat samples in a range from $10\text{-}50 \text{ mmol L}^{-1}$.

Finally, as a general conclusion, it is expected that this work will bring great enrichment to the literature on nanomaterials applied to chemical sensing. Appendix J presents the scientific contribution generated with the results obtained in this thesis. The experimental results proved that it is possible to develop such sensors on a laboratory scale, but also to take them to the field, facilitating the quality control of food products. Thus, a powerful alternative tool for the analysis of food additives will be offered, which will ensure benefits to the food production chain and consumer health.

REFERENCES

- ABDULLAEVA, Z. *et al.* Solvothermal Synthesis of Surface-Modified Graphene/C and Au-Fe₃O₄ Nanomaterials for Antibacterial Applications. **Materials Today: Proceedings**, [s. l.], v. 4, n. 7, p. 7044–7052, 2017.
- ADINARAYANA AVINASH CHUNDURI, Lakshmi *et al.* Single Step Synthesis of Carbon Quantum Dots from Coconut Shell: Evaluation for Antioxidant Efficacy and Hemotoxicity. **Journal of Materials Sciences and Applications**, [s. l.], v. 3, n. 6, p. 83–93, 2017. Disponível em: <http://www.aascit.org/journal/jmsa>. Acesso em: 9 fev. 2020.
- AF, Shaikh *et al.* Bioinspired Carbon Quantum Dots: An Antibiofilm Agents. **Journal of nanoscience and nanotechnology**, [s. l.], v. 19, n. 4, p. 2339–2345, 2019. Disponível em: <https://pubmed.ncbi.nlm.nih.gov/30486995/>. Acesso em: 1 set. 2021.
- AHMED, Gaber Hashem Gaber *et al.* Fluorescent carbon nanodots for sensitive and selective detection of tannic acid in wines. **Talanta**, [s. l.], v. 132, p. 252–257, 2015.
- ALARFAJ, Nawal Ahmad; EL-TOHAMY, Maha Farouk; ORABY, Hesham Farouk. CA 19-9 pancreatic tumor marker fluorescence immunosensing detection via immobilized carbon quantum dots conjugated gold nanocomposite. **International Journal of Molecular Sciences**, [s. l.], v. 19, n. 4, 2018. Disponível em: <http://www.ncbi.nlm.nih.gov/pubmed/29641488>. Acesso em: 9 fev. 2020.
- ALAVI, Mehran; JABARI, Erfan; JABBARI, Esmail. Functionalized carbon-based nanomaterials and quantum dots with antibacterial activity: a review. **Expert review of anti-infective therapy**, [s. l.], v. 19, n. 1, p. 35–44, 2021. Disponível em: <https://pubmed.ncbi.nlm.nih.gov/32791928/>. Acesso em: 4 jan. 2022.
- ALFÈ, Michela *et al.* Mesoporous TiO₂ from Metal-Organic Frameworks for Photoluminescence-Based Optical Sensing of Oxygen. **Catalysts** **2021**, Vol. **11**, Page **795**, [s. l.], v. 11, n. 7, p. 795, 2021. Disponível em: <https://www.mdpi.com/2073-4344/11/7/795/htm>. Acesso em: 10 out. 2021.
- AL-HASHIMI, Baraa; OMER, Khalid M.; RAHMAN, Heshu S. Inner filter effect (IFE) as a simple and selective sensing platform for detection of tetracycline using milk-based nitrogen-doped carbon nanodots as fluorescence probe. **Arabian Journal of Chemistry**, [s. l.], v. 13, n. 4, p. 5151–5159, 2020.
- ALI, Mumtaz *et al.* Microwave-assisted ultrafast in-situ growth of N-doped carbon quantum dots on multiwalled carbon nanotubes as an efficient electrocatalyst for photovoltaics. **Journal of Colloid And Interface Science**, [s. l.], 2020.
- AMALI, R. K.A. *et al.* Significance of nanomaterials in electrochemical sensors for nitrate detection: A review. **Trends in Environmental Analytical Chemistry**, [s. l.], v. 31, p. e00135, 2021.
- AN, Qingxiao *et al.* Electrochemical synthesis of carbon dots with a Stokes shift of 309 nm for sensing of Fe³⁺ and ascorbic acid. **Dyes and Pigments**, [s. l.], v. 185, p. 108878, 2021.

AN, Rui *et al.* Photostability and Photodegradation Processes in Colloidal CsPbI₃ Perovskite Quantum Dots. **ACS Applied Materials and Interfaces**, [s. l.], v. 10, n. 45, p. 39222–39227, 2018.

ANWAR, Ayaz *et al.* Synthesis of gold nanoparticles stabilized by a pyrazinium thioacetate ligand: A new colorimetric nanosensor for detection of heavy metal Pd(II). **Sensors and Actuators B: Chemical**, [s. l.], v. 257, p. 875–881, 2018.

ARAÚJO, Cleide S. T. *et al.* Moringa oleifera Lam. seeds as a natural solid adsorbent for removal of AgI in aqueous solutions. **Journal of the Brazilian Chemical Society**, [s. l.], v. 21, n. 9, p. 1727–1732, 2010.

ASLAM, Maria; *et al.* Determination of sodium benzoate in selected samples of fruit juices and squashes. **Ajahs**, [s. l.], v. 2, n. 1, p. 26–31, 2017.

ASLAN, Mikail; ESKALEN, Hasan. A study of carbon nanodots (carbon quantum dots) synthesized from tangerine juice using one-step hydrothermal method. **Fullerenes Nanotubes and Carbon Nanostructures**, [s. l.], v. 0, n. 0, p. 1–8, 2021.

ATCHUDAN, Raji *et al.* Leftover Kiwi Fruit Peel-Derived Carbon Dots as a Highly Selective Fluorescent Sensor for Detection of Ferric Ion. **Chemosensors 2021, Vol. 9, Page 166**, [s. l.], v. 9, n. 7, p. 166, 2021. Disponível em: <https://www.mdpi.com/2227-9040/9/7/166/htm>. Acesso em: 10 out. 2021.

ATCHUDAN, Raji *et al.* Sustainable synthesis of carbon quantum dots from banana peel waste using hydrothermal process for in vivo bioimaging. **Physica E: Low-Dimensional Systems and Nanostructures**, [s. l.], v. 126, p. 114417, 2021.

ATHIKA, Mattath *et al.* Carbon-quantum dots derived from denatured milk for efficient chromium-ion sensing and supercapacitor applications. **Materials Letters**, [s. l.], v. 241, p. 156–159, 2019. Disponível em: <https://www.sciencedirect.com/science/article/abs/pii/S0167577X19300965>. Acesso em: 10 set. 2019.

AYAZ, Saniya *et al.* Tunable ultraviolet sensing performance of Al-modified ZnO nanoparticles. **Journal of Alloys and Compounds**, [s. l.], v. 884, p. 161113, 2021.

BANG, Jae Hoon *et al.* Decoration of multi-walled carbon nanotubes with CuO/Cu₂O nanoparticles for selective sensing of H₂S gas. **Sensors and Actuators B: Chemical**, [s. l.], v. 344, p. 130176, 2021.

BANO, Daraksha *et al.* Synthesis of highly fluorescent nitrogen-rich carbon quantum dots and their application for the turn-off detection of cobalt (II). **Optical Materials**, [s. l.], v. 92, p. 311–318, 2019.

BAPTISTA, Frederico R. *et al.* Recent developments in carbon nanomaterial sensors. **Chemical Society Reviews**, [s. l.], v. 44, n. 13, p. 4433–4453, 2015. Disponível em: <https://pubs.rsc.org/en/content/articlehtml/2015/cs/c4cs00379a>. Acesso em: 2 set. 2021.

BARBERO, Nadia *et al.* A study of the interaction between fluorescein sodium salt and bovine serum albumin by steady-state fluorescence. **Dyes and Pigments**, [s. l.], v. 80, n. 3, p. 307–313, 2009. Disponível em: <https://www.sciencedirect.com/science/article/abs/pii/S0143720808001228>. Acesso em: 23 jun. 2019.

BASIRI, Sedigheh; MEHDINIA, Ali; JABBARI, Ali. A sensitive triple colorimetric sensor based on plasmonic response quenching of green synthesized silver nanoparticles for determination of Fe²⁺, hydrogen peroxide, and glucose. **Colloids and Surfaces A: Physicochemical and Engineering Aspects**, [s. l.], v. 545, p. 138–146, 2018.

BAYATI, Mohamed *et al.* Effect of water chemistry on the aggregation and photoluminescence behavior of carbon dots. **Journal of Environmental Sciences (China)**, [s. l.], v. 65, p. 223–235, 2018.

BELHUMEUR, P.N.; HESPANHA, J.P.; KRIEGMAN, D.J. Eigenfaces vs. Fisherfaces: recognition using class specific linear projection. **IEEE Transactions on Pattern Analysis and Machine Intelligence**, [s. l.], v. 19, n. 7, p. 711–720, 1997. Disponível em: <http://ieeexplore.ieee.org/document/598228/>. Acesso em: 18 jun. 2019.

BENER, Mustafa; ŞEN, Furkan Burak; APAK, Reşat. Novel pararosaniline based optical sensor for the determination of sulfite in food extracts. **Spectrochimica Acta - Part A: Molecular and Biomolecular Spectroscopy**, [s. l.], v. 226, 2020.

BHARATHI, D. *et al.* Understanding the interaction of carbon quantum dots with CuO and Cu₂O by fluorescence quenching. **Journal of Hazardous Materials**, [s. l.], v. 369, p. 17–24, 2019. Disponível em: <https://www.sciencedirect.com/science/article/pii/S0304389419301384>. Acesso em: 4 maio 2019.

BOZKURT, Ebru; GUL, Halise Inci. Fluorescence quenching of novel pyrazoline derivative with aniline in different solvents. **Journal of Photochemistry and Photobiology A: Chemistry**, [s. l.], v. 383, p. 111996, 2019.

CALDERÓN-JIMÉNEZ, B.; JOHNSON, M. E.; MONTORO BUSTOS, A. R.; MURPHY, K. E.; WINCHESTER, M. R.; BAUDRIT, J. R. V. Silver nanoparticles: Technological advances, societal impacts, and metrological challenges. **Frontiers in Chemistry**, v. 5, n. Feb, p. 6, 2017.

CALINK I. L. SANTOS *et al.* Síntese E Caracterização De Pontos Quânticos Ambientalmente Amigáveis, Um Meio Simples De Exemplificar E Explorar Aspectos Da Nanociência E Nanotecnologia Em Cursos De Graduação. **Química Nova**, [s. l.], v. 43, n. 6, p. 813–822, 2020.

CAO, Nan *et al.* A fluorescent sensor array based on silver nanoclusters for identifying heavy metal ions. **Microchemical Journal**, [s. l.], v. 159, p. 105406, 2020.

CAO, Yunrui *et al.* **Recent advances of molecularly imprinted polymer-based sensors in the detection of food safety hazard factors** *Biosensors and Bioelectronics* Elsevier Ltd, , 2019.

CARAMAZANA, Pablo *et al.* A review of the environmental impact of nanomaterial synthesis using continuous flow hydrothermal synthesis. **Current Opinion in Green and Sustainable Chemistry**, [s. l.], v. 12, p. 57–62, 2018.

CARNEIRO CRUZ, Antônio Alvernes *et al.* Fluorescence Based Platform to Discriminate Protein Using Carbon Quantum Dots. **ChemistrySelect**, [s. l.], v. 4, n. 19, p. 5619–5627, 2019. Disponível em: <https://onlinelibrary.wiley.com/doi/abs/10.1002/slct.201901014>. Acesso em: 26 jan. 2020.

CARNEIRO, S. V. *et al.* Highly sensitive sensing of food additives based on fluorescent carbon quantum dots. **Journal of Photochemistry and Photobiology A: Chemistry**, [s. l.], v. 411, p. 113198, 2021.

CARNEIRO, S. V. *et al.* Sensing strategy based on Carbon Quantum Dots obtained from riboflavin for the identification of pesticides. **Sensors and Actuators, B: Chemical**, [s. l.], v. 301, 2019.

CARVALHO, Joston *et al.* Hydrothermal Synthesis to Water-stable Luminescent Carbon Dots from Acerola Fruit for Photoluminescent Composites Preparation and its Application as Sensors. **Materials Research**, [s. l.], v. 22, n. 3, 2019. Disponível em: <http://dx.doi.org/10.1590/1980-5373-MR-2018-0920>. Acesso em: 29 mar. 2021.

CHAI, Lu xiao *et al.* Low-dimensional nanomaterials enabled autoimmune disease treatments: Recent advances, strategies, and future challenges. **Coordination Chemistry Reviews**, [s. l.], v. 432, p. 213697, 2021.

CHAROENSUK, Jiraporn *et al.* A simple and sensitive colorimetric sensor for cadmium (II) detection based on self-assembled trimethyl tetradecyl ammonium bromide and murexide on colloidal silica. **Microchemical Journal**, [s. l.], v. 160, p. 105666, 2021.

CHEN, Hai; ZHOU, Kai; ZHAO, Guanghua. Gold nanoparticles: From synthesis, properties to their potential application as colorimetric sensors in food safety screening. **Trends in Food Science & Technology**, [s. l.], v. 78, p. 83–94, 2018.

CHEN, Hengye *et al.* Nanomaterials as optical sensors for application in rapid detection of food contaminants, quality and authenticity. **Sensors and Actuators B: Chemical**, [s. l.], v. 329, p. 129135, 2021.

CHEN, Jiao *et al.* Functionalization of inorganic nanomaterials with pillar[n]arenes. **Chemical Communications**, [s. l.], v. 55, n. 48, p. 6817–6826, 2019. Disponível em: <https://pubs.rsc.org/en/content/articlehtml/2019/cc/c9cc03165k>. Acesso em: 2 set. 2021.

CHEN, Li *et al.* A ratiometric fluorescence sensor based on metal-organic frameworks and quantum dots for detection of ascorbic acid. **Optical Materials**, [s. l.], v. 121, p. 111622, 2021.

CHEN, Liyong *et al.* Carbon dots prepared in different solvents with controllable structures: Optical properties, cellular imaging and photocatalysis. **New Journal of Chemistry**, [s. l.], v. 42, n. 3, p. 1690–1697, 2018. a.

CHEN, Shuai *et al.* Multichannel fluorescent sensor array for discrimination of thiols using carbon dot–metal ion pairs. **Sensors and Actuators B: Chemical**, [s. l.], v. 266, p. 553–560, 2018. b. Disponível em: <https://www.sciencedirect.com/science/article/pii/S0925400518306725>. Acesso em: 27 jun. 2019.

CHEN, Teng *et al.* Construction of Time-Resolved Luminescence Nanoprobe and Its Application in As(III) Detection. **Nanomaterials** **2020**, Vol. 10, Page 551, [s. l.], v. 10, n. 3, p. 551, 2020. Disponível em: <https://www.mdpi.com/2079-4991/10/3/551/htm>. Acesso em: 10 out. 2021.

CHEN, Tongming *et al.* A fluorescent and colorimetric probe of carbyne nanocrystals coated Au nanoparticles for selective and sensitive detection of ferrous ions. **Carbon**, [s. l.], v. 167, p. 196–201, 2020.

CHHABRA, Varun A. *et al.* Synthesis and spectroscopic studies of functionalized graphene quantum dots with diverse fluorescence characteristics. **RSC Advances**, [s. l.], v. 8, n. 21, p. 11446–11453, 2018.

CHI, Hong *et al.* GO film on flexible substrate: An approach to wearable colorimetric humidity sensor. **Dyes and Pigments**, [s. l.], v. 185, p. 108916, 2021.

CHINNATHAMBI, Selvaraj; EUVERINK, Gert Jan Willem. Hydrothermally reduced graphene oxide as a sensing material for electrically transduced pH sensors. **Journal of Electroanalytical Chemistry**, [s. l.], v. 895, p. 115530, 2021.

COSTA, Rafael Souza da *et al.* An Alternative Route to Obtain Carbon Quantum Dots from Photoluminescent Materials in Peat. **Materials**, [s. l.], v. 11, n. 9, 2018. Disponível em: </pmc/articles/PMC6164320/>. Acesso em: 22 ago. 2021.

CRUZ, A.A.C. *et al.* Optical Sensing Strategy Based on Carbon Quantum Dots. *In*: REFERENCE MODULE IN BIOMEDICAL SCIENCES. [S. l.]: Elsevier, 2021.

D, Li *et al.* A supersensitive silicon nanowire array biosensor for quantitating tumor marker ctDNA. **Biosensors & bioelectronics**, [s. l.], v. 181, 2021. Disponível em: <https://pubmed.ncbi.nlm.nih.gov/33773219/>. Acesso em: 21 out. 2021.

DA SILVA JÚNIOR, Afonso Henrique *et al.* Polymeric Blends of Carboxymethyl Cellulose and Sodium Alginate Containing Functionalized Carbon Dots Result in Stable and Efficient Fluorescent Films for Silver and Iron (III) Sensing. **Journal of Environmental Chemical Engineering**, [s. l.], v. 9, n. 4, p. 105728, 2021.

DAHMAN, Yaser. **Nanotechnology and functional materials for engineers**. [S. l.: s. n.], [s. d.].

DAN CHANG *et al.* Lysosome-targeted red-fluorescent carbon dots for turn-on detection of permanganate and pH in vivo and in vitro. **Sensors and Actuators B: Chemical**, [s. l.], v. 349, p. 130774, 2021.

DAS, Ananya *et al.* On the Molecular Origin of Photoluminescence of Nonblinking Carbon Dot. [*s. l.*], 2017.

DAS, Sharmistha; RAKSHIT, Soumyadipta; DATTA, Anindya. Mechanistic Insights into Selective Sensing of Pb²⁺ in Water by Photoluminescent CdS Quantum Dots. **Journal of Physical Chemistry C**, [*s. l.*], v. 125, n. 28, p. 15396–15404, 2021.

DAULBAYEV, Chingis *et al.* 0D, 1D and 2D nanomaterials for visible photoelectrochemical water splitting. A Review. **International Journal of Hydrogen Energy**, [*s. l.*], v. 45, n. 58, p. 33325–33342, 2020.

DE BARROS, Anerise *et al.* Functionalized Advanced Carbon-Based Nanomaterials for Sensing. **Reference Module in Biomedical Sciences**, [*s. l.*], 2021.

DE MEDEIROS, Tayline V. *et al.* Microwave-assisted synthesis of carbon dots and their applications. **Journal of Materials Chemistry C**, [*s. l.*], v. 7, n. 24, p. 7175–7195, 2019.

DE YRO, Persia Ada N. *et al.* Hydrothermal synthesis of carbon quantum dots from biowaste for bio-imaging. In: AIP CONFERENCE PROCEEDINGS 2019, **Anais...** : AIP Publishing LLC , 2019. Disponível em: <http://aip.scitation.org/doi/abs/10.1063/1.5094310>. Acesso em: 22 jul. 2019.

DING, Hui *et al.* Full-Color Light-Emitting Carbon Dots with a Surface-State-Controlled Luminescence Mechanism. **ACS Nano**, [*s. l.*], v. 10, n. 1, p. 484–491, 2016. Disponível em: <http://pubs.acs.org/doi/abs/10.1021/acs.nano.5b05406>. Acesso em: 20 abr. 2017.

DING, Hui *et al.* Solvent-Controlled Synthesis of Highly Luminescent Carbon Dots with a Wide Color Gamut and Narrowed Emission Peak Widths. **Small**, [*s. l.*], v. 14, n. 22, p. 1–10, 2018.

DING, Hui *et al.* Surface states of carbon dots and their influences on luminescence. **Journal of Applied Physics**, [*s. l.*], v. 127, n. 23, 2020.

DING, Hui; WEI, Ji Shi; XIONG, Huan Ming. Nitrogen and sulfur co-doped carbon dots with strong blue luminescence. **Nanoscale**, [*s. l.*], v. 6, n. 22, p. 13817–13823, 2014.

DING, Yuanfei *et al.* Synthesis of short-chain passivated carbon quantum dots as the light emitting layer towards electroluminescence. **RSC Advances**, [*s. l.*], v. 7, n. 46, p. 28754–28762, 2017. Disponível em: <https://pubs.rsc.org/en/content/articlehtml/2017/ra/c7ra02421e>. Acesso em: 4 jul. 2021.

DISSANAYAKE, Niluka M. *et al.* Highly sensitive plasmonic metal nanoparticle-based sensors for the detection of organophosphorus pesticides. **Talanta**, [*s. l.*], v. 200, p. 218–227, 2019.

DONG, Chen *et al.* An ultra-sensitive colorimetric sensor based on smartphone for pyrophosphate determination. **Sensors and Actuators B: Chemical**, [*s. l.*], v. 329, p. 129066, 2021.

DONG, Jing *et al.* Sensing Properties of NH₂-MIL-101 Series for Specific Amino Acids via Turn-On Fluorescence. **Molecules** **2021**, Vol. **26**, Page **5336**, [s. l.], v. 26, n. 17, p. 5336, 2021. Disponível em: <https://www.mdpi.com/1420-3049/26/17/5336/htm>. Acesso em: 10 out. 2021.

DONG, Ren E. *et al.* Cation-exchange strategy for a colorimetric paper sensor: Belt-like ZnSe nanoframes toward visual determination of heavy metal ions. **Sensors and Actuators B: Chemical**, [s. l.], v. 312, p. 128013, 2020.

DONG, Yongqiang *et al.* Polyamine-Functionalized Carbon Quantum Dots as Fluorescent Probes for Selective and Sensitive Detection of Copper Ions. **Analytical Chemistry**, [s. l.], v. 84, n. 14, p. 6220–6224, 2012. Disponível em: <http://pubs.acs.org/doi/abs/10.1021/ac3012126>. Acesso em: 20 abr. 2017.

DOROODMAND, Mohammad Mahdi; ASKARI, Mohsen. Synthesis of a novel nitrogen-doped carbon dot by microwave-assisted carbonization method and its applications as selective probes for optical pH (acidity) sensing in aqueous/nonaqueous media, determination of nitrate/nitrite, and optical recognition of NO_x gas. **Analytica Chimica Acta**, [s. l.], v. 968, p. 74–84, 2017.

DU, Fuyou *et al.* Development of sulfur doped carbon quantum dots for highly selective and sensitive fluorescent detection of Fe²⁺ and Fe³⁺ ions in oral ferrous gluconate samples. **Spectrochimica Acta Part A: Molecular and Biomolecular Spectroscopy**, [s. l.], v. 226, p. 117602, 2020.

DU, Na *et al.* Fluorescent Sensor Array Constructed by Functionalized Carbon Nanodots for Qualitative and Quantitative Analysis of Urinary Organic Acids Biomarkers. **Sensors and Actuators B: Chemical**, [s. l.], p. 130825, 2021

EDISON, Thomas Nesakumar Jebakumar Immanuel *et al.* Microwave assisted green synthesis of fluorescent N-doped carbon dots: Cytotoxicity and bio-imaging applications. **Journal of Photochemistry and Photobiology B: Biology**, [s. l.], v. 161, p. 154–161, 2016

EDVINSSON, T. Optical quantum confinement and photocatalytic properties in two-, one- and zero-dimensional nanostructures. **Royal Society Open Science**, [s. l.], v. 5, n. 9, 2018. Disponível em: <https://royalsocietypublishing.org/doi/abs/10.1098/rsos.180387>. Acesso em: 6 set. 2021.

EL-SHAMY, Ahmed G.; ZAYIED, H. S.S. New polyvinyl alcohol/carbon quantum dots (PVA/CQDs) nanocomposite films: Structural, optical and catalysis properties. **Synthetic Metals**, [s. l.], v. 259, p. 116218, 2020.

FAN, Tianju *et al.* Controllable size-selective method to prepare graphene quantum dots from graphene oxide. **Nanoscale Research Letters**, [s. l.], v. 10, n. 1, 2015. Disponível em: </pmc/articles/PMC4385023/>. Acesso em: 1 set. 2021.

FECHINE, P. B. A. Avanços no desenvolvimento de nanomateriais. 1. ed. Fortaleza: Imprensa universitária, 2020.

FERREIRA, Márcia Miguel Castro. **Quimiometria: conceitos, métodos e aplicações**. [S. l.]: Editora da Unicamp, 2015.

FLORES, Mónica; TOLDRÁ, Fidel. **Chemistry, safety, and regulatory considerations in the use of nitrite and nitrate from natural origin in meat products**. [S. l.]: Elsevier Ltd, 2021.

FREIRE, R. M. *et al.* NH₂-rich Carbon Quantum Dots: A protein-responsive probe for detection and identification. **Sensors and Actuators B: Chemical**, [s. l.], v. 255, p. 2725–2732, 2018. Disponível em: <https://www.sciencedirect.com/science/article/pii/S0925400517317513>. Acesso em: 5 maio. 2018

FU, Yanzhao *et al.* A carbon dots-based fluorescent probe for turn-on sensing of ampicillin. **Dyes and Pigments**, [s. l.], v. 172, p. 107846, 2020.

GAI, Wenxiao; ZHAO, Die Ling; CHUNG, Tai Shung. Novel thin film composite hollow fiber membranes incorporated with carbon quantum dots for osmotic power generation. **Journal of Membrane Science**, [s. l.], v. 551, p. 94–102, 2018.

GAN, Lanlan *et al.* Exploration of pH-responsive carbon dots for detecting nitrite and ascorbic acid. **Applied Surface Science**, [s. l.], v. 530, p. 147269, 2020.

GAN, Ziyu *et al.* A dual-emission fluorescence sensor for ultrasensitive sensing mercury in milk based on carbon quantum dots modified with europium (III) complexes. **Sensors and Actuators, B: Chemical**, [s. l.], v. 328, p. 128997, 2021

GANAIE, M.A.; TANVEER, M. Fuzzy least squares projection twin support vector machines for class imbalance learning. **Applied Soft Computing**, [s. l.], p. 107933, 2021. Disponível em: <https://linkinghub.elsevier.com/retrieve/pii/S1568494621008553>. Acesso em: 16 out. 2021.

GAO, Wenli *et al.* Carbon Dots with Red Emission for Sensing of Pt²⁺, Au³⁺, and Pd²⁺ and Their Bioapplications in Vitro and in Vivo. **ACS Applied Materials and Interfaces**, [s. l.], v. 10, n. 1, p. 1147–1154, 2018.

GEHLEN, Marcelo H. **The centenary of the Stern-Volmer equation of fluorescence quenching: From the single line plot to the SV quenching map**. [S. l.]: Elsevier B.V., 2020.

GELLINI, Cristina; FEIS, Alessandro. Optothermal properties of plasmonic inorganic nanoparticles for photoacoustic applications. **Photoacoustics**, [s. l.], v. 23, p. 100281, 2021

GHALI, M. Static quenching of bovine serum albumin conjugated with small size CdS nanocrystalline quantum dots. **Journal of Luminescence**, [s. l.], v. 130, n. 7, p. 1254–1257, 2010.

GONG, Tingyuan *et al.* A facile fabrication of colorimetric graphene oxide reflecting films for ultrasensitive optical gas sensing. **Sensors and Actuators B: Chemical**, [s. l.], v. 261, p. 83–90, 2018.

GONG, Xiao *et al.* Fabrication of high-performance luminescent solar concentrators using N-doped carbon dots/PMMA mixed matrix slab. **Organic Electronics**, [s. l.], v. 63, p. 237–243, 2018.

GUO, Jiexiong *et al.* Ultrasensitive acetone sensor based on holey zinc oxide nanosheets doped by gold nanoparticles. **Materials Letters**, [s. l.], v. 302, p. 130443, 2021.

GUO, Ruiting *et al.* Functionalized carbon dots for advanced batteries. **Energy Storage Materials**, [s. l.], v. 37, n. November 2020, p. 8–39, 2021.

GUO, Ying *et al.* Green fluorescent carbon quantum dots functionalized with polyethyleneimine, and their application to aptamer-based determination of thrombin and ATP. **Microchimica Acta**, [s. l.], v. 186, n. 11, p. 1–8, 2019. Disponível em: <https://doi.org/10.1007/s00604-019-3874-y>. Acesso em: 29 mar. 2021.

GUO, Yongming *et al.* Hydrothermal synthesis of nitrogen and boron doped carbon quantum dots with yellow-green emission for sensing Cr(VI), anti-counterfeiting and cell imaging. **RSC Advances**, [s. l.], v. 7, n. 76, p. 48386–48393, 2017. Disponível em: <https://pubs.rsc.org/en/content/articlehtml/2017/ra/c7ra09785a>. Acesso em: 23 mar. 2021.

HAMEED, Rafal. Synthesis and physical properties of nanocomposite gold nanoparticles attached to graphene quantum dots prepared by laser ablation. **Materials Today: Proceedings**, [s. l.], v. 42, p. 1829–1833, 2021.

HAMMAMI, Inès *et al.* Gold nanoparticles: Synthesis properties and applications. **Journal of King Saud University - Science**, [s. l.], v. 33, n. 7, p. 101560, 2021.

HAN, Suqin; CHEN, Xiaoxia. Copper nanoclusters-enhanced chemiluminescence for folic acid and nitrite detection. **Spectrochimica Acta - Part A: Molecular and Biomolecular Spectroscopy**, [s. l.], v. 210, p. 315–320, 2019.

HAO, Ai Yue *et al.* A smartphone-combined ratiometric fluorescence probe for specifically and visibly detecting cephalixin. **Spectrochimica Acta Part A: Molecular and Biomolecular Spectroscopy**, [s. l.], v. 249, p. 119310, 2021.

HATZAKIS, Emmanuel. Nuclear Magnetic Resonance (NMR) Spectroscopy in Food Science: A Comprehensive Review. **Comprehensive Reviews in Food Science and Food Safety**, [s. l.], v. 18, n. 1, p. 189–220, 2019. Disponível em: <http://doi.wiley.com/10.1111/1541-4337.12408>. Acesso em: 22 ago. 2020.

HELPER, Gilson A. *et al.* PhotoMetrix: An Application for Univariate Calibration and Principal Components Analysis Using Colorimetry on Mobile Devices. **Journal of the Brazilian Chemical Society**, [s. l.], v. 28, n. 2, p. 328–335, 2016. Disponível em: <http://www.gnresearch.org/doi/10.5935/0103-5053.20160182>. Acesso em: 10 set. 2019.

HOU, Juying *et al.* Nitrogen-doped photoluminescent carbon nanospheres: Green, simple synthesis via hair and application as a sensor for Hg²⁺ ions. **RSC Advances**, [s. l.], v. 4, n. 70, p. 37342–37348, 2014. Disponível em: <https://pubs.rsc.org/en/content/articlehtml/2014/ra/c4ra04209c>. Acesso em: 4 jul. 2021.

HU, Chao *et al.* **Design and fabrication of carbon dots for energy conversion and storage.** [S. l.]: Royal Society of Chemistry, 2019.

HU, Ruoxin; LI, Lili; JIN, Wei Jun. Controlling speciation of nitrogen in nitrogen-doped carbon dots by ferric ion catalysis for enhancing fluorescence. **Carbon**, [s. l.], v. 111, p. 133–141, 2017.

HU, Tingting *et al.* Two-dimensional nanomaterials: fascinating materials in biomedical field. **Science Bulletin**, [s. l.], v. 64, n. 22, p. 1707–1727, 2019.

HUANG, Caoxing *et al.* Synthesis of carbon quantum dot nanoparticles derived from byproducts in bio-refinery process for cell imaging and in vivo bioimaging. **Nanomaterials**, [s. l.], v. 9, n. 3, 2019. Disponível em: /pmc/articles/PMC6473984/. Acesso em: 23 mar. 2021.

HUANG, Gengli *et al.* Dual-emission carbon dots based ratiometric fluorescent sensor with opposite response for detecting copper (II). **Dyes and Pigments**, [s. l.], v. 196, p. 109803, 2021.

HUANG, Ying *et al.* Chaos to order: An eco-friendly way to synthesize graphene quantum dots. **RSC Advances**, [s. l.], v. 4, n. 81, p. 43160–43165, 2014. Disponível em: <https://pubs.rsc.org/en/content/articlehtml/2014/ra/c4ra06757f>. Acesso em: 4 jul. 2021.

HUANGFU, Changxin; FENG, Liang. High-performance fluorescent sensor based on CsPbBr₃ quantum dots for rapid analysis of total polar materials in edible oils. **Sensors and Actuators, B: Chemical**, [s. l.], v. 344, n. February, p. 130193, 2021.

HUO, Xingyan *et al.* Facile synthesis of yellowish-green emitting carbon quantum dots and their applications for phoxim sensing and cellular imaging. **Analytica Chimica Acta**, [s. l.], p. 338685, 2021.

JAIN, Gunisha *et al.* One-step synthesis of strongly confined, defect-free and hydroxy-terminated ZnO quantum dots. [s. l.], 2020.

JALAB, Joud *et al.* Green synthesis of silver nanoparticles using aqueous extract of *Acacia cyanophylla* and its antibacterial activity. **Heliyon**, [s. l.], v. 7, n. 9, p. e08033, 2021.

JANA, Jayasmita *et al.* Blue emitting nitrogen-doped carbon dots as a fluorescent probe for nitrite ion sensing and cell-imaging. **Analytica Chimica Acta**, [s. l.], v. 1079, p. 212–219, 2019.

JANSI SANTHOSAM, A.; RAVICHANDRAN, K.; AHAMAD, Tansir. Donated free electrons induced enhancement in the NH₃ sensing ability of ZnO thin films - Effect of terbium loading. **Sensors and Actuators A: Physical**, [s. l.], v. 316, p. 112376, 2020.

JI, Xiaoyuan *et al.* Fluorescent quantum dots: Synthesis, biomedical optical imaging, and biosafety assessment. **Colloids and Surfaces B: Biointerfaces**, [s. l.], v. 124, p. 132–139, 2014.

JIA, Jing *et al.* Orange Luminescent Carbon Dots as Fluorescent Probe for Detection of Nitrite. **Chinese Journal of Analytical Chemistry**, [s. l.], v. 47, n. 4, p. 560–566, 2019.

JIA, Mingyan *et al.* Carbon dots with dual emission: A versatile sensing platform for rapid assay of Cr (VI). **Carbon**, [s. l.], v. 182, p. 42–50, 2021.

JIANG, Jie *et al.* Amino acids as the source for producing carbon nanodots: microwave assisted one-step synthesis, intrinsic photoluminescence property and intense chemiluminescence enhancement. **Chemical Communications**, [s. l.], v. 48, n. 77, p. 9634–9636, 2012. Disponível em: <https://pubs.rsc.org/en/content/articlehtml/2012/cc/c2cc34612e>. Acesso em: 1 set. 2021.

JIANG, Shan *et al.* Highly sensitive detection of mercury(II) ions with few-layer molybdenum disulfide. **Nano Research** 2015 8:1, [s. l.], v. 8, n. 1, p. 257–262, 2015. Disponível em: <https://link.springer.com/article/10.1007/s12274-014-0658-x>. Acesso em: 4 set. 2021.

JIANG, Xiaohua *et al.* Facile Preparation of Boron and Nitrogen Codoped Green Emission Carbon Quantum Dots for Detection of Permanganate and Captopril. **Analytical Chemistry**, [s. l.], v. 91, n. 17, p. 11455–11460, 2019. Disponível em: <https://pubs.acs.org/doi/abs/10.1021/acs.analchem.9b02938>. Acesso em: 2 mar. 2021.

JIANG, Yong Jian *et al.* Nitrogen and phosphorus doped polymer carbon dots as a sensitive cellular mapping probe of nitrite. [S. l.]: **Royal Society of Chemistry**, 2019. Disponível em: <https://pubs.rsc.org/en/content/articlehtml/2019/tb/c8tb02998a>. Acesso em: 29 mar. 2021.

JIGYASA; PRATIBHA; RAJPUT, Jaspreet Kaur. Alkali metal (Na/ K) doped graphitic carbon nitride (g-C₃N₄) for highly selective and sensitive electrochemical sensing of nitrite in water and food samples. **Journal of Electroanalytical Chemistry**, [s. l.], v. 878, p. 114605, 2020.

JIMÉNEZ-SALCEDO, Marta; TENA, María Teresa. Determination of cinnamaldehyde, carvacrol and thymol in feedstuff additives by pressurized liquid extraction followed by gas chromatography–mass spectrometry. **Journal of Chromatography A**, [s. l.], v. 1487, p. 14–21, 2017.

JIN, Hui *et al.* Carrot-derived carbon dots modified with polyethyleneimine and Nile blue for ratiometric two-photon fluorescence turn-on sensing of sulfide anion in biological fluids. **Talanta**, [s. l.], v. 169, p. 141–148, 2017. Disponível em: <http://www.ncbi.nlm.nih.gov/pubmed/28411804>. Acesso em: 22 out. 2018.

JIN, Hui *et al.* Zero-dimensional sulfur nanomaterials: Synthesis, modifications and applications. **Coordination Chemistry Reviews**, [s. l.], v. 438, p. 213913, 2021.

JOHN, Varsha Lisa; NAIR, Yamuna; VINOD, T. P. Doping and Surface Modification of Carbon Quantum Dots for Enhanced Functionalities and Related Applications. **Particle and Particle Systems Characterization**, [s. l.], v. 2100170, p. 1–28, 2021.

KANNAN, Veera Prabu; MOUNASAMY, Veena; MADANAGURUSAMY, Sridharan. Highly volatile dimethylamine vapour sensing studies using titanium-vanadium mixed oxide thin films. **Materials Today: Proceedings**, [s. l.], 2021.

KARWOWSKA, Małgorzata; KONONIUK, Anna. Nitrates/Nitrites in Food—Risk for Nitrosative Stress and Benefits. **Antioxidants**, [s. l.], v. 9, n. 3, 2020. Disponível em: [/pmc/articles/PMC7139399/](https://pmc/articles/PMC7139399/). Acesso em: 5 out. 2021.

KAUR, Jasjot *et al.* Highly photoluminescent and pH sensitive nitrogen doped carbon dots (NCDs) as a fluorescent sensor for the efficient detection of Cr (VI) ions in aqueous media. **Spectrochimica Acta - Part A: Molecular and Biomolecular Spectroscopy**, [s. l.], v. 227, p. 117572, 2020.

KAUR, Jasleen; SINGH, Harminder. Fabrication and analysis of piezoelectricity in 0D, 1D and 2D Zinc Oxide nanostructures. **Ceramics International**, [s. l.], v. 46, n. 11, p. 19401–19407, 2020.

KAZEMIFARD, Nafiseh; ENSAFI, Ali A.; REZAEI, Behzad. Green synthesized carbon dots embedded in silica molecularly imprinted polymers, characterization and application as a rapid and selective fluorimetric sensor for determination of thiabendazole in juices. **Food Chemistry**, [s. l.], v. 310, p. 125812, 2020.

KEERTHI VASAN, K.; SURENDIRAN, B. Dimensionality reduction using Principal Component Analysis for network intrusion detection. **Perspectives in Science**, [s. l.], v. 8, p. 510–512, 2016.

KHAN, Zubair M. S. H. *et al.* Hydrothermal treatment of red lentils for the synthesis of fluorescent carbon quantum dots and its application for sensing Fe³⁺. **Optical Materials**, [s. l.], v. 91, p. 386–395, 2019. Disponível em: <https://www.sciencedirect.com/science/article/pii/S0925346719302253>. Acesso em: 23 jun. 2019.

KIM, Ji Won *et al.* Enrichment of nitrite in onion powder using atmospheric pressure plasma and egg whites for meat curing. **LWT**, [s. l.], v. 135, p. 110050, 2021.

KIM, Soogeun *et al.* A facile, portable surface-enhanced Raman spectroscopy sensing platform for on-site chemometrics of toxic chemicals. **Sensors and Actuators B: Chemical**, [s. l.], v. 343, p. 130102, 2021.

KOLAHALAM, Lalitha A. *et al.* Review on nanomaterials: Synthesis and applications. **Materials Today: Proceedings**, [s. l.], v. 18, p. 2182–2190, 2019.

KOULOUMPIS, Antonios *et al.* Graphene/Carbon Dot Hybrid Thin Films Prepared by a Modified Langmuir–Schaefer Method. **ACS Omega**, [s. l.], v. 2, n. 5, p. 2090–2099, 2017. Disponível em: <https://pubs.acs.org/doi/10.1021/acsomega.7b00107>. Acesso em: 9 fev. 2020.

KOUSHKESTANI, Marjan *et al.* Simultaneous detection and identification of thiometon, phosalone, and prothioconazole pesticides using a nanoplasmonic sensor array. **Food and Chemical Toxicology**, [s. l.], v. 151, p. 112109, 2021.

KUMAR, Naveen *et al.* **Chemometrics tools used in analytical chemistry: An overview**. [S. l.]: Elsevier B.V., 2014.

KUMAR, Pawan. Proceedings Semiconductor (CdSe and CdTe) quantum dot: Synthesis, properties and applications. **Materials Today: Proceedings**, [s. l.], n. xxxx, 2021.

KURDEKAR, Aditya *et al.* Comparative performance evaluation of carbon dot-based paper immunoassay on Whatman filter paper and nitrocellulose paper in the detection of HIV infection. **Microfluidics and Nanofluidics**, [s. l.], v. 20, n. 7, 2016. Disponível em: <https://link.springer.com/epdf/10.1007/s10404-016-1763-9>. Acesso em: 2 mar. 2021.

KWAN, Melvin Ng Hau *et al.* Carbon-dot dispersal in PVA thin film for food colorant sensing. **Journal of Environmental Chemical Engineering**, [s. l.], v. 8, n. 3, p. 103187, 2019.

LAKOWICZ, Joseph R. **Principles of fluorescence spectroscopy**. [S. l.]: Springer, 2006.

LE, Ngoc D. B. *et al.* Cancer Cell Discrimination Using Host–Guest “Doubled” Arrays. **Journal of the American Chemical Society**, [s. l.], v. 139, n. 23, p. 8008–8012, 2017. Disponível em: <http://pubs.acs.org/doi/10.1021/jacs.7b03657>. Acesso em: 12 dez. 2018.

LETE, Cecilia *et al.* Nitrite electrochemical sensing platform based on tin oxide films. **Sensors and Actuators, B: Chemical**, [s. l.], v. 316, p. 128102, 2020.

LI, Cheng *et al.* A hybrid CO₂ ratiometric fluorescence sensor synergizing tetraphenylethene and gold nanoclusters relying on disulfide functionalized hyperbranched poly(amido amine). **Sensors and Actuators B: Chemical**, [s. l.], v. 346, p. 130513, 2021.

LI, Chunying; WEI, Chunying. DNA-templated silver nanocluster as a label-free fluorescent probe for the highly sensitive and selective detection of mercury ions. **Sensors and Actuators B: Chemical**, [s. l.], v. 242, p. 563–568, 2017.

LI, Fan *et al.* Mg/N double doping strategy to fabricate extremely high luminescent carbon dots for bioimaging. **RSC Advances**, [s. l.], v. 4, n. 7, p. 3201–3205, 2014. Disponível em: <https://pubs.rsc.org/en/content/articlehtml/2014/ra/c3ra43826k>. Acesso em: 2 mar. 2021.

LI, Gen *et al.* Carbon Quantum Dots Functionalized g-C₃N₄ nanosheets as Enhanced Visible-light Photocatalysts for Water Splitting. **Diamond and Related Materials**, [s. l.], p. 108242, 2021. Disponível em: <https://linkinghub.elsevier.com/retrieve/pii/S0925963521000054>. Acesso em: 18 jan. 2021.

LI, Huiyu *et al.* Synthesis of tiny carbon dots with high quantum yield using multi-walled carbon nanotubes as support for selective “turn-off-on” detection of rutin and Al³⁺. **Carbon**, [s. l.], v. 143, p. 391–401, 2019.

LI, Linlin *et al.* A nano-sensing composite platform combining magnetic and emissive features: Fabrication and performance. **Journal of Photochemistry and Photobiology A: Chemistry**, [s. l.], v. 408, p. 113099, 2021.

LI, Ping *et al.* A novel photoluminescence sensing system sensitive for and selective to bromate anions based on carbon dots. **RSC Advances**, [s. l.], v. 6, n. 66, p. 61891–61896, 2016. Disponível em: <https://pubs.rsc.org/en/content/articlehtml/2016/ra/c6ra12936f>. Acesso em: 29 mar. 2021.

- LI, Qingqing; CHEN, Baoliang; XING, Baoshan. Aggregation Kinetics and Self-Assembly Mechanisms of Graphene Quantum Dots in Aqueous Solutions: Cooperative Effects of pH and Electrolytes. **Environmental Science & Technology**, [s. l.], v. 51, n. 3, p. 1364–1376, 2017. Disponível em: <https://pubs.acs.org/doi/10.1021/acs.est.6b04178>. Acesso em: 9 fev. 2020.
- LI, Wenting *et al.* A smartphone-integrated ratiometric fluorescence sensor for visual detection of cadmium ions. **Journal of Hazardous Materials**, [s. l.], v. 408, p. 124872, 2021.
- LI, Xiangcao *et al.* **Advances and perspectives in carbon dot-based fluorescent probes: Mechanism, and application**. [S. l.]: Elsevier B.V., 2020.
- LI, Xin; WANG, John. One-dimensional and two-dimensional synergized nanostructures for high-performing energy storage and conversion. **InfoMat**, [s. l.], v. 2, n. 1, p. 3–32, 2020. Disponível em: <https://onlinelibrary.wiley.com/doi/full/10.1002/inf2.12040>. Acesso em: 2 set. 2021.
- LI, Zheng; ASKIM, Jon R.; SUSLICK, Kenneth S. The Optoelectronic Nose: Colorimetric and Fluorometric Sensor Arrays. **Chemical Reviews**, [s. l.], v. 119, n. 1, p. 231–292, 2019.
- LIANG, Aihui *et al.* Resonance scattering spectral detection of catalase activity using Au@Ag nanoparticle as probe and coupling catalase catalytic reaction with Fenton reaction. **Journal of fluorescence**, [s. l.], v. 19, n. 6, p. 1009–1015, 2009. Disponível em: <https://pubmed.ncbi.nlm.nih.gov/19533309/>. Acesso em: 4 jan. 2022.
- LIANG, Nini *et al.* A dual-signal fluorescent sensor based on MoS₂ and CdTe quantum dots for tetracycline detection in milk. **Food Chemistry**, [s. l.], v. 378, p. 132076, 2022.
- LIANG, Nini *et al.* Fluorescence and colorimetric dual-mode sensor for visual detection of malathion in cabbage based on carbon quantum dots and gold nanoparticles. **Food Chemistry**, [s. l.], v. 343, p. 128494, 2021.
- LIN, Xing. Phonon-assisted up-conversion photoluminescence of quantum dots. **Nature Communications**, [s. l.], 2021.
- LINO, C. M.; PENA, A. Occurrence of caffeine, saccharin, benzoic acid and sorbic acid in soft drinks and nectars in Portugal and subsequent exposure assessment. **Food Chemistry**, [s. l.], v. 121, n. 2, p. 503–508, 2010.
- LIU, Fang *et al.* A BCNO QDs-MnO₂ nanosheets based fluorescence “off-on-off” and colorimetric sensor with smartphone detector for the detection of organophosphorus pesticides. **Analytica Chimica Acta**, [s. l.], v. 1184, p. 339026, 2021.
- LIU, Jianfei *et al.* Mitochondria-targeted NIR fluorescent probe for sensing Hg₂⁺/HSO₃⁻ and its intracellular applications. **Talanta**, [s. l.], v. 234, p. 122606, 2021.
- LIU, Lei; ZHANG, Liguo; LIANG, Yong. Visual sensing of multiple proteins based on three kinds of metal nanoparticles as sensor receptors. **Colloids and Surfaces B: Biointerfaces**, [s. l.], v. 200, p. 111574, 2021.

LIU, Liang; MANDLER, Daniel. Using nanomaterials as building blocks for electrochemical deposition: A mini review. **Electrochemistry Communications**, [s. l.], v. 120, n. August, p. 106830, 2020.

LIU, Meng Li *et al.* Carbon dots: Synthesis, formation mechanism, fluorescence origin and sensing applications. **Green Chemistry**, [s. l.], v. 21, n. 3, p. 449–471, 2019.

LIU, Xiaojin *et al.* Visual detection of edible oil oxidation by using chitin-based colorimetric sensor for aldehydes. **Colloids and Surfaces A: Physicochemical and Engineering Aspects**, [s. l.], v. 628, p. 127303, 2021.

LIU, Yushan *et al.* Hydrothermal synthesis of green fluorescent nitrogen doped carbon dots for the detection of nitrite and multicolor cellular imaging. **Analytica Chimica Acta**, [s. l.], v. 1090, p. 133–142, 2019.

LOISEAU, Alexis *et al.* Silver-Based Plasmonic Nanoparticles for and Their Use in Biosensing. **Biosensors**, [s. l.], v. 9, n. 2, 2019. Disponível em: /pmc/articles/PMC6627098/. Acesso em: 4 jan. 2022.

LONG MA, Zhi *et al.* A multi-responsive luminescent indicator based on a Zn(II) metal-organic framework with “Turn on” sensing of pyridine and “Turn off” sensing of Fe³⁺, Cr₂O₇²⁻ and antibiotics in aqueous media. **Inorganica Chimica Acta**, [s. l.], v. 526, p. 120513, 2021.

LU, Changfang *et al.* New properties of carbon nanomaterials through zinc doping and application as a ratiometric fluorescence pH sensor. **Materials Research Bulletin**, [s. l.], v. 142, p. 111410, 2021.

LU, Shousi *et al.* Hydrothermal synthesis of nitrogen-doped carbon dots with real-time live-cell imaging and blood-brain barrier penetration capabilities. **International Journal of Nanomedicine**, [s. l.], v. 11, p. 6325–6336, 2016. Disponível em: <https://pubmed.ncbi.nlm.nih.gov/27932880/>. Acesso em: 2 mar. 2021.

LU, Xingxu *et al.* Solvent effects on the heterogeneous growth of TiO₂ nanostructure arrays by solvothermal synthesis. **Catalysis Today**, [s. l.], v. 360, n. October 2019, p. 275–283, 2021.

LUDMERCZKI, Robert *et al.* Carbon Dots from Citric Acid and its Intermediates Formed by Thermal Decomposition. **Chemistry – A European Journal**, [s. l.], v. 25, n. 51, p. 11963–11974, 2019. Disponível em: <https://onlinelibrary.wiley.com/doi/abs/10.1002/chem.201902497>. Acesso em: 26 jan. 2020.

MA, Y. *et al.* Off-on fluorescent switching of boron-doped carbon quantum dots for ultrasensitive sensing of catechol and glutathione. **Carbon**, [s. l.], v. 162, p. 234–244, 2020.

MAGDY, Galal *et al.* Green one-pot synthesis of nitrogen and sulfur co-doped carbon quantum dots as new fluorescent nanosensors for determination of salinomycin and maduramicin in food samples. **Food Chemistry**, [s. l.], v. 343, p. 128539, 2021.

MALEKZADEH, Mohammad *et al.* Laser pyrolysis synthesis of zinc-containing nanomaterials using low-cost ultrasonic spray delivery of precursors. **Powder Technology**, [s. l.], v. 376, p. 104–112, 2020.

MALIK, Rinki *et al.* Carbon quantum dots intercalated in polypyrrole (PPy) thin electrodes for accelerated energy storage. **Electrochimica Acta**, [s. l.], v. 364, p. 137281, 2020.

MANJUNATHA, J. G. A novel voltammetric method for the enhanced detection of the food additive tartrazine using an electrochemical sensor. **Heliyon**, [s. l.], v. 4, n. 11, 2018.

MANOTO, Sello Lebohang *et al.* Exploring optical spectroscopic techniques and nanomaterials for virus detection. **Saudi Journal of Biological Sciences**, [s. l.], v. 28, n. 1, p. 78–89, 2021.

MARTINS, Fernanda C.O.L.; SENTANIN, Michelle A.; DE SOUZA, Djenaine. **Analytical methods in food additives determination: Compounds with functional applications**. [S. l.]: Elsevier Ltd, 2019.

MARTYANOV, Timofey P. *et al.* Selective colorimetric sensor for cyanide anion based on 1-hydroxyanthraquinone. **Tetrahedron**, [s. l.], v. 93, p. 132312, 2021.

MAŠIĆ, Alma *et al.* Estimation of nitrite in source-separated nitrified urine with UV spectrophotometry. **Water Research**, [s. l.], v. 85, p. 244–254, 2015.

MATEA, Cristian T. *et al.* Quantum dots in imaging, drug delivery and sensor applications. **International Journal of Nanomedicine**, [s. l.], v. 12, p. 5421–5431, 2017. Disponível em: <https://pubmed.ncbi.nlm.nih.gov/28814860/>. Acesso em: 27 nov. 2020.

MATHIYALAGAN, Siva; MANDAL, Badal Kumar; LING, Yong Chien. Determination of synthetic and natural colorants in selected green colored foodstuffs through reverse phase-high performance liquid chromatography. **Food Chemistry**, [s. l.], v. 278, p. 381–387, 2019.

MAXIM, Askar A. *et al.* PMMA Thin Film with Embedded Carbon Quantum Dots for Post-Fabrication Improvement of Light Harvesting in Perovskite Solar Cells. **Nanomaterials 2020, Vol. 10, Page 291**, [s. l.], v. 10, n. 2, p. 291, 2020. Disponível em: <https://www.mdpi.com/2079-4991/10/2/291/htm>. Acesso em: 7 abr. 2022.

MAZARI, Shaukat Ali *et al.* Nanomaterials: Applications, waste-handling, environmental toxicities, and future challenges - A review. **Journal of Environmental Chemical Engineering**, [s. l.], v. 9, n. 2, p. 105028, 2021.

MESSAI, Habib *et al.* Chemometrics Methods for Specificity, Authenticity and Traceability Analysis of Olive Oils: Principles, Classifications and Applications. **Foods**, [s. l.], v. 5, n. 4, p. 77, 2016. Disponível em: <https://pubmed.ncbi.nlm.nih.gov/28231172/>. Acesso em: 24 jul. 2020.

MI, Xiaohu *et al.* Plasmonic sensing of Cu²⁺ via shell-etching of Au@Ag nanorods. **Materials Chemistry and Physics**, [s. l.], v. 259, p. 124036, 2021.

- MOHANRAJ, Jagannathan *et al.* Green synthesis of white light emitting carbon quantum dots: fabrication of white fluorescent film and optical sensor applications. **Journal of Hazardous Materials**, [s. l.], p. 125091, 2021. Disponível em: <https://linkinghub.elsevier.com/retrieve/pii/S0304389421000558>. Acesso em: 18 jan. 2021.
- MONCAYO, S. *et al.* Evaluation of supervised chemometric methods for sample classification by Laser Induced Breakdown Spectroscopy. **Chemometrics and Intelligent Laboratory Systems**, [s. l.], v. 146, p. 354, 2015.
- MONDAL, Tapas Kumar; GHORAI, Uttam Kumar; SAHA, Shyamal K. Dual-Emissive Carbon Quantum Dot-Tb Nanocomposite as a Fluorescent Indicator for a Highly Selective Visual Detection of Hg(II) in Water. **ACS Omega**, [s. l.], v. 3, n. 9, p. 11439–11446, 2018. Disponível em: <https://pubs.acs.org/sharingguidelines>. Acesso em: 23 mar. 2021.
- MONDAY, Yakubu Newman *et al.* Facile hydrothermal and solvothermal synthesis and characterization of nitrogen-doped carbon dots from palm kernel shell precursor. **Applied Sciences (Switzerland)**, [s. l.], v. 11, n. 4, p. 1–17, 2021.
- MOO, Y. C. *et al.* New development of optical fibre sensor for determination of nitrate and nitrite in water. **Optik**, [s. l.], v. 127, n. 3, p. 1312–1319, 2016.
- MURRAY, Eoin *et al.* Fully automated, low-cost ion chromatography system for in-situ analysis of nitrite and nitrate in natural waters. **Talanta**, [s. l.], v. 216, p. 120955, 2020.
- MUTHUSANKAR, Ganesan; DEVI, Ramadhass Keerthika; GOPU, Gopalakrishnan. Nitrogen-doped carbon quantum dots embedded Co₃O₄ with multiwall carbon nanotubes: An efficient probe for the simultaneous determination of anticancer and antibiotic drugs. **Biosensors & bioelectronics**, [s. l.], v. 150, n. December 2019, p. 111947, 2020.
- NASARUDDIN, Ricca Rahman *et al.* Roles of thiolate ligands in the synthesis, properties and catalytic application of gold nanoclusters. **Coordination Chemistry Reviews**, [s. l.], v. 368, p. 60–79, 2018.
- NEEMA, P. M.; TOMY, Ann Mary; CYRIAC, Jobin. Chemical sensor platforms based on fluorescence resonance energy transfer (FRET) and 2D materials. **TrAC Trends in Analytical Chemistry**, [s. l.], v. 124, p. 115797, 2020.
- NG HAU KWAN, Melvin *et al.* Carbon-dot dispersal in PVA thin film for food colorant sensing. **Journal of Environmental Chemical Engineering**, [s. l.], v. 8, n. 3, p. 103187, 2020.
- NGUYEN, Vanthan *et al.* Tuning photoluminescence of boron nitride quantum dots via surface functionalization by femtosecond laser ablation. **Journal of Molecular Structure**, [s. l.], v. 1244, p. 130922, 2021.
- NIROUMAND, Hamed; ZAIN, M.F.M. The Role of Nanomaterials in Nanoarchitecture. **Procedia - Social and Behavioral Sciences**, [s. l.], v. 89, p. 27–30, 2013.

- NORTON, Amie E. *et al.* A colorimetric/luminescence sensor for detecting MeCN in water: Towards direct detection of dissolved organic contaminants. **Sensors and Actuators B: Chemical**, [s. l.], v. 329, p. 129207, 2021.
- OMAR, Nur Alia Sheh *et al.* A sensing approach for manganese ion detection by carbon dots nanocomposite thin film-based surface plasmon resonance sensor. **Optik**, [s. l.], v. 243, p. 167435, 2021.
- OMAR, Nur Alia Sheh *et al.* Sensitive Detection of Dengue Virus Type 2 E-Proteins Signals Using Self-Assembled Monolayers/Reduced Graphene Oxide-PAMAM Dendrimer Thin Film-SPR Optical Sensor. **Scientific Reports** **2020** **10:1**, [s. l.], v. 10, n. 1, p. 1–15, 2020. Disponível em: <https://www.nature.com/articles/s41598-020-59388-3>. Acesso em: 26 out. 2021.
- ONYIA, A. I.; IKERI, H. I.; NWOBODO, A. N. Theoretical study of the quantum confinement effects on quantum dots using particle in a box model. **Journal of Ovonic Research**, [s. l.], v. 14, n. 1, p. 49–54, 2018.
- OROUJI, A.; ABBASI-MOAYED, S.; HORMOZI-NEZHAD, M. Reza. ThThnated Development of a pH assisted AgNP-based colorimetric sensor Array for simultaneous identification of phosalone and azinphosmethyl pesticides. **Spectrochimica Acta Part A: Molecular and Biomolecular Spectroscopy**, [s. l.], v. 219, p. 496–503, 2019.
- PANTHI, Gopal; PARK, Mira. Synthesis of metal nanoclusters and their application in Hg²⁺ ions detection: A review. **Journal of Hazardous Materials**, [s. l.], v. 424, p. 127565, 2022.
- PARK, Jae Jung *et al.* Colorimetric Visualization Using Polymeric Core–Shell Nanoparticles: Enhanced Sensitivity for Formaldehyde Gas Sensors. **Polymers** **2020**, **Vol. 12**, **Page 998**, [s. l.], v. 12, n. 5, p. 998, 2020. Disponível em: <https://www.mdpi.com/2073-4360/12/5/998/htm>. Acesso em: 13 out. 2021.
- PEARSON, Karl. LIII. On lines and planes of closest fit to systems of points in space. **The London, Edinburgh, and Dublin Philosophical Magazine and Journal of Science**, [s. l.], v. 2, n. 11, p. 559–572, 1901. Disponível em: <https://doi.org/10.1080/14786440109462720>.
- POURREZA, Nahid; GHOMI, Matineh. Green synthesized carbon quantum dots from Prosopis juliflora leaves as a dual off-on fluorescence probe for sensing mercury (II) and chemet drug. **Materials Science and Engineering C**, [s. l.], v. 98, p. 887–896, 2019.
- PRIYADARSHINI, E.; PRADHAN, N. Gold nanoparticles as efficient sensors in colorimetric detection of toxic metal ions: A review. **Sensors and Actuators B: Chemical**, [s. l.], v. 238, p. 888–902, 2017.
- PUTHIYEDATH, Thasnim; BAHULAYAN, Damodaran. A click derived triazole-coumarin derivative as fluorescence on-off PET based sensor for Ca²⁺ and Fe³⁺ ions. **Sensors and Actuators B: Chemical**, [s. l.], v. 272, p. 110–117, 2018.
- QIANG, Ruibin *et al.* Synthesis of carbon quantum dots with green luminescence from potato starch. **New Journal of Chemistry**, [s. l.], v. 43, n. 27, p. 10826–10833, 2019.

- QU, Dan *et al.* Tailoring color emissions from N-doped graphene quantum dots for bioimaging applications. **Light: Science & Applications**, [s. l.], v. 4, n. 12, p. e364–e364, 2015. Disponível em: www.nature.com/lsa. Acesso em: 4 jul. 2021.
- RAJAR, Kausar *et al.* Highly selective colorimetric onsite sensor for Co²⁺ ion detection by povidone capped silver nanoparticles. **Materials Chemistry and Physics**, [s. l.], v. 273, p. 125082, 2021.
- RAMALINGAM, Gopal *et al.* Quantum Confinement Effect of 2D Nanomaterials. **Quantum Dots - Fundamental and Applications**, [s. l.], 2020. Disponível em: <https://www.intechopen.com/chapters/70534>. Acesso em: 6 set. 2021.
- RAMDZAN, Nur Syahira Md *et al.* Detection of mercury ion using surface plasmon resonance spectroscopy based on nanocrystalline cellulose/poly(3,4-ethylenedioxythiophene) thin film. **Measurement**, [s. l.], v. 182, p. 109728, 2021.
- RAO, Longshi *et al.* Highly photoluminescent and stable n-doped carbon dots as nanoprobe for Hg²⁺ detection. **Nanomaterials**, [s. l.], v. 8, n. 11, 2018. Disponível em: [/pmc/articles/PMC6265737/](http://pmc/articles/PMC6265737/). Acesso em: 23 mar. 2021.
- RECKMEIER, C. J. *et al.* Luminescent colloidal carbon dots: optical properties and effects of doping [Invited]. **Optics Express**, [s. l.], v. 24, n. 2, p. A312, 2016. Disponível em: <https://pubmed.ncbi.nlm.nih.gov/26832584/>. Acesso em: 23 mar. 2021.
- RESHMA, V.G.; MOHANAN, P.V. Quantum dots: Applications and safety consequences. **Journal of Luminescence**, [s. l.], v. 205, p. 287–298, 2019. Disponível em: <https://www.sciencedirect.com/science/article/pii/S0022231318313334>. Acesso em: 15 jun. 2019.
- RIVADENEYRA, Almudena *et al.* Carbon Dots as Sensing Layer for Printed Humidity and Temperature Sensors. **Nanomaterials 2020, Vol. 10, Page 2446**, [s. l.], v. 10, n. 12, p. 2446, 2020. Disponível em: <https://www.mdpi.com/2079-4991/10/12/2446/htm>. Acesso em: 26 out. 2021.
- SACCENTI, Edoardo; CAMACHO, José. Multivariate Exploratory Data Analysis Using Component Models. *In*: REFERENCE MODULE IN FOOD SCIENCE. [S. l.]: Elsevier, 2020.
- SA-NGUANPRANG, Surisa; PHURUANGRAT, Anukorn; BUNKOED, Opas. An optosensor based on a hybrid sensing probe of mesoporous carbon and quantum dots embedded in imprinted polymer for ultrasensitive detection of thiamphenicol in milk. **Spectrochimica Acta Part A: Molecular and Biomolecular Spectroscopy**, [s. l.], v. 264, p. 120324, 2022.
- SANJUAN-NAVARRO, L. *et al.* In-tube solid phase microextraction coupled to miniaturized liquid chromatography for both, noble metal nanoparticle assessment and sensitive plasmonic assay development. **Analytica Chimica Acta**, [s. l.], v. 1171, p. 338665, 2021.

- ŠARIĆ, Ankica; DESPOTOVIĆ, Ines; ŠTEFANIĆ, Goran. Solvothermal synthesis of zinc oxide nanoparticles: A combined experimental and theoretical study. **Journal of Molecular Structure**, [s. l.], v. 1178, p. 251–260, 2019.
- SEDELNIKOVA, Olga V. *et al.* Role of interface interactions in the sensitivity of sulfur-modified single-walled carbon nanotubes for nitrogen dioxide gas sensing. **Carbon**, [s. l.], 2021.
- SEGKOS, Apostolos *et al.* Patterned carbon dot-based thin films for solid-state devices. **Nanoscale**, [s. l.], v. 12, n. 18, p. 10254–10264, 2020. Disponível em: <https://pubs.rsc.org/en/content/articlehtml/2020/nr/c9nr08904g>. Acesso em: 26 out. 2021.
- SHAJI, Ashin; ZACHARIAH, Ajesh K. Surface Area Analysis of Nanomaterials. **Thermal and Rheological Measurement Techniques for Nanomaterials Characterization**, [s. l.], v. 3, p. 197–231, 2017.
- SHAMSIPUR, Mojtaba; BARATI, Ali; KARAMI, Sara. **Long-wavelength, multicolor, and white-light emitting carbon-based dots: Achievements made, challenges remaining, and applications**. [S. l.]: Elsevier Ltd, 2017.
- SHARMA, Arjun *et al.* Molecular Origin and Self-Assembly of Fluorescent Carbon Nanodots in Polar Solvents. **Journal of Physical Chemistry Letters**, [s. l.], v. 8, n. 5, p. 1044–1052, 2017.
- SHARMA, Shivani; GHOSH, Kalyan Sundar. Recent advances (2017–20) in the detection of copper ion by using fluorescence sensors working through transfer of photo-induced electron (PET), excited-state intramolecular proton (ESIPT) and Förster resonance energy (FRET). **Spectrochimica Acta Part A: Molecular and Biomolecular Spectroscopy**, [s. l.], v. 254, p. 119610, 2021.
- SHAULOFF, Nitzan; BHATTACHARYA, Sagarika; JELINEK, Raz. Elastic carbon dot/polymer films for fluorescent tensile sensing and mechano-optical tuning. **Carbon**, [s. l.], v. 152, p. 363–371, 2019.
- SHEHALA *et al.* Efficient sensing of saccharin through interference synthesis of gum ghatti capped silver nanoparticles. **International Journal of Biological Macromolecules**, [s. l.], v. 182, p. 2003–2018, 2021.
- SHI, Xingbo *et al.* **Review on carbon dots in food safety applications** *Talanta* Elsevier B.V., , 2019.
- SHOBANA, J. *et al.* Visual sensing of Triethyl amine using *Sapindus mukorossi* – Silver nanoparticles. **Materials Today: Proceedings**, [s. l.], 2021.
- SHRIVASTAVA, Alankar; GUPTA, VipinB. Methods for the determination of limit of detection and limit of quantitation of the analytical methods. **Chronicles of Young Scientists**, [s. l.], v. 2, n. 1, p. 21, 2011.
- SINGH, K Anand. Fluorescence Spectroscopy as a Basic Tool of Analytical Chemists: A Review. **IOSR Journal of Applied Chemistry (IOSR-JAC)**, [s. l.], v. 9, p. 37–39, 2016.

Disponível em: www.iosrjournals.orgwww.iosrjournals.org37%7CPage. Acesso em: 5 out. 2021.

SONG, Haisheng *et al.* Quantitative detection of formaldehyde and ammonia using a yttrium-doped ZnO sensor array combined with a back-propagation neural network model. **Sensors and Actuators A: Physical**, [s. l.], v. 331, p. 112940, 2021.

SONG, Jinping *et al.* Fluorescent boron and nitrogen co-doped carbon dots with high quantum yield for the detection of nimesulide and fluorescence staining. **Spectrochimica Acta Part A: Molecular and Biomolecular Spectroscopy**, [s. l.], v. 216, p. 296–302, 2019.

SONIA *et al.* Gold nanoclusters: An ultrasmall platform for multifaceted applications. **Talanta**, [s. l.], v. 234, 2021. Disponível em: <https://pubmed.ncbi.nlm.nih.gov/34364432/>. Acesso em: 4 jan. 2022.

SOTOLONGO-GARCÍA, Roberto *et al.* Optimizing the Efficiency of a Cytocompatible Carbon-Dots-Based FRET Platform and Its Application as a Riboflavin Sensor in Beverages. **Nanomaterials 2021, Vol. 11, Page 1981**, [s. l.], v. 11, n. 8, p. 1981, 2021. Disponível em: <https://www.mdpi.com/2079-4991/11/8/1981/htm>. Acesso em: 10 out. 2021.

STEFANAKIS, Dimitrios *et al.* Synthesis of fluorescent carbon dots by a microwave heating process: structural characterization and cell imaging applications. **Journal of Nanoparticle Research 2014 16:10**, [s. l.], v. 16, n. 10, p. 1–10, 2014. Disponível em: <https://link.springer.com/article/10.1007/s11051-014-2646-1>. Acesso em: 26 ago. 2021.

STERN, E. A.; FERRELL, R. A. Surface plasma oscillations of a degenerate electron gas. **Physical Review**, [s. l.], v. 120, n. 1, p. 130–136, 1960.

SUI, Xiaoyu *et al.* Additive manufacturing and applications of nanomaterial-based sensors. **Materials Today**, [s. l.], 2021.

SUN, Jiefang *et al.* Polymer/inorganic nanohybrids: An attractive materials for analysis and sensing. **TrAC Trends in Analytical Chemistry**, [s. l.], v. 140, p. 116273, 2021.

SUN, Jingwei *et al.* A colorimetric sensor array for protein discrimination based on carbon nanodots-induced reversible aggregation of AuNP with GSH as a regulator. **Sensors and Actuators B: Chemical**, [s. l.], v. 296, p. 126677, 2019.

SUN, Jingwei *et al.* **Colorimetric sensor array based on gold nanoparticles: Design principles and recent advances**. [S. l.]: Elsevier B.V., 2020.

SUN, Lili *et al.* Chitosan-derived N-doped carbon dots for fluorescent determination of nitrite and bacteria imaging. **Spectrochimica Acta - Part A: Molecular and Biomolecular Spectroscopy**, [s. l.], v. 251, 2021. Disponível em: <https://pubmed.ncbi.nlm.nih.gov/33508683/>. Acesso em: 29 mar. 2021.

SUN, Zhonghui *et al.* Solvent-controlled synthesis strategy of multicolor emission carbon dots and its applications in sensing and light-emitting devices. **Nano Research**, [s. l.], v. 12, n. 1, p. 1–9, 2021.

SWAMINATHAN, Hariharan; BALASUBRAMANIAN, Karthikeyan. Förster resonance energy transfer between MoS₂ quantum dots and polyaniline for turn-on bovine serum albumin sensing. **Sensors and Actuators B: Chemical**, [s. l.], v. 264, p. 337–343, 2018.

TADESSE, Aschalew *et al.* Synthesis of nitrogen doped carbon quantum dots/magnetite nanocomposites for efficient removal of methyl blue dye pollutant from contaminated water. **RSC Advances**, [s. l.], v. 8, n. 16, p. 8528–8536, 2018. Disponível em: <https://pubs.rsc.org/en/content/articlehtml/2018/ra/c8ra00158h>. Acesso em: 2 mar. 2021.

TANG, Huang *et al.* Nitrogen-doped carbon dots based on arginine and maleic acid for fabrication of PVA composite films and iron fluorescence probes. **Journal of Molecular Structure**, [s. l.], v. 1251, p. 132034, 2022.

TANG, Qian *et al.* An optical sensing system with ratiometric and turn-off dual-mode of CDs@MnO₂ nanosheets for the determination of H₂O₂ and glucose based on a combination of first-order scattering, fluorescence, and second-order scattering. **Spectrochimica Acta Part A: Molecular and Biomolecular Spectroscopy**, [s. l.], v. 264, p. 120299, 2022.

TANG, Zhiyong; KOTOV, Nicholas A. One-Dimensional Assemblies of Nanoparticles: Preparation, Properties, and Promise. **Advanced Materials**, [s. l.], v. 17, n. 8, p. 951–962, 2005. Disponível em: <https://onlinelibrary.wiley.com/doi/full/10.1002/adma.200401593>. Acesso em: 4 jan. 2022.

TAO, Yingzhou *et al.* Quantitative gold nanorods based photothermal biosensor for glucose using a thermometer as readout. **Talanta**, [s. l.], v. 230, p. 122364, 2021.

TAPANGPAN, Pimchanok *et al.* Terbium metal organic framework: Microwave synthesis and selective sensing of nitrite. **Inorganic Chemistry Communications**, [s. l.], v. 111, p. 107627, 2020.

TORO-GONZÁLEZ, Miguel *et al.* New concept of radiolytic synthesis of gold nanoparticles in continuous flow. **Radiation Physics and Chemistry**, [s. l.], v. 188, p. 109614, 2021.

TRUSKEWYCZ, Adam *et al.* Incorporation of quantum carbon dots into a PVP/ZnO hydrogel for use as an effective hexavalent chromium sensing platform. **Analytica Chimica Acta**, [s. l.], v. 1099, p. 126–135, 2020.

VASHISHT, Devika *et al.* Solvothermal assisted phosphate functionalized graphitic carbon nitride quantum dots for optical sensing of Fe ions and its thermodynamic aspects. **Spectrochimica Acta - Part A: Molecular and Biomolecular Spectroscopy**, [s. l.], v. 228, p. 117773, 2020.

VASIMALAI, Nagamalai *et al.* Green synthesis of fluorescent carbon dots from spices for in vitro imaging and tumour cell growth inhibition. **Beilstein J. Nanotechnol**, [s. l.], v. 9, p. 530–544, 2018. Disponível em: <https://www.beilstein-journals.org/bjnano/content/pdf/2190-4286-9-51.pdf>. Acesso em: 27 jun. 2019.

VAZ, Roberto *et al.* High luminescent carbon dots as an eco-friendly fluorescence sensor for Cr(VI) determination in water and soil samples. **Journal of Photochemistry and Photobiology A: Chemistry**, [s. l.], v. 346, p. 502–511, 2017.

- VEDAMALAI, Mani *et al.* Carbon nanodots prepared from o-phenylenediamine for sensing of Cu²⁺ ions in cells. **Nanoscale**, [s. l.], v. 6, n. 21, p. 13119–13125, 2014. Disponível em: <https://pubs.rsc.org/en/content/articlehtml/2014/nr/c4nr03213f>. Acesso em: 4 jul. 2021.
- VENKATESWARA RAJU, Chikkili *et al.* Phosphorous doped carbon quantum dots as an efficient solid state electrochemiluminescence platform for highly sensitive turn-on detection of Cu²⁺ ions. **Electrochimica Acta**, [s. l.], v. 331, 2020.
- VILIAN, A. T.Ezhil *et al.* Pd–Cu nanospheres supported on Mo₂C for the electrochemical sensing of nitrites. **Journal of Hazardous Materials**, [s. l.], v. 408, p. 124914, 2021.
- VOON, Chun H.; LIM, Bee Y.; HO, Li N. Silicon Carbide Nanomaterials. **Synthesis of Inorganic Nanomaterials**, [s. l.], p. 213–253, 2018.
- WANG, Boyang *et al.* **Carbon dots as a new class of nanomedicines: Opportunities and challenges**. [S. l.]: Elsevier B.V., 2021.
- WANG, Kai *et al.* Differentiation of proteins and cancer cells using metal oxide and metal nanoparticles-quantum dots sensor array. **Sensors and Actuators B: Chemical**, [s. l.], v. 250, p. 69–75, 2017.
- WANG, Xiaohan *et al.* Colloidal carbon quantum dots as light absorber for efficient and stable ecofriendly photoelectrochemical hydrogen generation. **Nano Energy**, [s. l.], v. 86, n. April, p. 106122, 2021.
- WANG, Xiongbin; YU, Jiahao; CHEN, Rui. Optical Characteristics of ZnS Passivated CdSe/CdS Quantum Dots for High Photostability and Lasing. **Scientific Reports**, [s. l.], v. 8, n. 1, p. 1–7, 2018.
- WANG, Yan; TANG, Meng. Dysfunction of various organelles provokes multiple cell death after quantum dot exposure. **International Journal of Nanomedicine**, [s. l.], v. 13, p. 2729–2742, 2018.
- WANG, Yawen *et al.* Thermodynamics versus Kinetics in Nanosynthesis. **Angewandte Chemie International Edition**, [s. l.], v. 54, n. 7, p. 2022–2051, 2015.
- WANG, Yingte *et al.* Hydrothermal synthesis of carbon quantum dots as fluorescent probes for the sensitive and rapid detection of picric acid. **Analytical Methods**, [s. l.], v. 10, n. 23, p. 2775–2784, 2018.
- WANG, Zhen Xing *et al.* Ångstrom-Scale Silver Particles as a Promising Agent for Low-Toxicity Broad-Spectrum Potent Anticancer Therapy. **Advanced Functional Materials**, [s. l.], v. 29, n. 23, p. 1808556, 2019. Disponível em: <https://onlinelibrary.wiley.com/doi/full/10.1002/adfm.201808556>. Acesso em: 4 jan. 2022.
- WANG, Zijun *et al.* Carbon dots based nanocomposite thin film for highly efficient luminescent solar concentrators. **Organic Electronics**, [s. l.], v. 62, p. 284–289, 2018.

- WEI, Jianfei *et al.* Rapid preparation of homogeneous carbon dots with yellow fluorescence and formation mechanistic investigation. **Journal of Nanoparticle Research**, [s. l.], v. 21, n. 4, p. 1–12, 2019. Disponível em: <https://doi.org/10.1007/s11051-019-4510-9>. Acesso em: 4 jul. 2021.
- WEI, Na *et al.* One-pot facile synthesis of green-emitting fluorescent silicon quantum dots for the highly selective and sensitive detection of nitrite in food samples. **Dyes and Pigments**, [s. l.], v. 184, p. 108848, 2021.
- WEI, Wei *et al.* Carbon Dots Fluorescence-Based Colorimetric Sensor for Sensitive Detection of Aluminum Ions with a Smartphone. **Chemosensors 2021, Vol. 9, Page 25**, [s. l.], v. 9, n. 2, p. 25, 2021. Disponível em: <https://www.mdpi.com/2227-9040/9/2/25/htm>. Acesso em: 10 out. 2021.
- WU, Haocheng *et al.* Colorimetric sensor based on 4-mercaptophenylboronic modified gold nanoparticles for rapid and selective detection of fluoride anion. **Spectrochimica Acta Part A: Molecular and Biomolecular Spectroscopy**, [s. l.], v. 214, p. 393–398, 2019.
- WU, Peng *et al.* Hydrothermal synthesis of nitrogen-doped carbon quantum dots from microcrystalline cellulose for the detection of Fe³⁺ ions in an acidic environment. **RSC Advances**, [s. l.], v. 7, n. 70, p. 44144–44153, 2017. Disponível em: <https://pubs.rsc.org/en/content/articlehtml/2017/ra/c7ra08400e>. Acesso em: 2 mar. 2021.
- WU, Yiyang *et al.* Facile ultrasonic synthesized NH₂-carbon quantum dots for ultrasensitive Co²⁺ ion detection and cell imaging. **Talanta**, [s. l.], v. 205, p. 120121, 2019.
- XIANYU, Yunlei *et al.* Plasmonic sensing of β -glucuronidase activity via silver mirror reaction on gold nanostars. **Biosensors and Bioelectronics**, [s. l.], v. 190, p. 113430, 2021.
- XIE, Ruirui *et al.* Lanthanide-functionalized metal-organic frameworks based ratiometric fluorescent sensor array for identification and determination of antibiotics. **Talanta**, [s. l.], v. 231, p. 122366, 2021.
- XIE, Yanting *et al.* One-step hydrothermal synthesis of fluorescence carbon quantum dots with high product yield and quantum yield. **Nanotechnology**, [s. l.], v. 30, n. 8, 2019.
- XU, Dong; LIN, Qinlu; CHANG, Huan Tsung. Recent Advances and Sensing Applications of Carbon Dots. **Small Methods**, [s. l.], v. 4, n. 4, p. 1–17, 2020.
- XU, Hongda *et al.* Graphene oxide supported gold nanoclusters for the sensitive and selective detection of nitrite ions. **Analyst**, [s. l.], v. 140, n. 5, p. 1678–1685, 2015. Disponível em: www.rsc.org/analyst. Acesso em: 18 jan. 2021.
- XU, Li *et al.* Silver nanoparticles: Synthesis, medical applications and biosafety. **Theranostics**, [s. l.], v. 10, n. 20, p. 8996, 2020. Disponível em: [/pmc/articles/PMC7415816/](http://pmc/articles/PMC7415816/). Acesso em: 4 jan. 2022.
- XU, Xiaoyou *et al.* Electrophoretic Analysis and Purification of Fluorescent Single-Walled Carbon Nanotube Fragments. **Journal of the American Chemical Society**, [s. l.], v. 126, n.

40, p. 12736–12737, 2004. Disponível em: <https://pubs.acs.org/doi/10.1021/ja040082h>. Acesso em: 15 nov. 2019.

XU, Xuechao *et al.* **Nanomaterial-based sensors and biosensors for enhanced inorganic arsenic detection: A functional perspective.** [S. l.]: Elsevier B.V., 2020.

XU, Xumin *et al.* Nitrogen-doped carbon quantum dots for effective corrosion inhibition of Q235 steel in concentrated sulphuric acid solution. **Materials Today Communications**, [s. l.], v. 29, p. 102872, 2021.

XU, Yilan *et al.* The application of multifunctional nanomaterials in Alzheimer's disease: A potential theranostics strategy. **Biomedicine & pharmacotherapy = Biomedecine & pharmacotherapie**, [s. l.], v. 137, 2021. Disponível em: <https://pubmed.ncbi.nlm.nih.gov/33582451/>. Acesso em: 2 set. 2021.

XU, Zijun *et al.* Machine learning assisted dual-channel carbon quantum dots-based fluorescence sensor array for detection of tetracyclines. **Spectrochimica Acta - Part A: Molecular and Biomolecular Spectroscopy**, [s. l.], v. 232, p. 118147, 2020.

YANG, Min *et al.* Near infrared-response ratiometric fluorescence sensor for the sensitive detection of Cu²⁺. **Colloids and Surfaces A: Physicochemical and Engineering Aspects**, [s. l.], v. 624, p. 126812, 2021.

YANG, Pei *et al.* Microwave-assisted synthesis of xylan-derived carbon quantum dots for tetracycline sensing. **Optical Materials**, [s. l.], v. 85, p. 329–336, 2018.

YANG, Ting Ting *et al.* Synthesis and characterization of ErFeO₃ nanoparticles by a hydrothermal method for isopropanol sensing properties. **Vacuum**, [s. l.], v. 185, p. 110005, 2021.

YANG, Zhi *et al.* Nitrogen-doped, carbon-rich, highly photoluminescent carbon dots from ammonium citrate. **Nanoscale**, [s. l.], v. 6, n. 3, p. 1890–1895, 2014. Disponível em: <https://pubs.rsc.org/en/content/articlehtml/2014/nr/c3nr05380f>. Acesso em: 18 set. 2021.

YIN, Zipeng *et al.* Persistent luminescence nanorods-based autofluorescence-free biosensor for prostate-specific antigen detection. **Talanta**, [s. l.], v. 233, p. 122563, 2021.

YU, Lili *et al.* Progress of gold nanomaterials for colorimetric sensing based on different strategies. **TrAC Trends in Analytical Chemistry**, [s. l.], v. 127, p. 115880, 2020.

YUE, Xiaoyue *et al.* A green carbon dots-based fluorescent sensor for selective and visual detection of nitrite triggered by the nitrite-thiol reaction. **New Journal of Chemistry**, [s. l.], v. 44, n. 20, p. 8503–8511, 2020. Disponível em: <https://pubs.rsc.org/en/content/articlehtml/2020/nj/d0nj01025a>. Acesso em: 18 jan. 2021.

YUE, Xiaoyue *et al.* A portable smartphone-assisted ratiometric fluorescence sensor for intelligent and visual detection of malachite green. **Food Chemistry**, [s. l.], v. 371, p. 131164, 2022.

- ZAN, Minghui *et al.* A strong green fluorescent nanoprobe for highly sensitive and selective detection of nitrite ions based on phosphorus and nitrogen co-doped carbon quantum dots. **Sensors and Actuators, B: Chemical**, [s. l.], v. 262, p. 555–561, 2018.
- ZHAI, Hong *et al.* Colorimetric and Ratiometric Fluorescence Dual-Mode Sensing of Glucose Based on Carbon Quantum Dots and Potential UV/Fluorescence of o-Diaminobenzene. **Sensors 2019, Vol. 19, Page 674**, [s. l.], v. 19, n. 3, p. 674, 2019. Disponível em: <https://www.mdpi.com/1424-8220/19/3/674/htm>. Acesso em: 10 out. 2021.
- ZHANG, Dachuan *et al.* AdditiveChem: A comprehensive bioinformatics knowledge-base for food additive chemicals. **Food Chemistry**, [s. l.], p. 125519, 2019.
- ZHANG, Haimin *et al.* Fluorescence Determination of Nitrite in Water Using Prawn-Shell Derived Nitrogen-Doped Carbon Nanodots as Fluorophores. **ACS Sensors**, [s. l.], v. 1, n. 7, p. 875–881, 2016.
- ZHANG, Hao Chen; GUO, Yong Ming. **Advances of Carbon Quantum Dots for Fluorescence Turn-On Detection of Reductive Small Biomolecules**. [S. l.]: Chinese Academy of Sciences, 2021.
- ZHANG, Huadong *et al.* Wood-based carbon quantum dots for enhanced photocatalysis of MIL-88B(Fe). **Optical Materials**, [s. l.], v. 113, p. 110865, 2021.
- ZHANG, M. *et al.* Fabrication of HA/PEI-functionalized carbon dots for tumor targeting, intracellular imaging and gene delivery. **RSC Advances**, [s. l.], v. 7, n. 6, p. 3369–3375, 2017. Disponível em: www.rsc.org/advances. Acesso em: 29 mar. 2021.
- ZHANG, Qingwen *et al.* Wearable electrochemical biosensor based on molecularly imprinted Ag nanowires for noninvasive monitoring lactate in human sweat. **Sensors and Actuators B: Chemical**, [s. l.], v. 320, p. 128325, 2020.
- ZHANG, Shiwang *et al.* Study on the fluorescence properties of carbon dots prepared via combustion process. **Journal of Luminescence**, [s. l.], v. 206, p. 608–612, 2019. b.
- ZHANG, Shu Rong *et al.* One-step synthesis of N, P-doped carbon quantum dots for selective and sensitive detection of Fe²⁺ and Fe³⁺ and scale inhibition. **Journal of Molecular Structure**, [s. l.], v. 1246, p. 131173, 2021.
- ZHANG, Xiang Ping *et al.* Single gold nanocluster probe-based fluorescent sensor array for heavy metal ion discrimination. **Journal of Hazardous Materials**, [s. l.], v. 405, p. 124259, 2021.
- ZHANG, Yanpeng *et al.* Fluorescence Probe Based on Graphene Quantum Dots for Selective, Sensitive and Visualized Detection of Formaldehyde in Food. **Sustainability 2021, Vol. 13, Page 5273**, [s. l.], v. 13, n. 9, p. 5273, 2021. Disponível em: <https://www.mdpi.com/2071-1050/13/9/5273/htm>. Acesso em: 10 out. 2021.
- ZHANG, Yuewei *et al.* Porous graphitic carbon nitride synthesized via direct polymerization of urea for efficient sunlight-driven photocatalytic hydrogen production. **Nanoscale**, [s. l.], v.

4, n. 17, p. 5300–5303, 2012. Disponível em:

<https://pubs.rsc.org/en/content/articlehtml/2012/nr/c2nr30948c>. Acesso em: 9 set. 2021.

ZHANG, Zhiyang *et al.* Plasmonic colorimetric sensors based on etching and growth of noble metal nanoparticles: Strategies and applications. **Biosensors and Bioelectronics**, [s. l.], v. 114, p. 52–65, 2018.

ZHAO, Ke *et al.* Gold-silver nanoparticles modified electrochemical sensor array for simultaneous determination of chromium(III) and chromium(VI) in wastewater samples. **Chemosphere**, [s. l.], v. 281, p. 130880, 2021.

ZHAO, Lingzhi *et al.* A Colorimetric Sensor for the Highly Selective Detection of Sulfide and 1,4-Dithiothreitol Based on the In Situ Formation of Silver Nanoparticles Using Dopamine. **Sensors** **2017**, Vol. 17, Page 626, [s. l.], v. 17, n. 3, p. 626, 2017. Disponível em: <https://www.mdpi.com/1424-8220/17/3/626/htm>. Acesso em: 13 out. 2021.

ZHAO, Xun *et al.* Enhancing photoluminescence of carbon quantum dots doped PVA films with randomly dispersed silica microspheres. **Scientific Reports** **2020** **10:1**, [s. l.], v. 10, n. 1, p. 1–10, 2020. Disponível em: <https://www.nature.com/articles/s41598-020-62563-1>. Acesso em: 26 out. 2021.

ZHOU, Jie *et al.* Two-dimensional nanomaterial-based plasmonic sensing applications: Advances and challenges. **Coordination Chemistry Reviews**, [s. l.], v. 410, p. 213218, 2020.

ZHOU, Xiao *et al.* Chemical-tongue sensor array for determination of multiple metal ions based on trichromatic lanthanide-based nanomaterials. **Sensors and Actuators B: Chemical**, [s. l.], v. 343, p. 130107, 2021.

ZHOU, Zichun *et al.* A novel “turn-off” fluorescent sensor for Al³⁺ detection based on quinolinecarboxamide-coumarin. **Inorganic Chemistry Communications**, [s. l.], v. 121, p. 108168, 2020.

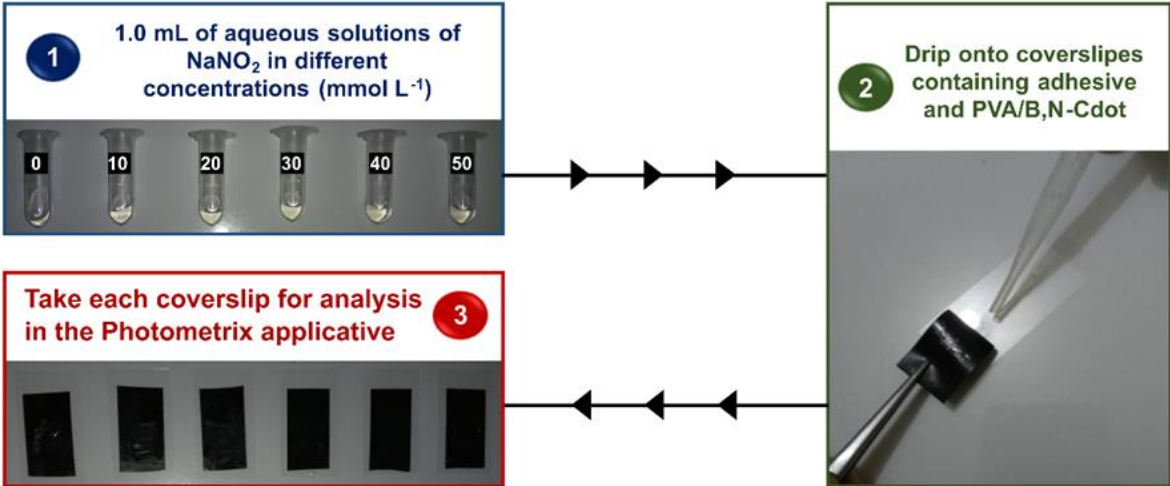
ZHU, Fudan *et al.* Disposable carbon electrodes modified by a bismuth selenide/carboxylic multiwalled carbon nanotubes composite for the effective electrocatalytic analysis of nitrite. **Sensors and Actuators B: Chemical**, [s. l.], p. 129454, 2021. Disponível em: <https://linkinghub.elsevier.com/retrieve/pii/S0925400521000228>. Acesso em: 18 jan. 2021.

ZOU, Chengyue *et al.* A paper-based visualization chip based on nitrogen-doped carbon quantum dots nanoprobe for Hg(II) detection. **Spectrochimica Acta Part A: Molecular and Biomolecular Spectroscopy**, [s. l.], v. 265, p. 120346, 2022.

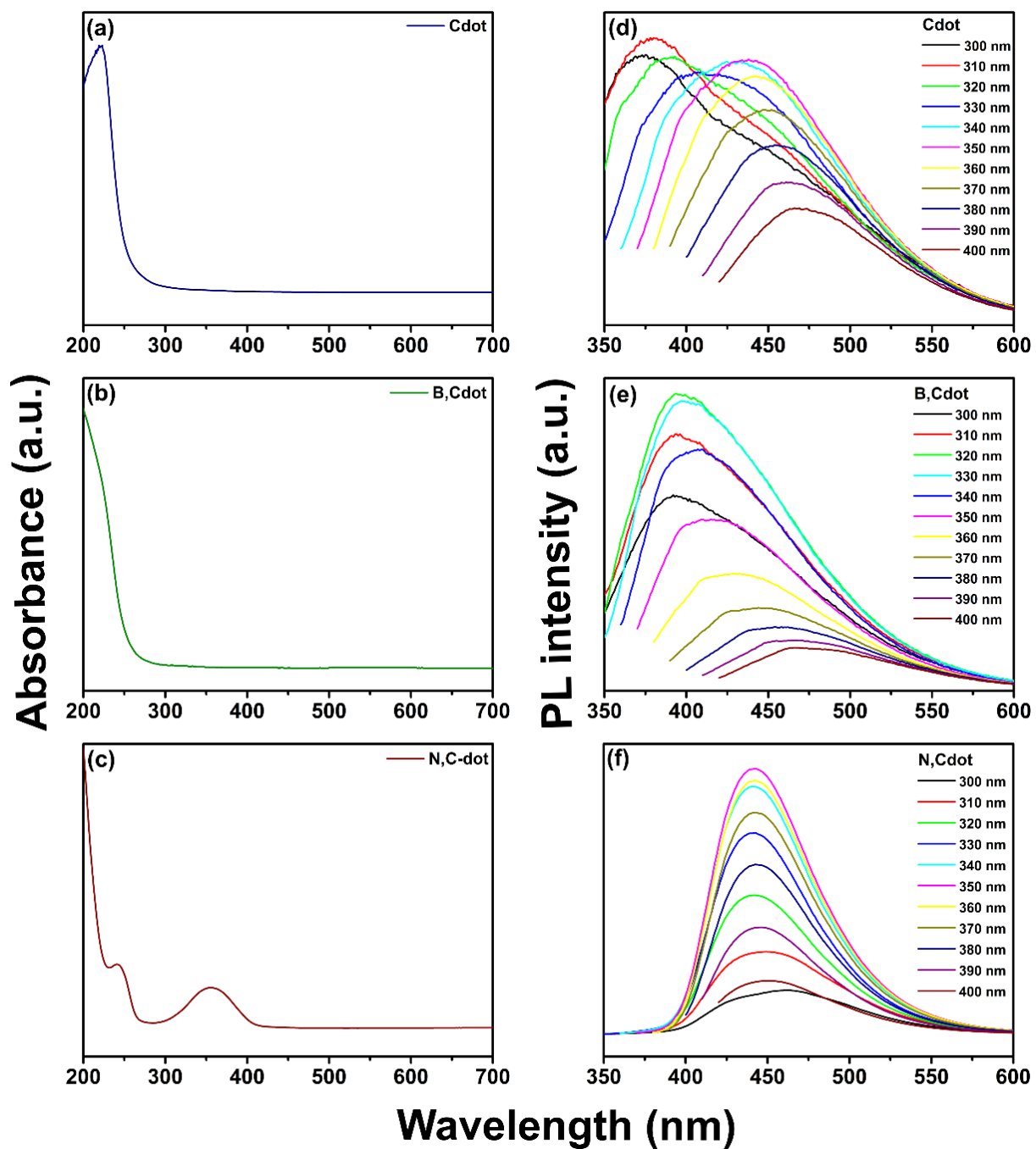
ZU, Fanlin *et al.* The quenching of the fluorescence of carbon dots: A review on mechanisms and applications. **Microchimica Acta**, [s. l.], v. 184, n. 7, p. 1899–1914, 2017.

ZULFAJRI, Muhammad *et al.* Cranberry Beans Derived Carbon Dots as a Potential Fluorescence Sensor for Selective Detection of Fe³⁺ Ions in Aqueous Solution. **ACS Omega**, [s. l.], v. 4, n. 13, p. 15382–15392, 2019.

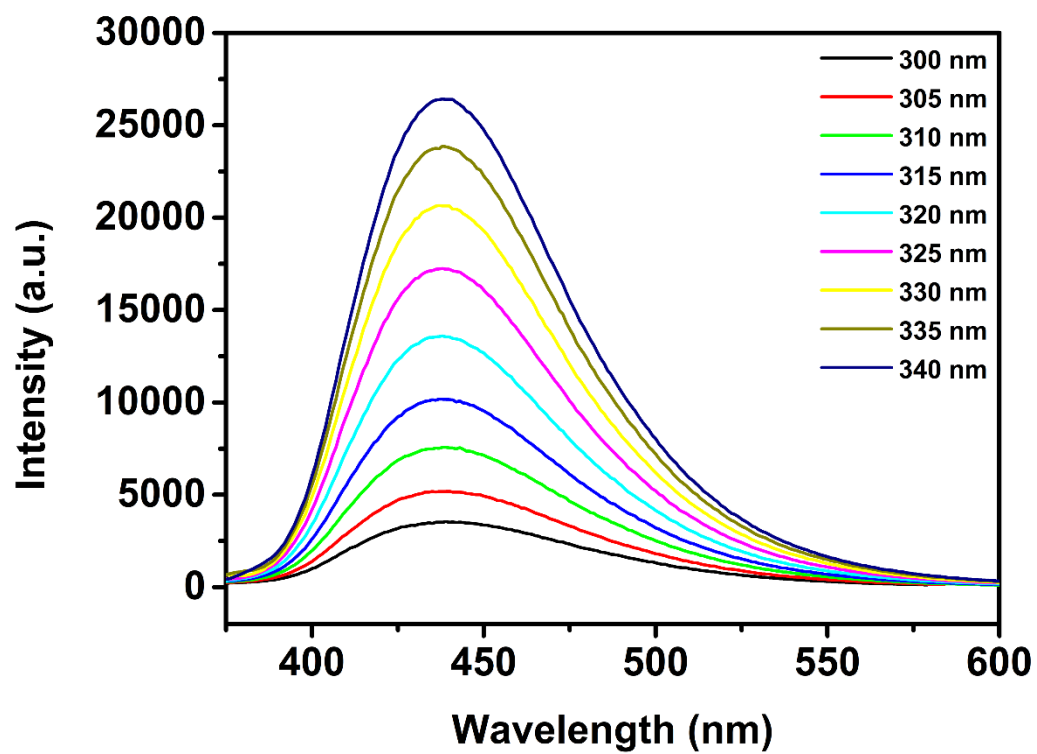
**APPENDIX A – PROCEDURE PROPOSAL FOR THE USE OF THE DEVICE
CONSISTING OF THE PVA/B,N-CDOT THIN FILM, IN FIELD ANALYSIS**



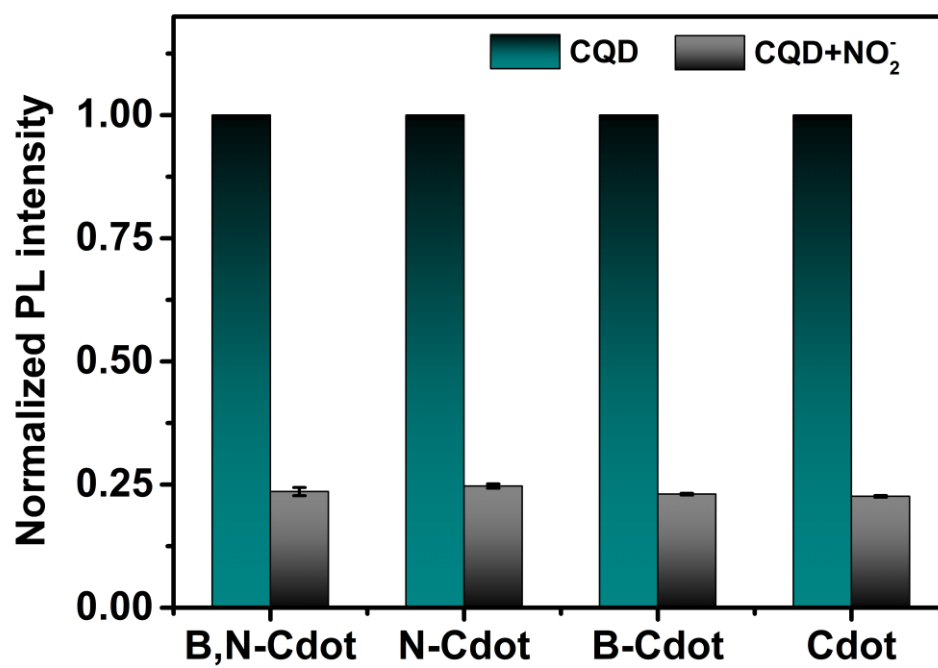
APPENDIX B – (a)-(c) UV-VIS SPECTRUM; (d)-(f) PHOTOLUMINESCENCE
SPECTRUM OF CQDS SYNTHESIZED IN THIS WORK



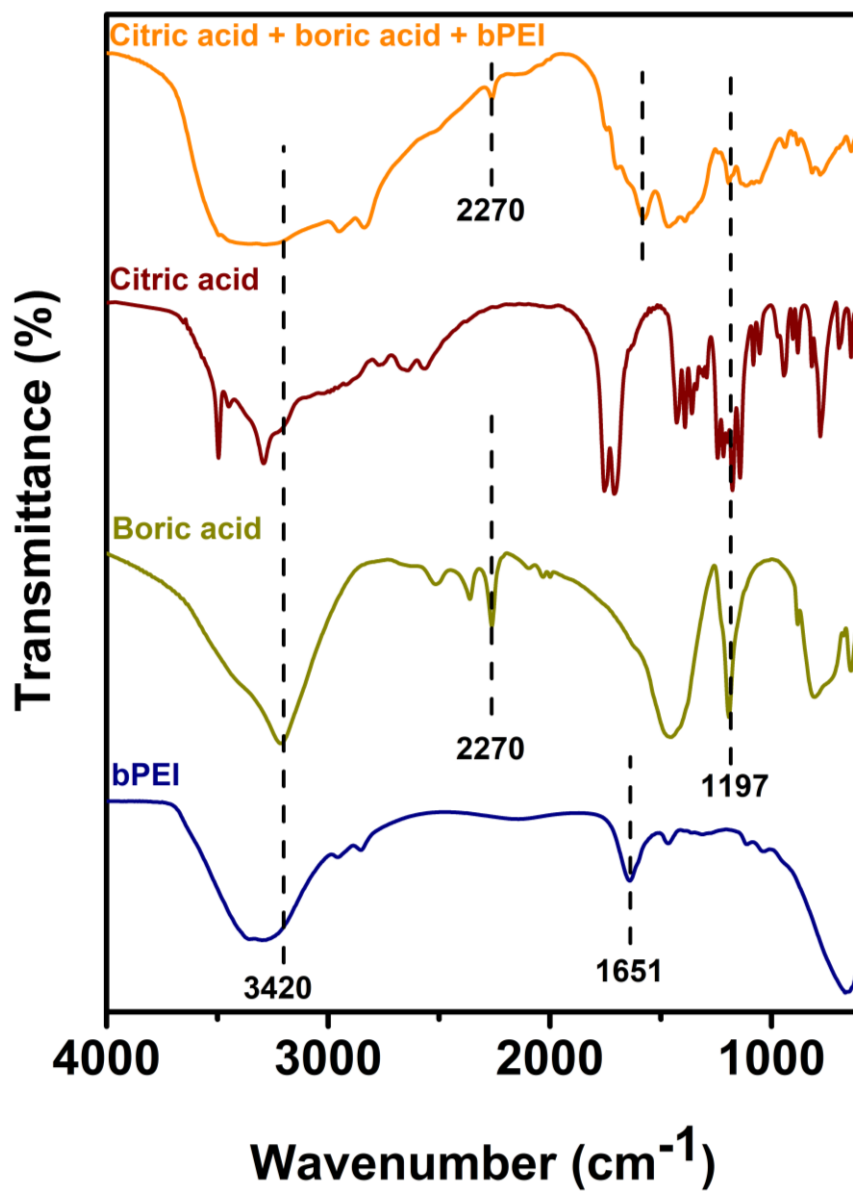
**APPENDIX C – PHOTOLUMINESCENCE SPECTRA WITH DIFFERENT
EXCITATION WAVELENGTHS (300 TO 340 NM) OF B,N-CDOT**



APPENDIX D – EFFECT OF THE DOPING AND FUNCTIONALIZATION OF CQDS
IN THE DETECTION OF NO_2^- IONS

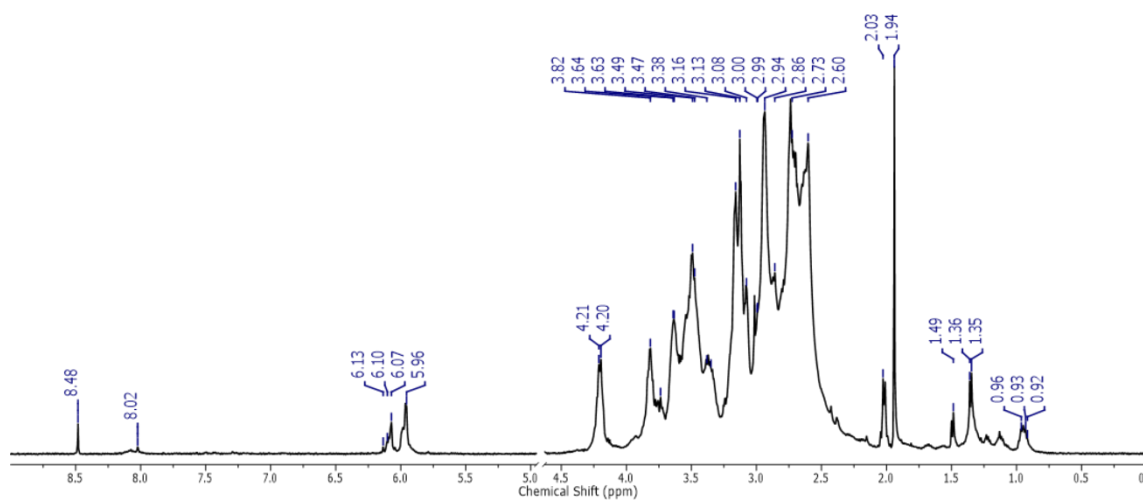


APPENDIX E – FTIR OF THE B,N-CDOT PRECURSORS

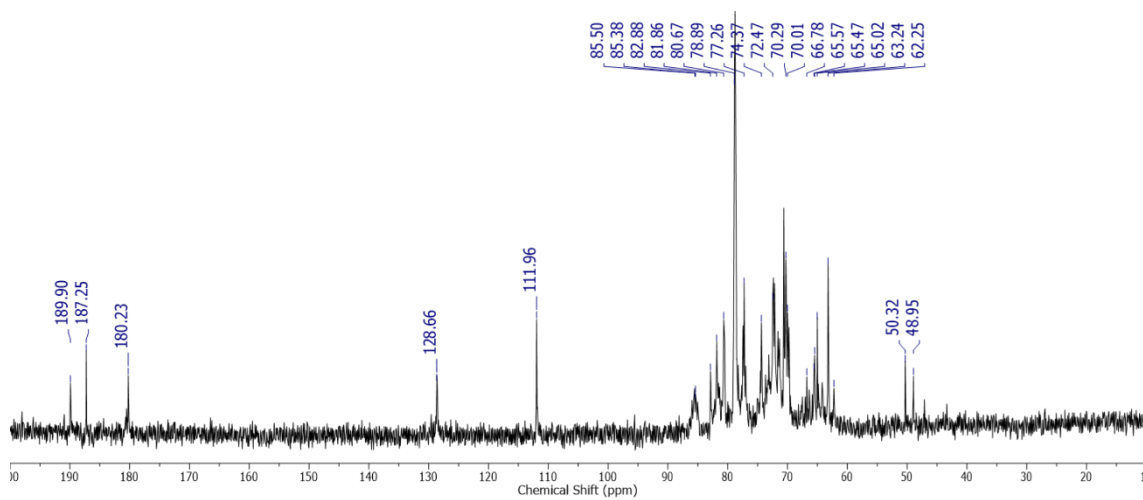


APPENDIX F – NMR SPECTRA OF B₃N-CDOT: (a) ¹H NMR AND (b) ¹³C NMR.

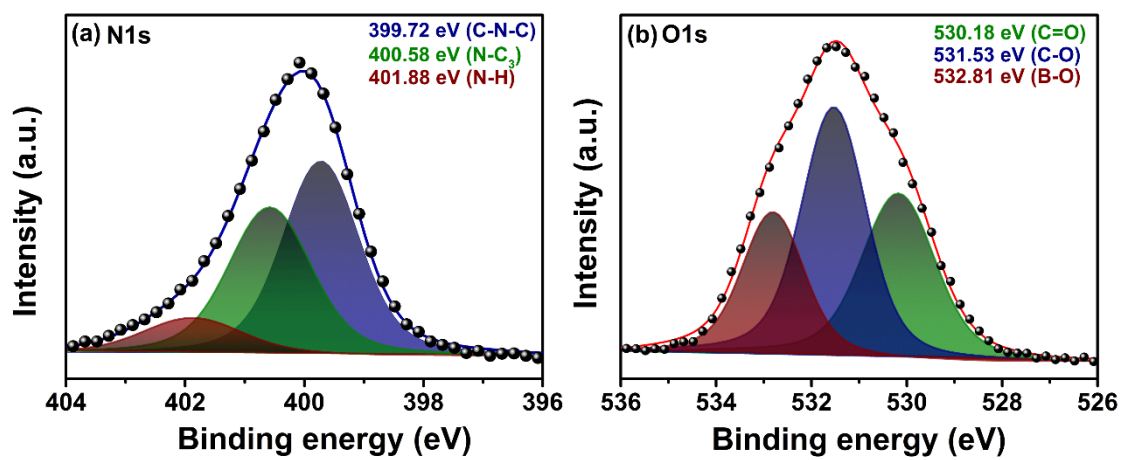
(a)



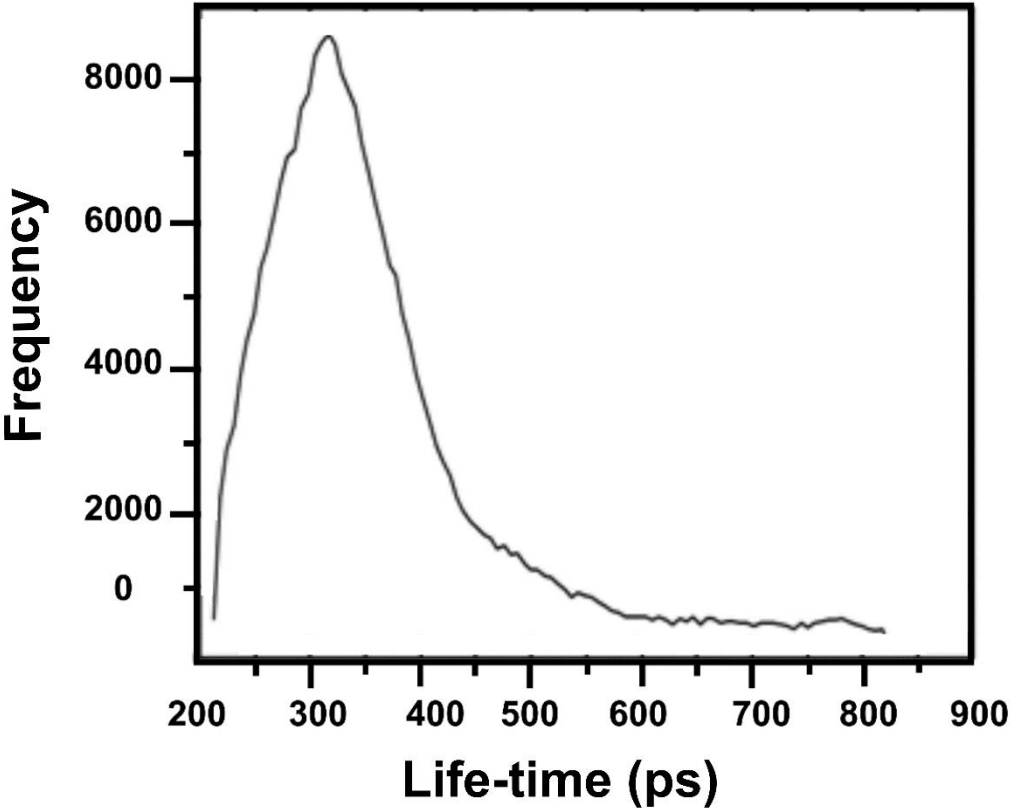
(b)



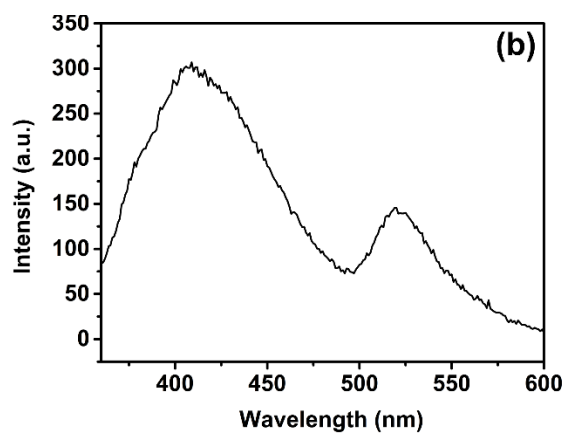
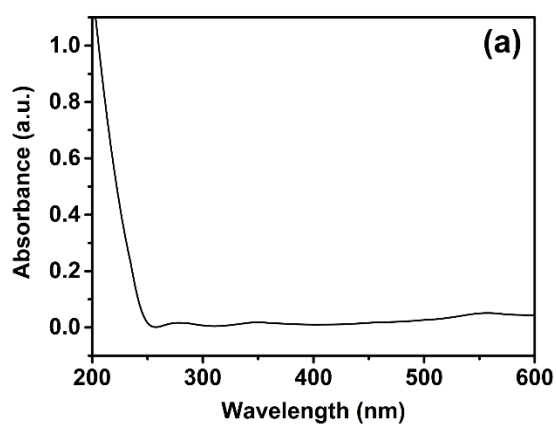
APPENDIX G – HIGH-RESOLUTION SPECTRA OF B,N-CDOT: (a) N1s; (b) O1s.



APPENDIX H – HISTOGRAM OF THE LIFE-TIME DECAYS FREQUENCY.



APPENDIX I – (a) UV-Vis SPECTRUM AND (b) PHOTOLUMINESCENCE SPECTRE OF PVA THIN FILM USING EXCITATION WAVELENGTH OF 340 NM



APPENDIX J – SCIENTIFIC PRODUCTION RELATED TO THE THESIS

Paper 1: Highly sensitive sensing of food additives based on fluorescent carbon quantum dots.

Status: published

Authors: CARNEIRO, S.V.; HOLANDA, M.H.B.; CUNHA, H.O.; OLIVEIRA, J.J.P.; PONTES, S.M.A.; CRUZ, A.A.C.; FECHINE, L.M.U.D.; MOURA, T.A.; PASCHOAL, A.R.; ZAMBELLI, R.A.; FREIRE, R.M.; FECHINE, P.B.A.

Periodic: Journal of Photochemistry and Photobiology A-Chemistry

Year: 2021.



Highly sensitive sensing of food additives based on fluorescent carbon quantum dots



S.V. Carneiro^a, M.H.B. Holanda^b, H.O. Cunha^a, J.J.P. Oliveira^a, S.M.A. Pontes^a, A.A.C. Cruz^a, L.M.U.D. Fechine^a, T.A. Moura^c, A.R. Paschoal^c, R.A. Zambelli^b, R.M. Freire^{d,e}, P.B. A. Fechine^{a,*}

^a Grupo de Química de Materiais Avançados (GQMat), Departamento de Química Analítica e Físico-Química, Universidade Federal do Ceará – UFC, Campus do Pici, CP 12100, CEP 60451-970, Fortaleza, CE, Brasil

^b Laboratório de Biomateriais Alimentícios (LBMA), Departamento de Engenharia de Alimentos, Universidade Federal do Ceará – UFC, Campus do Pici, CP 12100, CEP 60451-970, Fortaleza, CE, Brasil

^c Departamento de Física, Universidade Federal do Ceará – UFC, Campus do Pici, CP 12100, CEP 60451-970, Fortaleza, CE, Brasil

^d Institute of Applied Chemical Sciences, Universidad Autónoma de Chile, 8910060, Santiago, Chile

^e Center for the Development of Nanoscience and Nanotechnology (CEDENNA), 9170124, Santiago, Chile

ARTICLE INFO

Keywords:

Carbon quantum dots
Fluorescence
Sensing platform
Linear discriminant analysis
Food additives
Pickled olives

ABSTRACT

A robust fluorescence-based sensing strategy was designed considering relevance of analyzing chemical additives in industrialized food. In this study, a sensing approach was developed using fluorescent carbon quantum dots (CQDs) as a chemometric tool. CQDs were synthesized by a simple one-step hydrothermal route using the American natural seed *Caesalpinia pulcherrima*, and further characterized regarding their chemical structure. Five food additives were identified, citric acid, lactic acid, ascorbic acid, sodium benzoate and potassium sorbate, which showed a highly sensitive response with a limit of detection (LOD) as low as 252 ng mL⁻¹. The sensing platform was designed using the supervised method for recognizing patterns of linear discriminant analysis (LDA), where we could identify different concentrations of additives, after optimization of experimental parameters. Furthermore, the sensing strategy successfully identified all tested additives in a pickled olives sample with 95 % of confidence, where 100 % of combinations were correctly identified based on classification matrix. Overall, the obtained results evidence the accuracy and potential of CQDs-based fluorescence sensing in the identification of food additives.

Paper 2: Doped carbon quantum dots/PVA nanocomposite as a platform to sense nitrite ions in meat.

Status: submitted

Authors: CARNEIRO, S.V.; OLIVEIRA, J.J.P; FECHINE, L.M.U.D.; ANTUNES, R.A.; NETO, M. L.A.; MOURA, T.A.; LENS, C.; CARVALHO, H.; PASCHOAL, A.R.; FREIRE, R.M.; FECHINE, P.B.A.

Periodic: ACS Applied Materials & Interfaces.

Year: 2022.

This document is confidential and is proprietary to the American Chemical Society and its authors. Do not copy or disclose without written permission. If you have received this item in error, notify the sender and delete all copies.

**DOPED CARBON QUANTUM DOTS/PVA NANOCOMPOSITE AS
A PLATFORM TO SENSE NITRITE IONS IN MEAT**

Journal:	<i>ACS Applied Materials & Interfaces</i>
Manuscript ID	am-2021-19964w
Manuscript Type:	Article
Date Submitted by the Author:	15-Oct-2021
Complete List of Authors:	Carneiro, Samuel; Universidade Federal do Ceara, Physical-chemistry Oliveira, José; Universidade Federal do Ceara, Physical-chemistry Fechine, Lillian; Universidade Federal do Ceara, Antunes, Renato A; Universidade Federal do ABC, Engn Modeling & Appl Social Sci Ctr Neto, Manoel; Universidade Federal do Ceara, Physical-chemistry Moura, Thiago; Universidade Federal do Ceara, Physical-chemistry Lens, Carlos; Universidade Federal do Ceara Carvalho, Hernandes; Universidade Estadual de Campinas, Paschoal, Alexandre; Universidade Federal do Ceara, Physics Freire, Rafael; Instituto de Investigaciones Agropecuarias Fechine, Pierre; Universidade Federal do Ceara, Physical-chemistry

VI Congresso regional da Sociedade Brasileira de Biofísica (SBBf):

Título do trabalho: Pontos Quânticos de Carbono obtidos de fonte natural e sua aplicação para o sensoriamento de aditivos alimentares

Ano: 2021



Prêmio Ícaro de Sousa Moreira:

Título do trabalho: Sensing strategy based on Carbon Quantum Dots from riboflavin for the identification of pesticides.

Ano: 2020

